October 2012 Vol. 37 No. 10
www.mrs.org/bulletin

MRS Bulletin

MRS MATERIALS RESEARCH SOCIETY
Advancing materials. Improving the quality of life.

Thermal-barrier coatings for more efficient gas-turbine engines

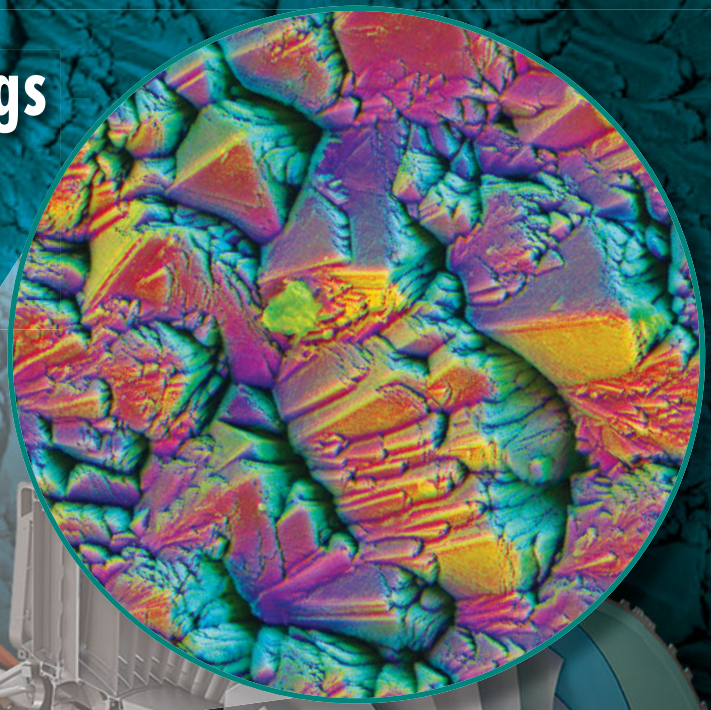

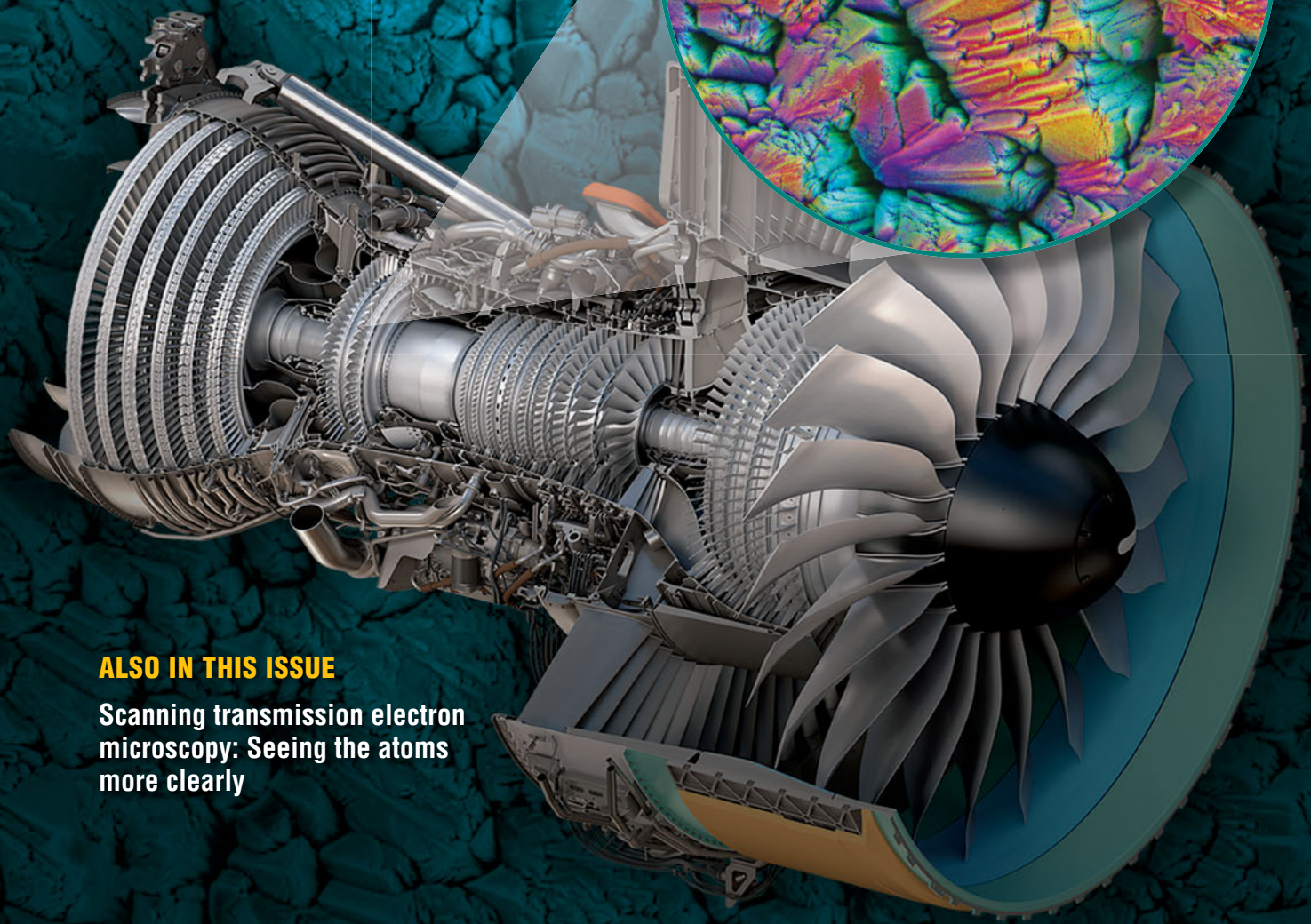

ALSO IN THIS ISSUE

Scanning transmission electron microscopy: Seeing the atoms more clearly

CAMBRIDGE
UNIVERSITY PRESS

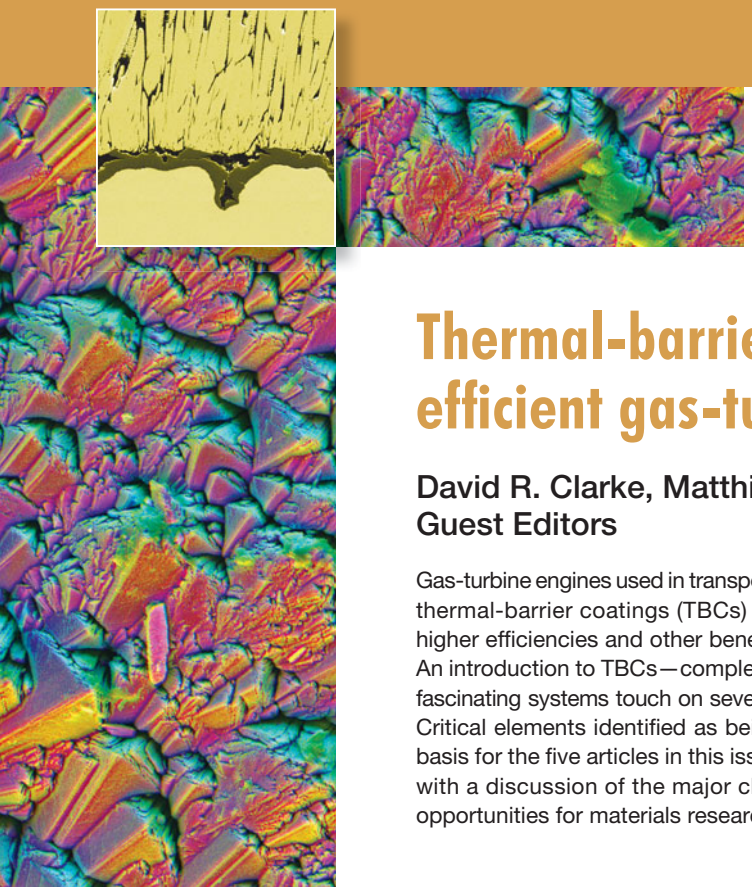

Thermal-barrier coatings for more efficient gas-turbine engines

David R. Clarke, Matthias Oechsner, and Nitin P. Padture, Guest Editors

Gas-turbine engines used in transportation, energy, and defense sectors rely on high-temperature thermal-barrier coatings (TBCs) for improved efficiencies and power. The promise of still higher efficiencies and other benefits is driving TBCs research and development worldwide. An introduction to TBCs—complex, multi-layer evolving systems—is presented, where these fascinating systems touch on several known phenomena in materials science and engineering. Critical elements identified as being important to the development of future TBCs form the basis for the five articles in this issue of *MRS Bulletin*. These articles are introduced, together with a discussion of the major challenges to improved coating development and the rich opportunities for materials research they provide.

Introduction

Thermal-barrier coatings (TBCs) are refractory-oxide ceramic coatings applied to the surfaces of metallic parts in the hottest part of gas-turbine engines (**Figures 1 and 2**), enabling modern engines to operate at significantly higher gas temperatures than their predecessors (see recent reviews[1–6]). Gas-turbine engines, used to propel aircraft and to generate electricity, are Carnot engines where their efficiency and core power are directly related to the gas temperature entering the turbine section.[7,8] Further increases in the energy efficiency of gas-turbine engines, both to increase the electricity output and, for jet engines, the thrust-to-weight ratio and durability, will rely on further improvements in TBCs. At the same time, as gas temperatures are increased in the pursuit of higher engine efficiency, there are new challenges to existing TBCs.

To place this in context, gas-turbine engines are a $42 billion industry worldwide (2010), with ~65% of the sales accounting for jet engines and the remainder land-based engines for electricity generation.[9] The latter, fueled by natural gas or liquid fuels, produce ~25% of all electricity in the United States and ~20% worldwide (2010).[10] With the anticipated worldwide growth of electricity demand and the recent discovery of vast shale gas resources, the number of gas-turbine engines in service will inevitably grow in the coming decades.[9] Similarly, airline traffic is expected to double in the next 20 years,[11] while at the same time, there is a need to reduce high-altitude NO_x pollution produced by jet engine exhausts.[12] Together, these developments will require continued innovation in gas turbine technology and high-temperature engine materials, including TBCs and associated technologies.

Many engineering design factors influence the overall efficiency of gas-turbine engines, but a major step in increasing engine temperature and engine efficiency was the introduction of TBCs. Typically made of ~7 wt% Y_2O_3-stabilized ZrO_2 (7YSZ) ceramics, TBCs provide thermal insulation to the metallic/superalloy engine parts. These parts include the combustor (Figures 1 and 2); stationary guide vanes, rotating blades (Figure 1), blade outer air-seals, and shrouds in the high-pressure section behind the combustor; and afterburners in the tail section of jet engines. As illustrated in **Figure 3**, the gas-temperature increase facilitated by the use of TBCs, in conjunction with innovative air-cooling approaches, has been much greater than that enabled by earlier materials development, including the development of single-crystal Ni-based superalloys.

Originally, TBCs were introduced to extend the useful life of stationary engine parts such as the combustor, but in the late 1980s, TBCs were first used on rotating blades.[13] However, TBCs were not "prime reliant"; in other words, the ceramic coating was not considered in the design of the temperature capability of the underlying metal parts. Today, TBCs are critical components in gas-turbine engines, and because the gas temperatures are typically higher than the melting point of

David R. Clarke, School of Engineering and Applied Sciences, Harvard University; clarke@seas.harvard.edu
Matthias Oechsner, Center for Structural Materials, Technische Universitaet Darmstadt, Germany; Oechsner@mpa-ifw.tu-darmstadt.de
Nitin P. Padture, School of Engineering, Brown University; nitin_padture@brown.edu
DOI: 10.1557/mrs.2012.232

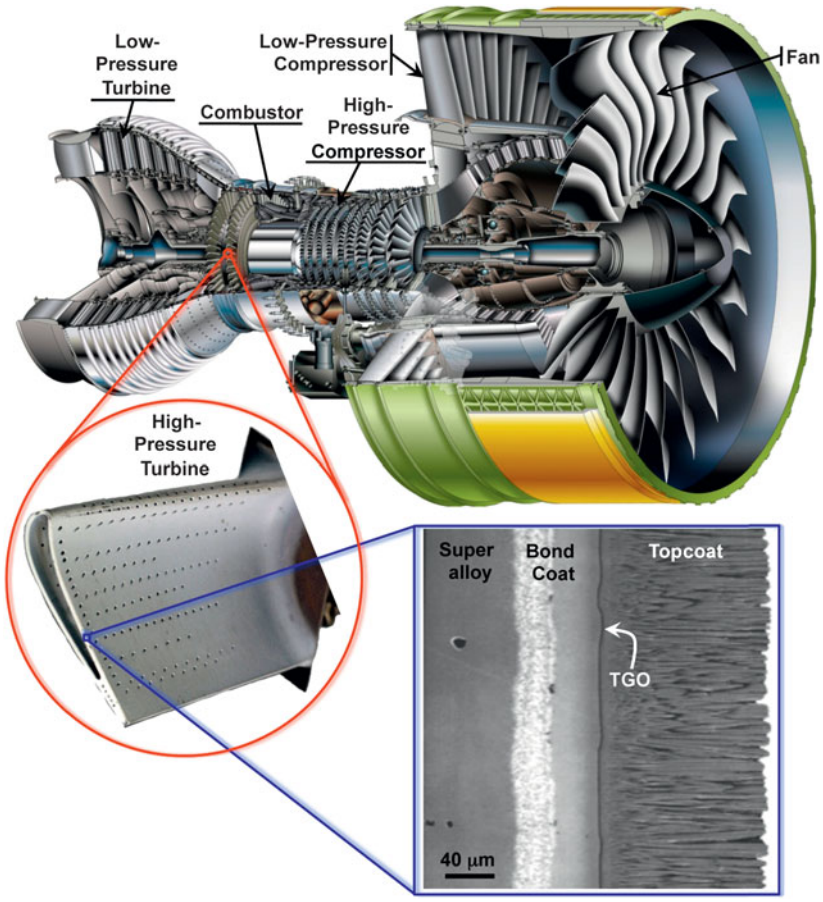

Figure 1. Cutaway view of Engine Alliance GP7200 aircraft engine, photograph of a turbine blade (~10 cm long) with thermal-barrier coating (TBC) from the high-pressure hot section of an engine, and a scanning electron microscope (SEM) image of a cross-section of an electron beam physical vapor deposited 7 wt% yttria-stabilized zirconia TBC. (Engine image courtesy of Engine Alliance, turbine blade photograph courtesy of YXLON, and the SEM micrograph is from Reference 44.) TGO, thermally grown oxide.

the underlying metal parts, any TBC failure can endanger the engine.[14] Furthermore, because of the coupled diffusional and mechanical interactions between the oxide ceramic coating and the underlying alloys at these high temperatures, it is essential to consider TBCs as a complex, interrelated, and evolving material system, consisting not only of the oxide ceramic coating (topcoat) itself but also the underlying superalloy engine part, and two other layers in between. These include a metallic bond-coat layer that is more oxidation resistant than the superalloy, and a thin, thermally grown oxide (TGO) layer that forms between the topcoat and the bond coat as result of bond-coat oxidation in-service. The bond-coat composition is designed to result in a TGO made of α-Al_2O_3—a mechanically robust, effective barrier to oxygen diffusion. **Figure 4** illustrates this multilayer structure in a typical TBC system.

During service, several kinetic processes occur in parallel. Interdiffusion between the bond coat and the underlying superalloy occurs, driven by chemical potential gradients; Al diffuses from the bond coat to form the TGO; and microstructural, chemical, and phase changes occur in all the materials, including in the ceramic topcoat itself, changing their very properties. Since all of these are thermally activated processes, the rates at which they occur are expected to increase exponentially with temperature, albeit with different activation energies. Furthermore, the processes generally lead to degradation and failure of the coating.

TBCs are also multifunctional: they must provide thermal insulation to protect the underlying superalloy engine parts, have strain compliance to minimize thermal-expansion-mismatch stresses with the superalloy parts on heating and cooling, and must also reflect much of the radiant heat from the hot gas, preventing it from reaching the metal alloy. Furthermore, TBCs must maintain thermal protection for prolonged service times and thermal cycles without failure. Typically, these times are 1000s of hours for jet engines being cycled numerous times between a maximum temperature of ~1300°C and room temperature (takeoff/landing and on-ground), and 10,000s of hours for power-generation engines with fewer thermal cycles (maintenance shut-downs). However, the latter are now being increasingly employed to stabilize the electric grid connected to renewable sources (wind, solar), and, thus, these engines experience more frequent cycles to compensate for the inherent intermittency of renewables. TBCs need to do this without separating from the engine parts while also withstanding extreme thermal gradients (~1°C μm^{-1}) and energy fluxes (~1 MW m^{-2}). Not only are these demands extremely exacting but also are often conflicting: TBCs must have both low thermal conductivity and low weight; they must remain intact while withstanding large stress variations, both due to heating and cooling as well as under thermal shock; they must be chemically compatible with the underlying metal and the TGO; and they must operate in an oxidizing environment at maximum pressures of ~10 atmospheres and maximum gas velocities exceeding Mach 1.

These demands and the desire to operate at higher temperatures reliably for longer times are driving new TBC innovations based on exploration of the underlying materials, processing sciences, and mechanistic understanding of degradation/failure and its mitigation. Several but not all of these key areas are highlighted in this issue of *MRS Bulletin*.

In this issue

Ceramic topcoat processing

Sampath et al. describe the oxide ceramic topcoat deposition processes and microstructures. Unlike more traditional thin films used in microelectronics and in materials-growth studies,

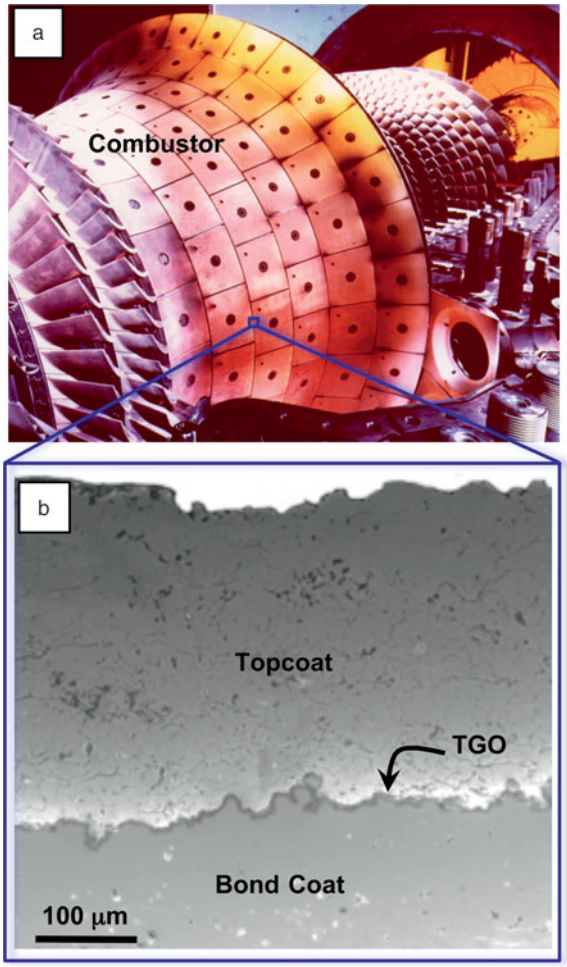

Figure 2. (a) Photograph of an annular combustor with thermal-barrier coating (TBC) and (b) cross-sectional scanning electron microscopy image showing an air plasma-sprayed 7 wt% yttria-stabilized zirconia TBC.[2] TGO, thermally grown oxide. Combustor image courtesy of Siemens Energy Inc.

these coatings are of intermediate thickness (100 μm to 1 mm), and they must be deposited at a high rate to incorporate porosity. Typical TBC porosity is ~15%, which is essential for high strain compliance and reduced thermal conductivity, yet the TBCs need to be mechanically robust to resist fracture, erosion, and foreign object damage (FOD). Furthermore, TBCs need to be deposited on complex-shaped parts with highly curved surfaces, and at the same time the TBCs must have reproducible thermal and mechanical properties. Currently, TBCs are deposited by air plasma-spraying (APS)[15] or by electron beam physical vapor deposition (EBPVD).[16] Typically, the low-cost APS method is used to deposit TBCs on stationary engine parts (combustor, shroud, vanes), whereas EBPVD TBCs are used on the most demanding hot-section parts in jet engines such as blades and vanes. Today, both stationary and rotating hot-section parts in electricity-generation engines, which tend to be much larger than those in jet engines, use APS TBCs. The microstructures of APS and EBPVD TBCs are vastly different (see Figures 1 and 2),

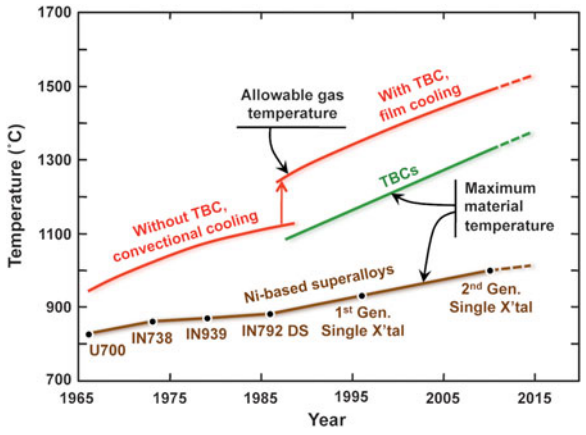

Figure 3. Progression of temperature capabilities of Ni-based superalloys and thermal-barrier coating (TBC) materials over the past 50 years. The red lines indicate progression of maximum allowable gas temperatures in engines, with the large increase gained from employing TBCs. Based on a diagram from the late Professor Tony Evans.

and each offer different advantages in terms of properties and performance. While processing science and technology of depositing 7YSZ TBCs is well established, the widespread introduction of improved TBCs of alternative compositions will ultimately depend on their reproducible and successful deposition commercially. Alternative TBC deposition methods with added advantages and versatilities are also being pursued.[17–20]

TBCs testing and evaluation

An equally big hurdle to developing improved TBCs is the sheer complexity and variety of failure modes and their dependence on engine operating conditions. Superficially, the failures are similar; the coating spalls off the engine part exposing the underlying metal to rapid oxidation or melting. However, a variety of mechanisms can be responsible for the observed failure.[1] In some instances, the TGO grows to exceed a critical thickness and spalls off, causing TBC failure.[21,22] In others, the initially flat bond coat and TGO undergo a complex morphological instability—"rumpling" (**Figure 5**)—causing local separations that grow in size with thermal cycling until linking up to form a spall.[23–25] In still others, cavitation occurs in the bond coat and grows under thermal cycling.[26] In each of these cases, the failure location depends on the actual thermal and mechanical loading conditions in the coating. Typically, at moderate heat fluxes but high temperatures at the bond coat, failure is dominated by processes related to TGO formation and bond-coat inelastic behavior, where fracture occurs in the bond-coat/topcoat interface region. With increasing topcoat surface temperature and thermal-gradient, thermal-expansion mismatch starts to play a more dominant role, and fracture location typically shifts to within the ceramic topcoat.

In some cases, spallation occurs as a result of impact from particles (FOD) carried along with the hot, combusted gas.[27] In other cases, thermal-shock spallation of the coating can occur

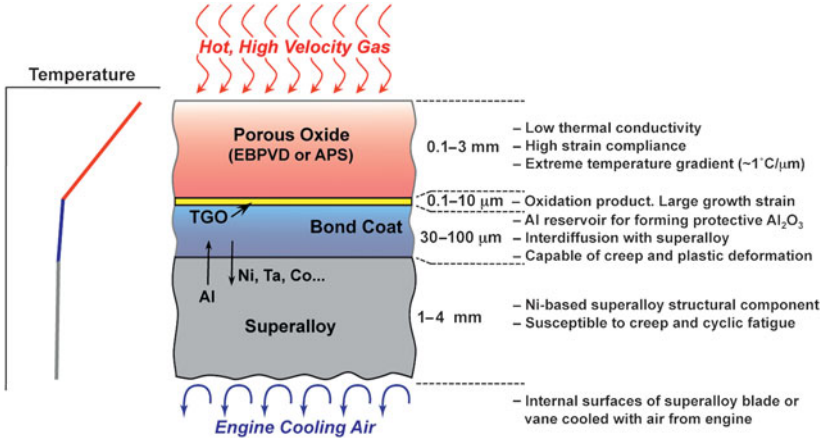

Figure 4. Schematic illustration of the multilayer, multifunctional nature of the thermal-barrier coating system (not to scale). The ceramic topcoat is deposited by electron beam physical vapor deposition (EBPVD) or air plasma-spraying (APS). Sandwiched between the topcoat and the metallic bond coat is the thermally grown oxide (TGO). Properties/functions and approximate thicknesses of the different layers are indicated.

during rapid cooling. In still other cases, fine sand and particulates ingested into the engine (including volcanic ash) can melt into a silicate glass at high temperatures (>1200°C) on the TBC surface and wick into the TBC, decreasing its strain compliance and causing spallation upon cooling.

Both the crack driving force and the fracture resistance offered by the material also depend on the mechanical and thermophysical properties of the TBC system. These can change significantly with time at temperature. Also, these properties can be influenced significantly by the coating microstructure, which in turn is influenced by the process parameters used during the coating deposition. Even small variations of these parameters can lead to significant changes in coating microstructure, and thus to a wide variation in mechanical and thermophysical properties, resulting in a large scatter in system reliability, durability, and predictability. Thus, deterministic approaches for predicting TBC life can be often misleading, requiring the use of probabilistic approaches for predicting TBC life. From a manufacturing, as well as materials selection perspective, clarifying mechanisms of failure and being able to predict life remains an essential and central task in optimizing the coating system.

This has motivated the development of TBC testing methods and non-destructive evaluation techniques, especially under realistic conditions pertinent to engine operation, which can include high pressures (up to 10 atm.), high temperatures (up to 1400°C), steep thermal gradients (temperature differences up to 300°C), high gas velocities, and the presence of detrimental environmental species (e.g., water vapor, sand, ash, salt). The article by Vaβen et al. describes some of the common TBC failure modes and innovations in TBC testing and evaluation.

Topcoat ceramics

The majority of TBCs in use today are ZrO_2-based having a composition containing ~7 wt% Y_2O_3 (7YSZ). Originally, this ceramic was selected empirically based on its low thermal conductivity, high melting point, resistance to sintering, a demonstrated manufacturing capability for depositing it with constant composition, and long life in the resulting TBCs.[13,28–30] Unlike the cubic ZrO_2 used in oxide fuel cells, oxygen sensors, and fake diamonds, which have higher Y_2O_3 content, 7YSZ is a metastable tetragonal phase (t').[4] 7YSZ has been shown to have unusually high fracture toughness due to ferroelastic toughening.[31,32] Unlike other transformation-toughened ZrO_2-based ceramics, so-called "ceramic steels,"[33] used in bearings, cutting tools, and knives, the toughness in 7YSZ does not arise from the martensitic transformation (an irreversible and diffusionless collective movement of atoms) from the tetragonal to monoclinic phase but rather from reversible ferroelastic domain switching from one tetragonal variant to another when stressed.[31,32] Also, unlike transformation toughening, ferroelastic toughening can operate at high temperatures, typical of those at engine temperatures. High fracture toughness in TBCs is important not only for resisting impact and erosion but also spallation.

Despite these intrinsic advantages, there is a worldwide search under way for oxides with superior, high-temperature properties that could replace 7YSZ. Much of this activity is presently directed to identifying oxides with lower thermal conductivity,[34] as discussed in the article by Pan et al. Although the underlying physics of thermal conductivity in solids was firmly established more than 30 years ago, the challenge is to translate the concepts to identify prospective low conductivity compounds in terms of crystal structure and bonding, especially when little or nothing is known about the phonon (lattice wave) properties of almost all poly-ionic oxides. The bulk of heat transport in these oxides occurs via phonons, and their scattering governs the oxide thermal resistance. Fortunately, at high temperatures, the majority of lattice phonons can be expected to be fully thermally activated, so classical descriptions of thermal conductivity can guide the search for low conductivity oxides. This search has, for instance, revealed that natural superlattice structures have exceptionally low thermal conductivity[35–37] as do oxides with a large number of ions per unit cell that also can exhibit extensive solid solution.[38] Another insight, gained from molecular dynamics simulations, is that in YSZ, phonons are highly delocalized and transport diffusively, akin to a phonon glass, despite the crystal perfection measured by x-ray diffraction.[39]

Bond-coat alloys and oxidation

In many respects, the most stringent constraints are imposed on the bond coat. Its primary function is to provide a reservoir from which Al can diffuse to form a protective α-Al_2O_3 TGO while maintaining cohesion with the TBC without reacting with it. Mechanics modeling[40] indicates that, ideally, the TGO

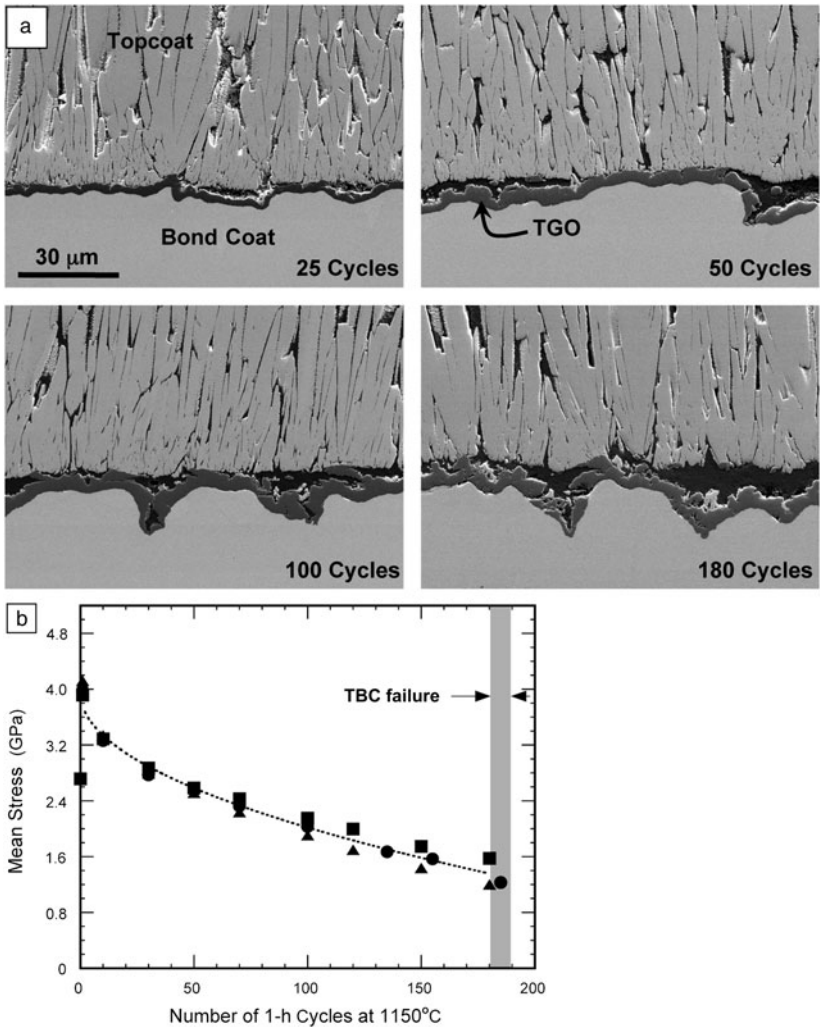

Figure 5. (a) Cross-sectional scanning electron microscopy images showing the progression of thermally grown oxide (TGO) thickening and the evolution of local interface separations in an electron beam physical vapor deposited 7 wt% yttria-stabilized zirconia thermal-barrier coating (TBC) on a Pt-modified nickel aluminide bond coat with number of 1-h thermal cycles (1150°C peak temperature). (b) The plot shows the mean stress in the TGO stress measured through the topcoat using the photoluminescence piezo-spectroscopy technique. The different symbols refer to measurements on different coatings from the same deposition run. (Based on information from Reference 25.)

should remain elastic to the highest temperatures and not creep to prevent "rumpling"[23,24] or cavitation on thermal cycling[26] that can, in turn, lead to the development of local separations at the TBC interface (Figure 5).[25] At the same time, it has to operate at the highest temperature possible to minimize the amount of air used to cool the vanes and blades, without reacting with the underlying superalloy and melting. This presently implies that the maximum bond-coat temperature cannot be allowed to exceed ~1150°C. Currently, there are two main bond-coat alloys in use, a Ni-rich nickel aluminide and a compositionally more complex MCrAlY (M=Ni, Co+Ni, or Fe) alloy. While these are very different alloys metallurgically, the challenges are similar, as described in the article by Pollock et al.: how to minimize deformation at intermediate and operating temperatures, how to minimize interdiffusion with the underlying superalloy to prevent the formation of brittle intermetallics, and how to deliver critical elements in addition to Al, such as Hf and Y, to the growing TGO to minimize its inelastic plastic deformation under thermal cycling.

Critical to understanding the performance of the TBC system is the formation, growth, and properties of the TGO that forms underneath the 7YSZ topcoat by oxidation of the bond-coat alloy (TBC microstructures are highly defective with porosity and cracks, and 7YSZ is an oxygen conductor, hence oxidation of the bond coat cannot be prevented). The bond-coat compositions are selected to form an α-Al_2O_3 TGO because it is the slowest growing oxide at high temperatures and forms an impervious, adherent layer with excellent mechanical integrity. This is important because TBC failure can occur when the TGO growth exceeds a critical thickness. The essential mechanics of this form of failure are similar to the origin of a critical thickness for the loss of coherence of epitaxial thin films, namely when the release of stored elastic strain energy in the growing film exceeds the fracture resistance.[41] There are two contributions to the stress in the TGO, one is associated with the growth strain as new oxide is created at the grain boundaries of the TGO, and the other is the mismatch stress with the superalloy generated by differences in thermal expansion on cooling. The growth strain consists of two components: one that leads to a simple thickening and the other that motivates lateral expansion of the TGO that, in turn, drives out-of-plane instabilities as well as other mechanical responses.[40] The origin of the lateral growth strain is poorly understood but is generally attributed to the counter-diffusion of inward diffusing O^{2-} and outward diffusing Al^{3+}, resulting in the plating out of new Al_2O_3 in the TGO grain boundaries.[42] There have been a limited number of measurements of the growth strain in the TGO absent the TBC itself using x-ray synchrotron sources[43] but not nearly enough to follow the evolution during oxidation or thermal cycling. More revealing have been non-contact measurements by photoluminescence piezo-spectroscopy of the strains measured through the topcoat.[44] In this technique, a laser beam is used to penetrate through the topcoat and excite the *R*-line luminescence from trace Cr^{3+} ions invariably present in the TGO. The local mean stress in the TGO is proportional to the frequency shift of the *R*-lines. This has enabled correlations to be mapped between luminescence shifts and the development of local damage as the bond coat and TGO rumple, as shown in **Figures** 5 and **6**.[23,25,45] There remain several important unresolved questions about the lateral

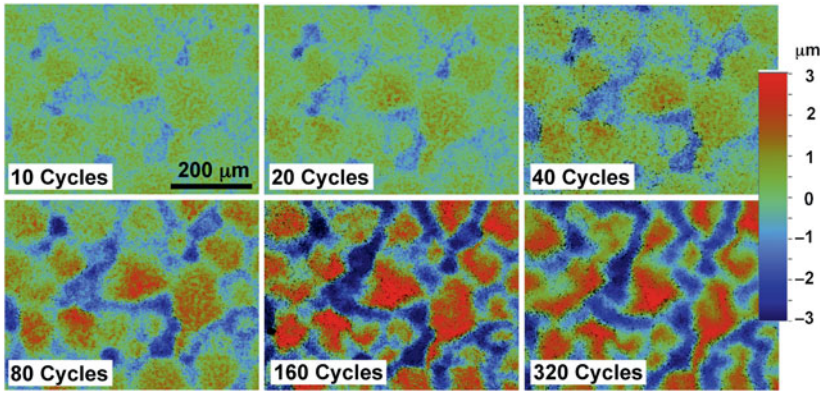

Figure 6. Topographic profilometer (optical) images (top view) of the identical area of an aluminized bond coat (without a ceramic topcoat) after polishing flat and then thermal cycled (1-h cycles) between room temperature and 1150°C for the cycles indicated. As is evident from the sequence of images, the magnitude of the rumpling surface instability increases with cycling, but the microstructural scale does not. The color scale at the right indicates the rumpling height variation. (Based on information from Reference 45.)

growth strain whose resolution could impact oxidation of other metallic alloys. These include how minor elements, at the ppm level and above, affect the growth and mechanical behavior of the TGO. Of particular interest are the elements Y, Zr, and Hf that segregate, on account of their large ionic radii, to the grain boundaries of the TGO. Among the key questions being raised are whether these elements alter the counter-diffusion along the TGO grain boundaries that creates the lateral growth strain and how they affect the high-temperature creep and plasticity of the TGO. It is known that rare-earth ions dramatically increase the creep resistance of alumina ceramics.[46]

Attack by molten deposits and its mitigation

Higher engine temperatures are also creating new materials issues in ceramic topcoats, namely degradation of 7YSZ TBCs due to molten silicate deposits,[47–52] formed by the ingestion of fine particulates from the environment (sand,[49] volcanic ash[53,54]) (see the Levi et al. article in this issue). Because of the major components in the silicate glass formed, this phenomenon is commonly referred to as CMAS (calcium-magnesium-alumino-silicate) attack. This primarily affects high-performance jet engines on account of their higher maximum temperatures and electricity-generation engines in some locations, but it will likely affect more engines as operation temperatures are increased in pursuit of greater engine efficiencies. In the case of land-based electricity-generation engines, it is not always practical to filter out the finest particles that can be carried along with the input air and from alternative fuels such as syngas.[55,56] It appears that wetting of TBCs by the molten CMAS glass, and dissolution/reprecipitation of YSZ grains in that glass, contribute to the CMAS attack of 7YSZ TBCs.[50,51] This manifests itself as continued penetration of the CMAS glass into the TBC and affects both APS and EBPVD TBCs alike. For example, **Figure 7** shows complete penetration of an EBPVD 7YSZ TBC by molten CMAS in a laboratory test.[57] Therefore, being able to mitigate CMAS attacks becomes an additional critical requirement for future TBCs.

While this area of TBC research is relatively new, important insights into CMAS attack and mitigation mechanisms have started to emerge. For instance, for a TBC ceramic to be highly effective against CMAS attack, wetting should be prevented, and/or it must readily interact with the CMAS to form a crystalline sealing layer arresting further penetration of the molten CMAS.[51,58–63] By corollary, TBCs made from ceramics that are inert or stable in contact with molten CMAS may not be effective in resisting CMAS wetting and attack. Thus, tailoring of TBC compositions and microstructures for resistance against molten silicate deposits is becoming an important area of TBC research. An example of APS TBC of designed composition (7YSZ containing Al_2O_3 and TiO_2) resisting attack by molten ash from the Eyjafjallajökull volcano in a laboratory test is shown in **Figure 8**a–b.[54]

Outlook

The sheer complexity of the interactions between the four principal layers and materials in the thermal-barrier coating (TBC) system—ceramic topcoat, thermally grown oxide, metallic bond coat, base superalloy—and their evolution with time at

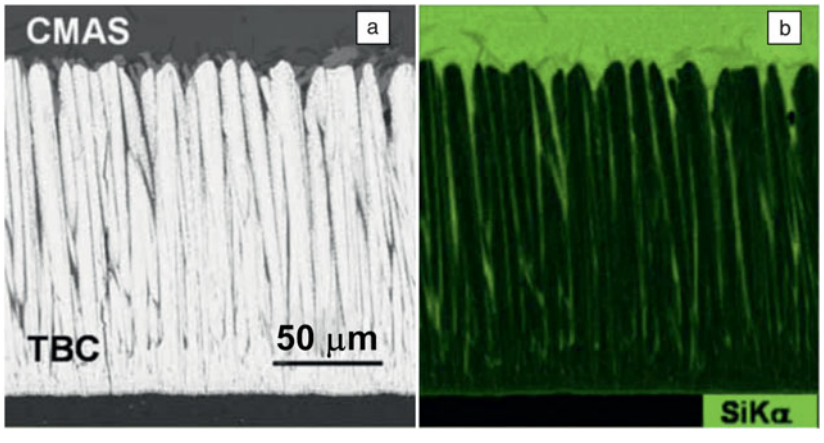

Figure 7. (a) Cross-sectional scanning electron microscopy micrograph of electron beam physical vapor deposited 7 wt% yttria-stabilized zirconia (7YSZ) thermal-barrier coating (TBC) fully penetrated by a model calcium-magnesium-aluminosilicate (CMAS) melt in a laboratory experiment. Crystalline phases with different compositions from the parent 7YSZ material (lighter gray) are noted (a) at the interface between the coating and the melt. (b) The corresponding Si elemental map showing the extensive CMAS penetration. (Based on information from Reference 57.)

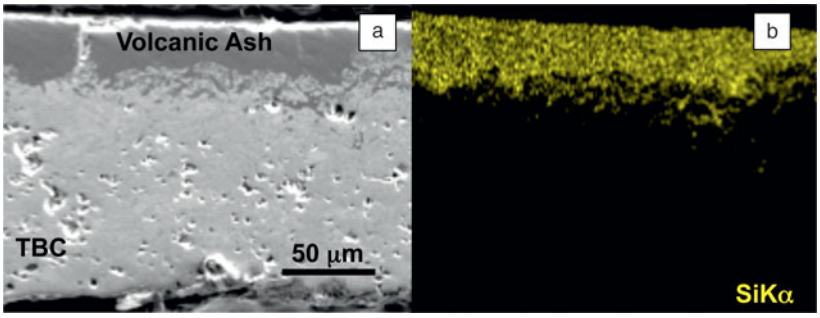

Figure 8. (a) Cross-sectional scanning electron microscopy micrograph of an air plasma-sprayed thermal-barrier coating of a new composition (7 wt% yttria-stabilized zirconia containing Al_2O_3 and TiO_2) showing resistance to penetration of molten ash from the Eyjafjallajökull volcano eruption in Iceland in laboratory experiments. (b) The corresponding Si elemental map illustrates the arrest of the molten ash penetration front. (Based on information from Reference 54.)

temperature make it essential that synergistic progress be made in all areas to enable TBCs to operate reliably at still higher temperatures in the future. Three major challenges stand out. The first is to increase the reproducibility of the coating deposition so that full temperature capabilities of existing TBCs can be utilized with greater confidence. Indeed, at present, engine designers only take into account about half of the possible temperature increase afforded by the thermal properties of current TBCs because of the lack of processing reproducibility. The second challenge is to have more comprehensive modeling of the evolution of the coating system and its failure, as well as a better description of the material properties, especially at high temperatures. This will require a concerted modeling effort spanning multiple length and temporal scales, supported by experimental validation that will greatly benefit the development and implementation of future TBCs. The third major challenge is tackling new issues that arise with higher temperatures. One such issue is radiative heat transport through the TBC. New approaches will be needed to reflect and/or scatter radiation and prevent it from reaching the metallic parts. Another important issue is calcium-magnesium-alumino-silicate (CMAS) attack and its mitigation. This will require new TBC compositions and microstructures that not only resist CMAS penetration but also meet a suite of other requirements at those higher temperatures.

While the use of TBCs has already resulted in dramatic improvements in the efficiency and the power output of gas-turbine engines, the challenges described in this and the companion articles present new materials research opportunities essential for turbine engine designers to take full advantage of recent advances in materials, processing, and reliability. This will become even more crucial in bridging the growing energy and transportation demands of society until large scale energy generation from renewable sources (solar, wind) becomes economically more viable. Indeed, because gas turbines already play a major role in electricity generation and aircraft propulsion, even minor improvements in engine efficiency will have an immediate and significant positive impact on the overall energy portfolio of the world.

Acknowledgments

D.R.C. is grateful for the long-term support of his research in TBCs from the Office of Naval Research. M.O. acknowledges the German Research Society (DFG) and the Forschungsvereinigung Verbrennungskraftmaschinen e.V. (FVV-6011081). N.P.P. is grateful for continued support from the Office of Naval Research and the Department of Energy for his research in the area of TBCs. We acknowledge the contributions of all the authors in this theme issue and discussions with several others too numerous to list.

References

1. A.G. Evans, D.R. Mumm, J.W. Hutchinson, G.H. Meier, F.S. Pettit, *Prog. Mater. Sci.* **46**, 505 (2001).
2. N.P. Padture, M. Gell, E.H. Jordan, *Science* **296**, 280 (2002).
3. C.G. Levi, *Curr. Opin. Solid State Mater. Sci.* **8**, 77 (2002).
4. D.R. Clarke, C.G. Levi, *Annu. Rev. Mater. Sci.* **33**, 383 (2003).
5. A.G. Evans, D.R. Clarke, C.G. Levi, *J. Eur. Ceram. Soc.* **28**, 1405 (2008).
6. R. Vaßen, M. Ophelia-Jarligo, T. Steinke, D. Emil-Mack, D. Stöver, *Surf. Coat. Technol.* **205**, 938 (2010).
7. W.W. Bathie, *Fundamentals of Gas Turbines—Second Edition* (Wiley, New York, 1996).
8. J.H. Perepezko, *Science* **326**, 1068 (2009).
9. L.S. Langston, *Mech. Eng.* **133**, 30 (2011).
10. US Energy Information Administration, *Annual Energy Review*; www.eia.gov/totalenergy/data/annual/index.cfm (accessed June 2012).
11. Federal Aviation Administration, *FAA Forecast Predicts Air Travel to Double in Two Decades*; www.faa.gov/news/press_releases/news_story.cfm?newsId=12439 (accessed June 2012).
12. International Civl Aviation Organization, ICAO Environment Report, www.icao.int/environmental-protection/Pages/EnvReport10.aspx (accessed June 2010).
13. U. Schulz, K. Fritscher, C. Leyens, M. Peters, W.A. Kaysser, *JOM* **49** (1997).
14. Anon., *The Economist* **290**, 60 (2009).
15. H. Herman, S. Sampath, R. McCune, *MRS Bull.* **25**, 17 (2000).
16. U. Schulz, C. Leyens, K. Fritscher, M. Peters, B. Saruhan-Brings, O. Lavigne, J.M. Dorvaux, M. Poulain, R. Mevrel, M.L. Caliez, *Aerosp. Sci. Technol.* **7**, 73 (2003).
17. N.P. Padture, K.W. Schlichting, T. Bhatia, A. Ozturk, B. Cetegen, E.H. Jordan, M. Gell, S. Jiang, T.D. Xiao, P.R. Strutt, E. Garcia, P. Miranzo, M.I. Osendi, *Acta Mater.* **49**, 2251 (2001).
18. P. Fauchais, G. Montavon, *J. Therm. Spray Technol.* **19**, 226 (2010).
19. A. Hospach, G. Mauer, R. Vaßen, D. Stöver, *J. Therm. Spray Technol.* **20**, 116 (2011).
20. K. von Niessen, M. Gindrat, *J. Therm. Spray Technol.* **20**, 736 (2011).
21. K. Chan, S. Cheruvu, R. Vishwanathan, *ASME Turbo Expo 2003, Atlanta* (2003), p. 591.
22. K.W. Schlichting, N.P. Padture, E.H. Jordan, M. Gell, *Mater. Sci. Eng., A* **342**, 120 (2003).
23. V.K. Tolpygo, D.R. Clarke, *Acta Mater.* **52**, 5115 (2004).
24. M. Wen, E.H. Jordan, M. Gell, *Surf. Coat. Technol.* **201**, 3289 (2006).
25. B. Heeg, V.K. Tolpygo, D.R. Clarke, *J. Am. Ceram. Soc.* **94**, S112 (2011).
26. V.K. Tolpygo, *Surf. Coat. Technol.* **2002**, 617 (2007).
27. X. Chen, R. Wang, N. Yao, A.G. Evans, K.J.J.W. Hutchinson, R.W. Bruce, *Mater. Sci. Eng. A* **352**, 221 (2003).
28. S. Stecura, *Am. Ceram. Soc. Bull.* **56**, 1082 (1977).
29. S. Stecura, H. Curt, US Patent No. 4,005,705 (1977).
30. R.L. Jones, in *Metallurgical and Ceramic Coatings*, K.H. Stern, Ed. (Chapman & Hall, London, UK, 1996).
31. A.V. Virkar, *Key Eng. Mater.* **153–154**, 183 (1998).
32. C. Mercer, J.R. Williams, D.R. Clarke, A.G. Evans, *Proc. R. Soc. London, Ser. A* **463**, 1393 (2007).
33. D.J. Green, R.H.J. Hannink, M.V. Swain, *Transformation Toughening of Ceramics* (CRC Press, Boca Raton, FL, 1989).

34. M.R. Winter, D.R. Clarke, *J. Am. Ceram. Soc.* **90**, 533 (2007).
35. Y. Shen, D.R. Clarke, P.A. Fuierer, *Appl. Phys. Lett.* **93**, 102907 (2008).
36. A. Chernatynskiy, R.W. Grimes, M.A. Zurbuchen, D.R. Clarke, *Appl. Phys. Lett.* **95**, 161906 (2009).
37. T.D. Sparks, P.A. Fuierer, D.R. Clarke, *J. Am. Ceram. Soc.* **93**, 1136 (2010).
38. Z. Qu, T.D. Sparks, W. Pan, D.R. Clarke, *Acta Mater.* **59**, 3841 (2011).
39. P.K. Schelling, S.R. Phillpot, *J. Am. Ceram. Soc.* **84**, 2997 (2001).
40. D.S. Balint, J.W. Hutchinson, *J. Mech. Phys. Solids* **53**, 949 (2005).
41. L.B. Freund, S. Suresh, *Thin Film Materials: Stess, Defect Formation and Surface Evolution* (Cambridge University Press, Cambridge, UK, 2003).
42. F.N. Rhines, J.S. Wolf, *Metall. Mater. Trans. A* **1**, 1701 (1970).
43. P.Y. Hou, A.P. Paulikas, B.W. Beal, *JOM* **61**, 51 (2009).
44. R.J. Christensen, D.M. Lipkin, D.R. Clarke, K. Murphy, *Appl. Phys. Lett.* **69**, 3754 (1996).
45. S. Dryepondt, J. Porter, D.R. Clarke, *Acta Mater.* **57**, 1717 (2009).
46. J. Cho, C.M. Wang, H.M. Chan, J.M. Rickman, M.P. Harmer, *Acta Mater.* **47**, 4197 (1999).
47. J.L. Smialek, F.A. Archer, R.G. Garlick, *JOM* **46**, 39 (1994).
48. F.H. Stott, D.J. DeWet, R. Taylor, *MRS Bull.* **19**, 46 (1994).
49. M.P. Borom, C.A. Johnson, L.A. Peluso, *Surf. Coat. Technol.* **86–87**, 116 (1996).
50. S. Kramer, J. Yang, C.G. Levi, C.A. Johnson, *J. Am. Ceram. Soc.* **89**, 3167 (2006).
51. A. Aygun, A.L. Vasiliev, N.P. Padture, X. Ma, *Acta Mater.* **55**, 6734 (2007).
52. A.G. Evans, J.W. Hutchinson, *Surf. Coat. Technol.* **201**, 7905 (2007).
53. J. Kim, M.G. Dunn, A.J. Baran, D.P. Wade, E.L. Tremba, *ASME J. Eng. Gas Turbines Power* **115**, 641 (1993).
54. J.M. Drexler, A.D. Gledhill, K. Shinoda, A.L. Vasiliev, K.M. Reddy, S. Sampath, N.P. Padture, *Adv. Mater.* **23**, 2419 (2011).
55. J.P. Bons, J. Crosby, J.E. Wammack, B.I. Bentley, T.H. Fletcher, *ASME J. Eng. Gas Turbines Power* **129**, 135 (2007).
56. A.D. Gledhill, K.M. Reddy, J.M. Drexler, K. Shinoda, S. Sampath, N.P. Padture, *Mater. Sci. Eng. A* **58**, 7214 (2011).
57. M.-P. Bacos, J.-M. Dorvaux, S. Landais, O. Lavigne, R. Mevrel, M. Poulain, C. Rio, M.-H. Vidal-Setif, in *Aerospace Lab: The ONERA Journal*. ONERA, Chatillon, France, **3** (2011).
58. M. Freling, M.J. Maloney, D.A. Litton, K.W. Schlichting, J.G. Smeggil, D.B. Snow, US Patent No. 7,455,913 (2008).
59. S. Kramer, S. Faulhaber, M. Chambers, D.R. Clarke, C.G. Levi, J.W. Hutchinson, A.G. Evans, *Mater. Sci. Eng. A* **490**, 26 (2008).
60. D.A. Litton, K.W. Schlichting, M. Freling, J.G. Smeggil, D.B. Snow, M.J. Maloney, US Patent No. 7,662,489 (2010).
61. J.M. Drexler, K. Shinoda, A.L. Ortiz, D. Li, A.L. Vasiliev, A.D. Gledhill, S. Sampath, N.P. Padture, *Acta Mater.* **58**, 6835 (2010).
62. J.M. Drexler, C.-H. Chen, A.D. Gledhill, K. Shinoda, S. Sampath, N.P. Padture, *Surf. Coat. Technol.* **206**, 3911 (2012).
63. J.M. Drexler, A.L. Ortiz, N.P. Padture, *Acta Mater.* **60**, 5437 (2012). □

David R. Clarke
Guest Editor for this issue of *MRS Bulletin*

School of Engineering and Applied Sciences, Harvard University, 29 Oxford St., Cambridge, MA 02138, USA; tel. 617-495-4140; and email clarke@seas.harvard.edu.

Clarke is a Gordon McKay Professor of Materials and Applied Physics in the Harvard School of Engineering and Applied Sciences. He holds a PhD degree in physics from the University of Cambridge, a BSc degree in applied sciences from Sussex University, and was awarded a ScD degree from the University of Cambridge. A member of the National Academy of Engineering, he shared the 2008 Japanese NIMS Award for Recent Breakthroughs in Materials Science for Energy and Environment and is a Distinguished Life Member of the American Ceramic Society. Clarke has published more than 450 papers in areas of materials ranging from thermal-barrier coatings to dielectric elastomers to fundamentals of oxidation to microelectronics reliability and the electrical and optical properties of ZnO and GaN.

Matthias Oechsner
Guest Editor for this issue of *MRS Bulletin*

Center for Structural Materials (MPA/IfW), Technische Universitaet Darmstadt, Grafenstrasse 2, 64289 Darmstadt, Germany; tel. 49-6151-160-2251; and email Oechsner@mpa-ifw.tu-darmstadt.de.

Oechsner is a professor of materials technology in mechanical engineering and director of the State Materials Testing Laboratory at the Technical Universitaet in Darmstadt, Germany. He holds a doctoral degree in mechanical engineering from Universitaet Karlsruhe, Germany. Prior to joining the university as a professor in 2010, he held positions with Siemens Energy in gas-turbine engineering and manufacturing in Germany, the United States, and China. His research focus includes the structure—property relation, the mechanical behavior, and in particular the reliability analysis—of structural materials, including high-temperature applications and coatings.

Nitin P. Padture
Guest Editor for this issue of *MRS Bulletin*

School of Engineering, Brown University, 184 Hope St., Box D, Providence, RI 02912, USA; tel. 401-863-2859; and email nitin_padture@brown.edu.

Padture is a professor of Engineering and director of the Center for Advanced Materials Research at Brown University. He holds a PhD degree (1991) from Lehigh University, a MS degree (1987) from Alfred University, and a BTech degree (1985) from IIT-Bombay. Before joining Brown, he was professor and founding director of the NSF Materials Research Science and Engineering Center at The Ohio State University. His research interests include structural ceramics/coatings/composites and functional nanomaterials. Padture has published more than 125 journal papers, which have been cited over 5,000 times. He has co-invented four patents and delivered about 150 invited talks. A fellow of the American Ceramic Society, he also has received the society's Snow, Coble, and Fulrath awards. Padture is recipient of the Office of Naval Research Young Investigator Award, is an AAAS fellow, and is principal editor of the MRS *Journal of Materials Research*.

Aleksandr Chernatynskiy
Department of Materials Science and Engineering, University of Florida, Gainesville, FL 32611, USA; tel. 352-392-6609; and email avtche01@gmail.com.

Chernatynskiy is a postdoctoral research associate at the University of Florida. He received his BS degree in theoretical physics from Perm State University, Russia, in 1999, and his PhD degree in physical chemistry from the University of Louisville in 2005. His research focuses on the simulation of material properties based on atomistic techniques, including first-principles methods. Particular applications of interest are phonons thermal transport in technologically important systems such as nuclear fuels and thermal-barrier coatings.

Kevin J. Hemker
Department of Mechanical Engineering, Whiting School of Engineering, The Johns Hopkins University; tel. 410-516-4489; and email hemker@jhu.edu.

Hemker is the Alonzo G. Decker Chair of Mechanical Engineering at Johns Hopkins University. He and his students seek to identify the underlying atomic-scale processes that govern the mechanical response of advanced materials. Their research involves the mechanical stability of nanocrystalline thin films, development and characterization of MEMS materials, optimization and synthesis of materials with controlled microscale architectures, ceramics in extreme environments, high-temperature alloys, and thermal protection systems.

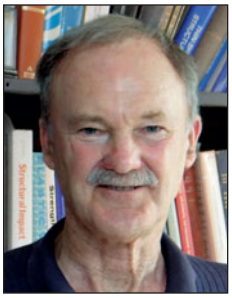

John W. Hutchinson
School of Engineering and Applied Sciences, Harvard University; tel. 617-495-2848; and email Hutchinson@husm.harvard.edu.

Hutchinson is the Abbott and James Lawrence Professor in the School of Engineering and Applied Sciences at Harvard University. His research focuses on problems in solid mechanics concerned with engineering materials and structures, including the mechanics of films and multilayers and the development of a mechanics framework for assessing the durability of thermal-barrier coatings for gas turbines. He is a member of the National Academies of Engineering and Sciences and of the American Academy of Arts and Sciences.

Maria Ophelia Jarligo
Institute of Energy and Climate Research (IEK-1), Forschungszentrum Jülich GmbH, Jülich, 52428, Germany; tel. 49-2461-612877; and email m.o.jarligo@fz-juelich.de.

Jarligo is a postdoctoral researcher in the Materials Synthesis and Processing Department of the Institute of Energy and Climate Research at the research center in Jülich (Germany). She received her DEng degree in materials processing at Tohoku University (Japan). While her specialties range from design, synthesis, processing, and characterization of advanced materials for thermal-barrier coating applications, Jarligo's current work also involves design and fabrication of gas separation membranes.

DOI: 10.1557/mrs.2012.240

Curtis A. Johnson
GE Global Research and Center for Thermal Spray Research, Stony Brook University, New York; email johnsonca@nycap.rr.com.

Johnson retired in 2008 from his position of principal scientist in Ceramics and Metallurgy Technologies at General Electric (GE) Research, but continues to consult actively for GE and elsewhere. He earned BS and PhD degrees in metallurgy from The Pennsylvania State University. In 1973, he joined GE's Corporate Research and Development Center (now GE Research) in Niskayuna, NY. In 2010, Johnson was appointed adjunct professor in the Department of Materials Science and Engineering at Stony Brook University. He is a Fellow of the American Ceramic Society.

Yutaka Kagawa
Research Center for Advanced Science and Technology, The University of Tokyo, 4–6-1 Komaba, Meguro-ku, Tokyo 153–8904, Japan; tel. 81-3-5452-5-86; and email kagawa@rcast.u-tokyo.ac.jp.

Kagawa is currently a professor at the University of Tokyo and a National Institute for Materials Science research fellow. He received his DEng degree from Waseda University, Tokyo, Japan. His current research interests include design and performance of thermal-barrier coatings, environmental barrier coatings, advanced fiber-reinforced ceramic composites, and fracture of solid materials. Emphasis is placed on understanding of mechanical behavior through experimental and theoretical approaches. Kagawa also is a Fellow of the American Ceramic Society.

Seiji Kuroda
National Institute for Materials Science, 1–2-1 Sengen, Tsukuba-city Ibaraki 305–0047, Japan; tel. 81-29-859-2444; and email Kuroda.Seiji@nims.go.jp.

Kuroda is currently the director of the High Temperature Materials Unit at the National Institute for Materials Science (NIMS) and a visiting professor at Chiba Institute of Technology and Warsaw University of Technology. After receiving his doctoral degree in instrumentation engineering at Keio University, Yokohama, Japan, he has spent most of his career at NIMS. Kuroda's major research interests lie in surface modification of materials, especially by using thermal-spray processes. He is a Fellow of ASM International and an associate editor of the *Journal of Thermal Spray Technology*.

Carlos G. Levi
Materials Department, University of California, Santa Barbara; tel. 805-893-2381; and email levic@engineering.ucsb.edu.

Levi is a professor of materials and mechanical engineering at the University of California, Santa Barbara. He holds a PhD degree from the University of Illinois at Urbana-Champaign (1981). His research focuses on the fundamental understanding of microstructure evolution in ceramics and metals and its application to the conceptual design of improved structural and functional materials. The current emphasis of his research is on high temperature coatings for advanced energy systems, including the effects of CMAS on TBCs and EBCs. Levi is a Fellow of the American Ceramic Society.

Don M. Lipkin
GE Global Research, Niskayuna, NY; email lipkin@ge.com.

Lipkin is a senior materials scientist at GE Global Research, where he has worked since 1996. He received his PhD degree in materials science from the University of California, Santa Barbara, and a BS degree in materials science from Northwestern University. His current research is focused on developing advanced alloys, coatings, and coating processes for high-temperature and structural applications. These include oxidation-resistant, thermal-barrier, and environmental-barrier coatings for industrial and aero turbine applications, as well as refractory alloys and coatings for medical imaging and power generation applications.

Wei Pan
State Key Lab of New Ceramics and Fine Processing, Tsinghua University, Beijing 100084, China; tel. 86-10-62772858; and email panw@mail.tsinghua.edu.cn.

Pan is a professor and director of the State Key Lab of New Ceramics and Fine Processing at Tsinghua University, China. He received his BS degree (1982) from the University of Science and Technology Beijing, China, and his MS (1987) and PhD degrees (1990) from Nagoya University in Japan. His research interests include low thermal conductivity ceramics for gas-turbines, solid-electrolytes, and nanomaterials. Pan is a member of the standing-committee of the Chinese Ceramic Society and member of the editorial board of several international journals. He is also a Fellow of the School of Engineering at the University of Tokyo.

Simon R. Phillpot
Department of Materials Science and Engineering, University of Florida, Gainesville, FL 32611, USA; tel. 35-846-3782; and email sphil@mse.ufl.edu.

Phillpot is a professor of materials science and engineering at the University of Florida. He received his BA degree from Oxford University in 1980 and PhD degree from the University of Florida in 1985, both in physics. He spent 16 years at Argonne National Laboratory in Chicago prior to joining the University of Florida in 2003. His research focuses on using atomistic and electronic-structure simulation methods to address issues in phonon-mediated heat transfer, ferroelectric and dielectric behavior, defect properties in oxides, mechanical behavior of metals, and tribology. He also works on developing advanced potentials for multifunctional systems. Phillpot is a Fellow of the American Physical Society, the American Association for the Advancement of Science, the Institute of Physics (UK), and the Institute of Materials, Minerals and Mining (UK).

Tresa Pollock
Materials Department, University of California, Santa Barbara; tel. 805-893-3810; and email Pollock@engineering.ucsb.edu.

Pollock is the Alcoa Professor of Materials at the University of California, Santa Barbara. She graduated with a BS degree from Purdue University and a PhD degree from the Massachusetts Institute of Technology in 1989. Her current research focuses on the processing and properties of structural materials and coatings and on the use of ultrafast lasers for microfabrication and materials diagnostics. Pollock is a member of the United States National Academy of Engineering, a Fellow of TMS and ASM International, and was the 2005–2006 president of TMS.

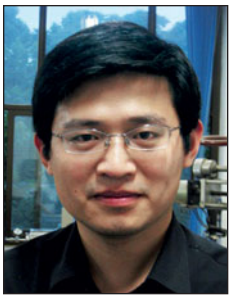

Zhixue Qu
College of Materials Science and Engineering, Beijing University of Technology, Beijing 100124, China; tel. 86-10-67392755; and email quzhixue@bjut.edu.cn.

Qu is an assistant professor in the College of Materials Science and Engineering at Beijing University of Technology in China. He received his PhD degree in materials science and engineering from Tsinghua University (2009). His research interests include the defect chemistry and thermophysical properties of materials, as well as the synthesis and characterization of magnetic materials for high-frequency applications. Qu has authored or co-authored more than 20 publications in these fields.

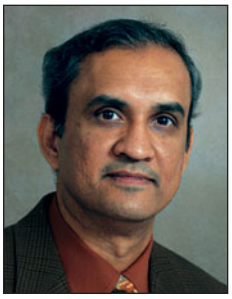

Sanjay Sampath
Center for Thermal Spray Research, Department of Materials Science & Engineering, Stony Brook University, NY 11794, USA; tel. 631-632-9512; and email sanjay.sampath@stonybrook.edu.

Sampath is the director of the Center for Thermal Spray Research at Stony Brook University and a professor of materials science and engineering. He received his PhD degree from Stony Brook in 1989, after which he spent four years in industry before returning to Stony Brook to start his academic career. His research interests lie in thermal-spray processing, multifunctional coatings, and direct write technologies. Sampath is a Fellow of ASM International and the American Ceramic Society. He has received numerous best paper awards from the Thermal Spray Society, was a recipient of the R&D 100 Award, and recently elevated to the rank of distinguished professor of the State University of New York system. He has approximately 150 articles and 15 patents to his credit.

Uwe Schulz
German Aerospace Center (DLR), Institute of Materials Research, 51170 Cologne, Germany; tel. 49-2203-601-2543; and email Uwe.Schulz@dlr.de.

Schulz is head of the High Temperature and Functional Coatings department at the German Aerospace Center's (DLR) Institute of Materials Research in Cologne, Germany. He studied materials science at the Technical University Mining Academy Freiberg, where he received his PhD degree in 1995. In 1991, he joined DLR to perform research on the development, manufacture, characterization, and testing of EBPVD thermal-barrier coating systems for turbine applications. Schulz is in charge of various in-house, national, and European projects, funded by industry and government. His major research focus is on thermal-barrier coatings and protective coatings for aerospace applications deposited by PVD methods. He holds 6 patents and is the author of 50 papers and co-author of more than 70 additional papers.

Ramesh Subramanian
Siemens Energy Inc., 4400 Alafaya Trail MC303, Orlando, FL 32826, USA; tel. 407-736-3310; and email Ramesh.Subramanian@siemens.com.

Subramanian is a principal technical expert and Core Competency Owner for Coatings Technology and Development, within Gas Turbine Engineering, at Siemens Energy. He received his PhD degree from Cornell University in materials science and engineering. He is responsible for the strategic direction and guiding coatings selection for gas-turbine components across different product lines. He has 49 patents and has authored 33 papers. Subramanian was also awarded as the Siemens Inventor of the Year (2001) and Siemens Top Innovator (2007).

Robert Vaßen
Institute of Energy and Climate Research (IEK-1), Forschungszentrum Jülich GmbH, 52425 Jülich, Germany; tel. 49 2461 616108; and email r.vassen@fz-juelich.de.

Vaßen is a section head at the IEK-1 within the Forschungszentrum Jülich GmbH, where he is responsible for the development of materials for advanced power plants. He studied physics and received his PhD degree from the RWTH in Aachen. Vaßen has been with the Forschungszentrum Jülich GmbH since 1990. His main research topics are materials developments for gas turbines, fusion reactors, membranes, and solid oxide fuel cells. He has authored and co-authored more than 250 papers, has given an H-index of 26, and has received 15 patents. In 2007, he received a professorship at the Ruhr University in Bochum. He has also held a guest professorship with University West, Sweden, since 2009.

Marie-Hélène Vidal-Sétif
Department of Metallic Materials and Structures, Onera, the French Aerospace Lab, 29 Ave. de la Division Leclerc, 92322 Châtillon, France; tel. 33-1-46-73-44-79; and email marie-helene.vidal-setif@onera.fr.

Vidal-Sétif has been working as a senior scientist on thermal-barrier systems for gas-turbine engines at Onera, the French Aerospace Lab, for the past seven years. She graduated as a chemist engineer from the Ecole Supérieure de Physique et Chimie Industrielles in Paris and obtained a PhD degree in physical chemistry from the University of Paris-Sud XI. She joined Onera in 1987, where she was successively involved in the development of metal-matrix composites (MMC), corrosion behavior of MMC, and aluminum alloys.

Chunlei Wan
Graduate School of Engineering, Nagoya University, Nagoya 464–8603, Japan; tel. 81-52-789-3330; and email chunlei.wan@gmail.com.

Wan is an assistant professor in the Graduate School of Engineering at Nagoya University in Japan. He received his PhD degree from Tsinghua University, China, in 2008. His research interests cover both phonon and electron-transport phenomena in solid-state materials. He has extensively worked on novel thermal-barrier coating materials and thermoelectric materials with low thermal conductivity. Wan has co-authored more than 20 peer-reviewed publications and two book chapters.

Dongming Zhu
Durability and Protective Coatings Branch, Structures and Materials Division, NASA Glenn Research Center, Cleveland, OH 44135, USA; tel. 216-433-5422; and email dongming.zhu@nasa.gov.

Zhu is a senior materials engineer at the NASA Glenn Research Center. He received his PhD degree from the University of Minnesota in 1996. Since joining NASA in 1996, he has developed simulated high-heat-flux and environment high pressure testing capabilities for the laboratory. His research interests include the development of thermal- and environmental-barrier coatings for turbine engine applications. Zhu has received many awards, including the NASA Exceptional Technology Achievement Medal (2009) and the R&D 100 Award (2007). He is a Fellow of the American Ceramic Society, has authored 100 archival publications, and been awarded seven patents.

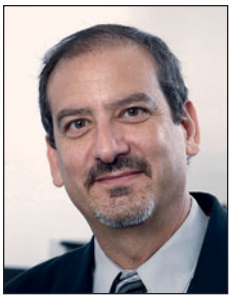

Paul Zombo
Engine and Component Diagnostics, Siemens Energy Inc., Orlando, FL 32826, USA; tel. 407-736-5138; and email Paul.Zombo@siemens.com.

Zombo has been working in the fields of metallurgy, failure analysis, and NDE for 26 years since earning a degree in metallurgical engineering. His fields of involvement include welding, casting, forging, coating, machining, failure analysis, and composites used in power generation, aerospace, and heavy industry. Zombo has 36 patents and 29 publications in the fields of NDE, *in situ* inspection, welding, and metallurgy. He was recently awarded "Siemens Inventor of the Year 2009" for outstanding innovation.

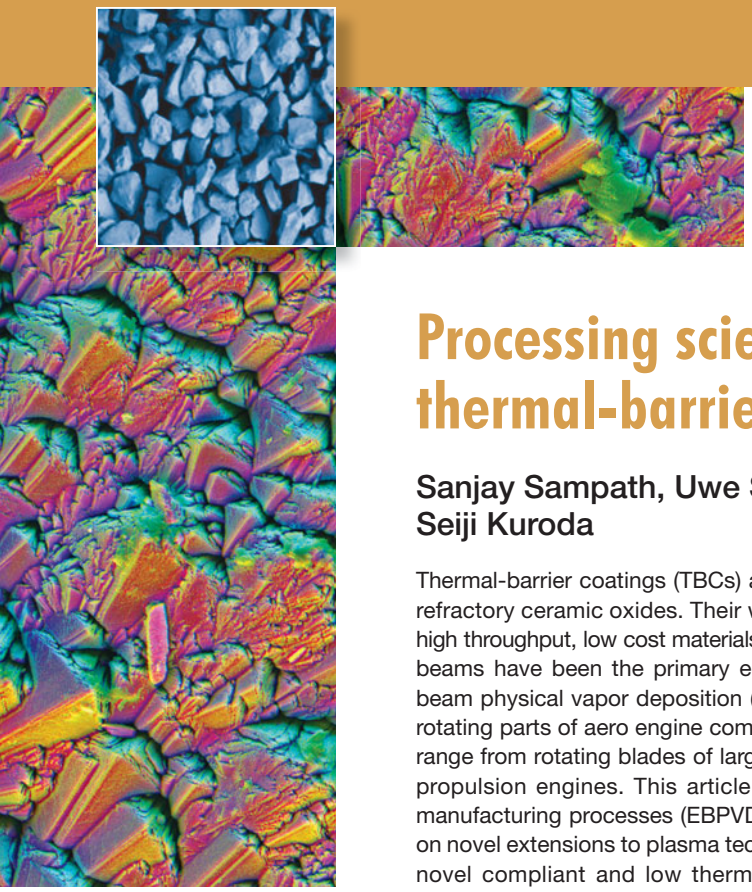

Processing science of advanced thermal-barrier systems

Sanjay Sampath, Uwe Schulz, Maria Ophelia Jarligo, and Seiji Kuroda

Thermal-barrier coatings (TBCs) are complex, defected, thick films made of zirconia-based refractory ceramic oxides. Their widespread applicability has necessitated development of high throughput, low cost materials manufacturing technologies. Thermal plasmas and electron beams have been the primary energy sources for processing of such systems. Electron-beam physical vapor deposition (EBPVD) is a sophisticated TBC fabrication technology for rotating parts of aero engine components, while atmospheric plasma sprays (APS) span the range from rotating blades of large power generation turbines to afterburners in supersonic propulsion engines. This article presents a scientific description of both contemporary manufacturing processes (EBPVD, APS) and emerging TBC deposition technologies based on novel extensions to plasma technology (suspension spray, plasma spray-PVD) to facilitate novel compliant and low thermal conductivity coating architectures. TBCs are of vital importance to both performance and energy efficiency of modern turbines with concomitant needs in process control for both advanced design and reliable manufacturing.

Introduction

The widespread utilization of ceramic thermal-barrier coatings (TBCs) in both energy and propulsion systems has, to a large extent, been enabled by the development of advanced deposition technologies. The refractory nature of TBC materials such as yttria partially stabilized zirconia (YSZ) with melting points approaching or in excess of 3000 K requires ultrahigh temperature materials processing capabilities. Hence, thermal plasmas and electron beam sources have become primary and preferred methods of manufacturing. The former involves melt fabrication of powdered ceramics, while the latter is based on evaporation and vapor deposition from ceramic ingots.

A remarkable attribute of this process development is the scale of implementation of such advanced materials. According to various industrial sources, some 1–1.5 million kilograms of YSZ was atmospheric plasma sprayed (APS) onto engine components in 2011 alone. Aero-engine components benefiting from APS TBCs include combustors, vanes, and turbine shrouds, while TBCs are plasma sprayed onto both rotating and stationary parts of large land-based power-generation engines. On the other hand, virtually all hot section rotating turbine blades of aircraft-engines contain TBCs deposited via electron-beam physical vapor deposition (EBPVD) processes. These applications are expected to grow in the next two decades, especially as the importance of TBCs continues to grow due to ever increasing demands for fuel efficiency.

A critical aspect of ceramic TBCs, in addition to the material, is the coating defect architecture facilitated by processing. Both APS and EBPVD TBCs are comprised of some 10–30% porosity, which reduces the already low thermal conductivity of YSZ by an additional 100–150%.[1,2] EBPVD coatings display conductivities from 45 to 65% of bulk values, depending on process conditions, while as-deposited APS coatings can show properties as low as 20% of bulk values. This substantial reduction in thermal conductivity is attributed to the assortment of deposition-induced defects in these coatings, including pores of various sizes and morphologies, as well as a myriad array of interfaces of different character and length scales. **Figure 1** shows exemplary scanning electron micrographs of these coatings identifying the nature and dimensions of these defects.

Given the scale of reduction of thermal properties due to these defects, their manipulation and control via processing have been an important research endeavor. In recent years,

Sanjay Sampath, Center for Thermal Spray Research, Department of Materials Science and Engineering, Stony Brook University; sanjay.sampath@stonybrook.edu
Uwe Schulz, German Aerospace Center, Institute of Materials Research, Germany; Uwe.Schulz@dlr.de
Maria Ophelia Jarligo, Institute of Energy and Climate Research (IEK-1), Forschungszentrum Jülich GmbH, Germany; m.o.jarligo@fz-juelich.de
Seiji Kuroda, National Institute for Materials Science, Japan; Kuroda.Seiji@nims.go.jp
DOI: 10.1557/mrs.2012.233

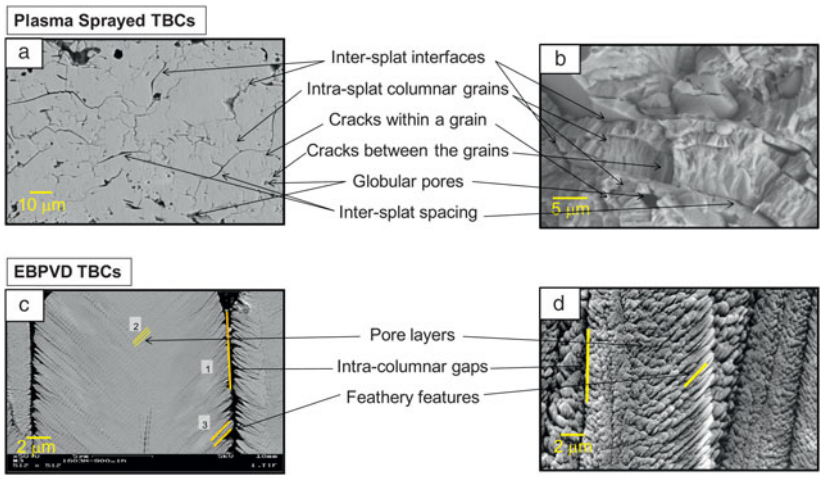

Figure 1. Microstructures and defect components of atmospheric plasma sprayed and electron-beam physical vapor deposition (EBPVD) thermal-barrier coatings (TBCs). (a,c) Scanning electron micrograph of polished coating cross-sections; (b,d) scanning electron micrographs of fractured cross-sections revealing the grain elements and interfacial features. In the plasma sprayed case, inter-splat gaps and interfaces are seen, which provide substantial reduction to thermal conductivity. For the EBPVD case, intra-columnar gaps perpendicular to the surface are shown, which impart in-plane compliance, while the feathery features formed by rotation and resultant shadowing effects provide reduction to through-thickness conductivity.

manufacturing reliability and reproducibility of these controlled defected structures has become paramount given the scale of the industrial applications and the importance of the coatings in energy and propulsion systems.

Defects also impart compliance to the TBC system, an essential property as the ceramic coating is fabricated on metallic substrates and subjected to thermal cycling and thermomechanical loading. In some ways, the emergence of YSZ as the preferred material of choice has been fortuitous, as YSZ displays higher than usual thermal expansion coefficients for ceramics and is more closely matched with that of the metal. However, during sustained exposure, the evolution of thermally grown alumina at the interface between the metal and the TBC complicates the mismatch effects warranting careful control of coating compliance.[3]

The EBPVD coating possesses a feathery microstructure with vertical separations that offers excellent compliance to thermal cycling. EBPVD coatings exhibit enhanced durability under aero-engine thermal loading situations. A typical APS coating, on the other hand, displays a layered architecture built up via discrete "splats" (impacted and solidified droplets). This brick wall structure with interpenetrating porosity and interfaces also offers compliance, although to a lesser extent than the vertical separations. Recent research has pointed to the fact that pores, cracks, and interfaces in APS coatings contribute to nonlinear elastic stress–strain response with hysteresis, together described as anelastic. Recent work further suggests that these novel mechanisms contribute to significant coating compliance and thus durability during thermal cycling.[4–6] Of further importance is our ability to measure and control these advanced properties via processing, which enables improved coating design and predicted performance in service.

There has been significant progress both in industry and academia to build ideal microstructures that combine the unique capabilities of EBPVD and APS. Of particular interest is the development of dense vertically cracked (DVC) or segmented crack microstructures synthesized via advanced APS processing. These structures display vertical separations similar to those of EBPVD, but the conditions required to generate vertical macrocracks result in increased coating density between the cracks and hence much higher thermal conductivity compared to typical layered APS coatings. To compensate for this higher conductivity, DVC coatings are typically sprayed to much greater thickness. These coatings have been employed in advanced engines for more than 15 years.[7,8]

The introduction of suspension and solution precursor plasma spraying further hybridizes the benefits of feathery EBPVD coatings and vertical cracking of the DVC structures. Such structures, produced through introduction of slurries/solutions into the thermal plasma rather than powder, introduce new complexities to the process with concomitant opportunities for research.[9] Similar attempts have emerged to produce advanced vapor deposited structures, for instance through the electron-beam directed vapor deposition (EBDVD) process, which combines a flowing carrier gas, as in thermal spray processes, with thermal vaporization of the material and PVD-based growth of the coating from the vapor phase.[10] In yet another nuance, the plasma spray process has been used to produce vapor phase deposition through the development of advanced high vacuum plasma spray technology (termed plasma spray PVD or PSPVD), resulting in high rate deposition of vapor phase materials.

This article will cover the underlying principles of both contemporary manufacturing methods (EBPVD and APS), modifications to traditional APS processes (segmented TBCs and suspension/solution sprays), and lastly, emerging hybrid technologies that combine attributes of particle based techniques and vapor processes (PSPVD).[11]

Current approaches to TBC processing

Electron-beam physical vapor deposition of TBC ceramics

EBPVD processing relies on evaporation of a material from a melt, utilizing a high vapor pressure over an overheated molten pool.[11] A highly energetic electron beam is scanned over the ceramic material to melt and evaporate it within a vacuum chamber. Preheated substrates are positioned in the vapor cloud, and the vapor is deposited onto the substrates at deposition rates of μm/minute. To achieve a defined stoichiometry of the

zirconia, oxygen is bled into the deposition chamber to compensate for the deficit caused by dissociation. Rotation of the parts is mandatory if the substrates or blades need to be coated on all sides. Due to the formation of the coating from the vapor phase and combined actions of surface diffusion, shadowing, and crystallographic growth selection, a columnar microstructure of the TBC can be achieved, providing a high level of strain tolerance (Figure 1c–d). To ensure continuous growth of the ceramic coating, cylindrical ingots of the ceramic are bottom-fed into the crucibles.

Formation of the microstructure of EBPVD TBCs is closely connected to processing conditions used.[12] Columns and inter-columnar gaps originate from vapor phase condensation and macroscopic shadowing caused by the curved column tips, triggered by rotation of the parts during deposition. Since shadowing occurs primarily along the plane of vapor incidence, columns are significantly wider in the direction parallel to the rotation axis than perpendicular to it, leading to an anisotropy of the in-plane compliance with notable consequences to the strain tolerance of the TBC system.

Globular and elongated spheroid pores are a consequence of rotation. They are arranged in layers inward from the edge to the center of the columns nearly parallel to the substrate surface, more precisely parallel to the individual column tip at that very location during growth. Each layer represents one revolution. These features are believed to consist mostly of closed porosity. Due to the sunset-sunrise situation as the object rotates perpendicular to the direction of deposition, bent sub-columns within each layer may be visible, depending on rotational speed, cutting direction of the cross-section for SEM with regard to the rotational axis, and thickness of the TBC.

The last microstructural feature, often referred to as "feather arms" (Figure 1d), is a consequence of shadowing by growth steps on the column tips near the center of a column. Since energetic reasons favor {111} planes to build the facets of a column tip while the column tip is curved for macroscopic shadowing reasons, a multitude of growth steps is formed that act as shadowing centers during further growth, leading to mostly opened porosity aligned at angles of between 35 and 50° (often 45°) to the main column axis. These feather arms might partly transform into lines of small nanometer-sized globular pores already during deposition, mainly driven by minimization of surface energy, overshadowing effects, and gas entrapment. This is found more often in the center area of a column. Recent investigations using ultra-small angle x-ray diffraction (USAXS) and small-angle neutron diffraction (SANS) indicate that the distribution of most elongated and feathery pores is also highly anisotropic.[13] Intra-columnar pores are a combination of globular and elongated spheroids and range between 18 and 25 nm in size. Image analyses indicate opening dimensions of 200–250 nm at feathery features with a typical aspect ratio of 1 to 10. To lower thermal conductivity, EBPVD TBCs rely mainly on elongated and feathery pores (intra-columnar porosity), while inter-columnar porosity primarily provides compliance.[2]

The microstructural factors regarding intra-columnar porosity are size, distribution, concentration, and morphology, all of which can be manipulated via processing, including deposition temperature, rotational speed, chamber pressure, pattern of vapor incidence, condensation rate, and partial shadowing. Hence, microstructure tailoring is feasible, within limits, which might be set by durability, processing cost issues, and physical restrictions due to shadowing.[14] Examples of different microstructures are given in **Figure 2**, together with the resulting thermal conductivities.

In summary, the major advantage of EBPVD is the columnar structure that provides strain tolerance and pseudo-plasticity. In comparison to plasma-sprayed TBCs, a higher erosion resistance, a smoother surface finish that offers aerodynamic advantages, and the fact that cooling holes stay open through the processing stages are key benefits. On the other hand, high cost, higher thermal conductivity, and limits in chemical variability due to vapor pressure issues are drawbacks along with a low utilization of the raw material.

Atmospheric plasma spray deposition of TBC ceramics

Thermal plasma spray is molten droplet deposition technology in which tens of micrometer-sized particles of metals and ceramics are introduced in powder form into an arc-plasma jet, entrained therein, and projected onto a prepared substrate. The particles acquire thermal energy and momentum from the thermal plasma, undergo melting, followed by impact and rapid solidification. Typically, for oxides and even most metallic alloys, plasma sprays are conducted under ambient conditions, hence the term atmospheric plasma spraying (oxidation sensitive metals can be sprayed in a low pressure environment). The resultant spray-deposited materials are comprised of an assemblage of "splats" of rapidly solidified materials assembled to form a brick-wall structure. Typical powder particle sizes range from 10–100 micrometers with resultant splats of the order of a few microns in thickness and upward of 100–150 micrometers in diameter. Under typical APS conditions, most particles solidify independently, resulting in a chaotic assemblage of the deposited microstructure that consists of splat-interfaces and unfilled regions resulting in porosity. **Figure 3** provides an illustrative description of the process, including source material (feedstock powder), the building blocks of the microstructure (splats), and assemblage of many splats as depicted in the cross-section micrograph of the deposit. The two critical properties of importance, namely thermal conductivity and non-linear stress–strain behavior, are shown for different types of coating microstructures.

As one can envision, the characteristics of the deposited microstructure are strongly dependent on processing.[15] Parameters of critical importance include the characteristics of the spray stream (particle trajectory and thermal and kinetic state, including degree of melting); the location and state of the substrate, including roughness, temperature, position, part geometry, and relative movement; and speed of the torch and part. Both characteristics of the feedstock powder as well as

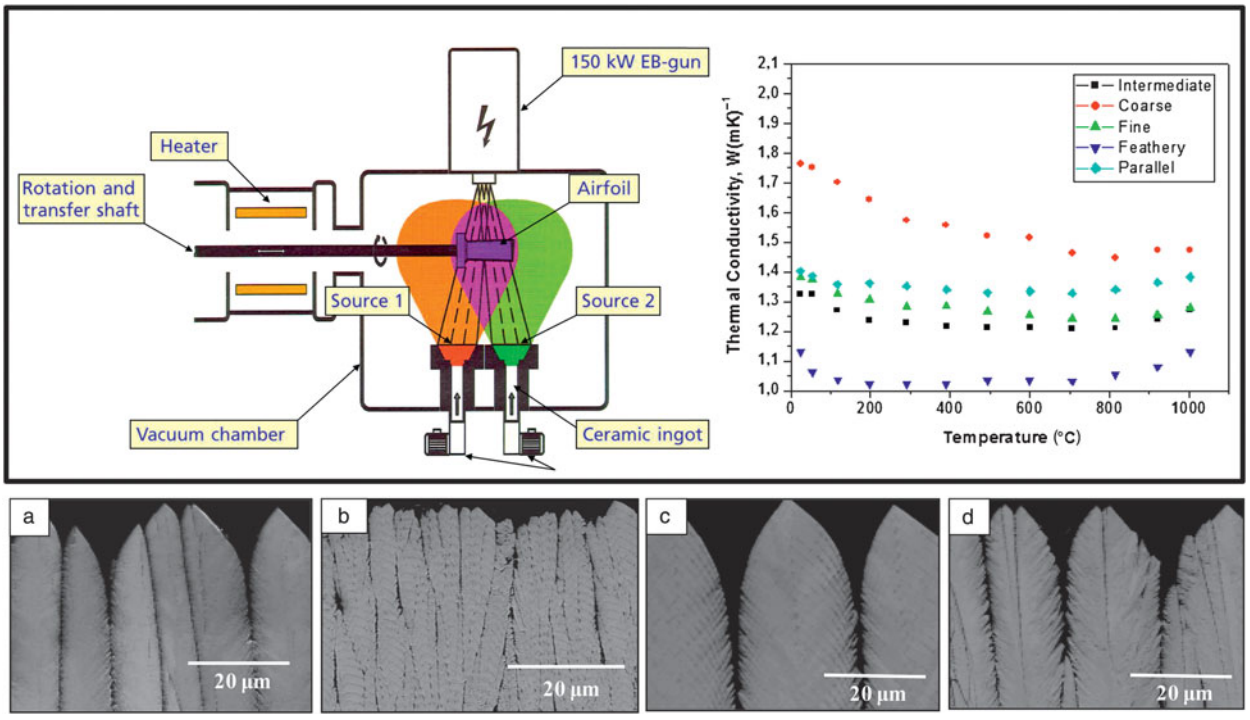

Figure 2. A schematic of electron-beam physical vapor deposition (EBPVD) processing is shown, where the orange and green represent two vapor clouds of different chemistry that can be mixed on the airfoil. (a–d) Electron micrographs showing cross-sections of the column tips found in EBPVD coatings, demonstrate the variability of microstructure achievable by varying important EBPVD process parameters such as substrate temperature and rotational speed, including variation in column diameter, porosity, and width of inter-columnar gaps. The plot shows their corresponding thermal conductivity values.[2]

the attributes of the spray device are of significance. All of the mentioned processing attributes govern the nature of the deposit buildup and, as such, both the extrinsic microstructural character (porosity, interfaces) as well as intrinsic or material dependent attributes (grain size, texture, cracking, phase evolution, and stability). With respect to TBC systems based on the YSZ polymorph, the critical microstructural elements include splat and interpass interfaces (the latter is a temporal effect associated with torch movement), intra-splat cracking due to relief of very large quenching stresses upon impact and solidification, and finally incompletely filled layers resulting in highly varied porosity.[16]

Much progress has been achieved in our ability to characterize the interplay between processing and microstructure and hence the performances of this complex defect containing system. Although the processing conditions can affect the defect quantity and type in a very significant way for YSZ, there has been specific and steady progress not only in macroscopic quantification of the structure-property relationship (e.g., porosity-thermal conductivity relations) but also in the underlying fundamentals in terms of the generation of the defect type and their characteristics.[17] This is particularly significant for monitoring and controlling coating compliance, which in recent years has been attributed to the unique nonlinear/anelastic response of the porous ceramic coating on metallic substrates.[3,18] An illustrative example of the link between processing and porosity properties is provided in the plots in Figure 3d–e, where thermal conductivity and compliance are described for different microstructures. These developments have not only enhanced the applicability of YSZ TBC systems, but have also paved the way for expanded opportunities for other oxide systems.

In recent years, much of the scientific and technological efforts have focused on process control to achieve reliable manufacturing of TBC coatings. TBCs are fabricated by small to large factories all over the world to specifications defined by the engine manufacturer. As these spray factories are entitled to use any available (approved) spray device and powder, the specifications tend to be rather wide to accommodate microstructural variation. This has, to some extent, resulted in design engineers reducing their reliance on the coating for reliable performance and focusing more on life extension of the underlying superalloy components. However, as the engine inlet temperatures increase, the need for reliable and controlled coatings is becoming increasingly critical. As such, advancements in process science have been sought to develop methodologies not only for process control, but also effective materials science descriptions for microstructural control.

Segmented cracked TBCs via advanced APS strategies

Both APS and EBPVD coatings, which are now used in mainstream TBC manufacturing, offer benefits in terms of both

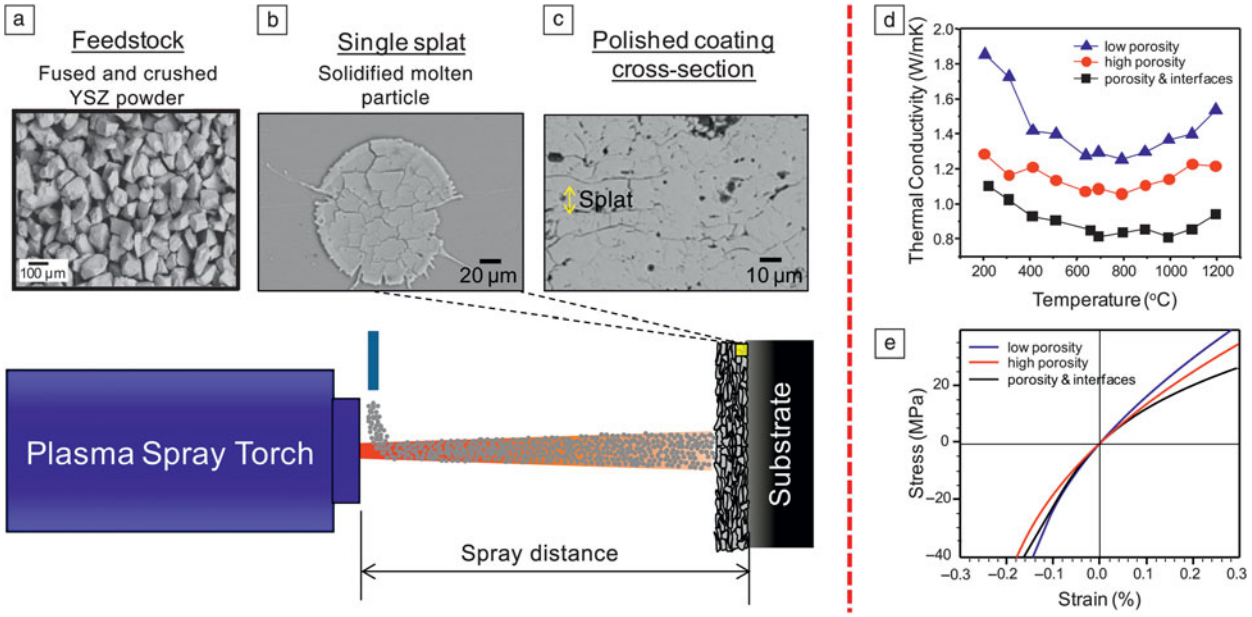

Figure 3. Illustrative description of atmospheric plasma spray deposition process for thermal-barrier coatings in which a ceramic feedstock (gray dots) is carried to the substrate by a plasma spray. Electron micrographs show (a) the feedstock powder, (b) an individual component of the coating assembly (splat), and (c) a polished cross-section of an aggregated coating. On the right are (d) thermal conductivities of three different coatings with different pore/interface content, along with (e) non-linear stress–strain relations as obtained from curvature measurements. Detailed description of the parametric effects can be found in References 4, 18, and 19.

compliance and conductivity due to their defected structure. Typical APS coatings offer lower conductivity, but EBPVD coatings provide for better compliance and erosion resistance. As outlined earlier, there is significant interest to incorporate the benefits of EBPVD into APS coatings, particularly for large component TBC applications in power systems. This has led to both industrial and academic research on segmented or vertically cracked ceramic coatings and their successful implementation in gas turbines.[7,8,20,21]

Plasma sprayed zirconia splats undergo extremely rapid quenching (10^8 K s^{-1}) as they impact a substrate or the surface of already deposited layers, spread into sheets of a few µm thickness, and are cooled down predominantly by thermal conduction to the underlying solid body. As a result, if one observes a single ceramic splat formed on a flat metal substrate, an intricate network of microcracks can be seen (Figure 3b). The patterns and the principle behind the formation of these cracks are similar to mud cracking or crazing on some porcelain pieces, where the shrinkage of the surface layer is restricted by the underlying massive body, resulting in large lateral tensile stresses and consequent cracking during cooling. Since the coefficient of thermal expansion of YSZ is approximately 10^{-5} K^{-1}, and the temperature drop ΔT that plasma sprayed splats undergo is more than 2000 K, the amount of strain that must be incorporated is approximately 2×10^{-2}, which is an order of magnitude larger than the failure strain of most ceramics, including zirconia.

As a result, APS ceramic coatings usually contain a large number of microcracks. When the deposition temperature is raised significantly, an interesting tendency has been observed to transition from splat level microcracking to large macroscale cracking (i.e., so-called segmentation cracks or dense vertical cracks). **Figure 4** provides an illustrative description of the phenomenon indicating the role of substrate temperature on the segmentation crack density.[20] It has been shown that the density of segmentation cracks increases at the expense of micropores as the substrate/deposition temperature increases.[21] This transition is related to both the improvement of wetting between overlaid splats at high deposition temperatures and the reduction of the temperature drop ΔT. As the wetting among several splats improves and multiple splats are connected at high temperature, they start to behave more or less as a larger single body. There is also evidence of columnar grains grown across multiple splats when observations are made on fractured cross-sections. As a result, cracks between thicker masses of zirconia are formed associated with more macroscopic temperature variations experienced during APS. Recent experiments to detect acoustic emission during APS to some extent support this hypothesis, but further investigation is needed.[22] Significant improvement in terms of thermal cycle life has been reported for such vertically cracked TBCs, and this technology has been used in industry for more than a decade.

Despite the industrial acceptance of these techniques, several fundamental issues remain, such as what optimal crack density is needed to achieve optimum performance as a TBC. Furthermore, thermal conductivity is somewhat sacrificed, as there is greater vertical connection of splats as compared to TBCs sprayed in a conventional manner, where significant

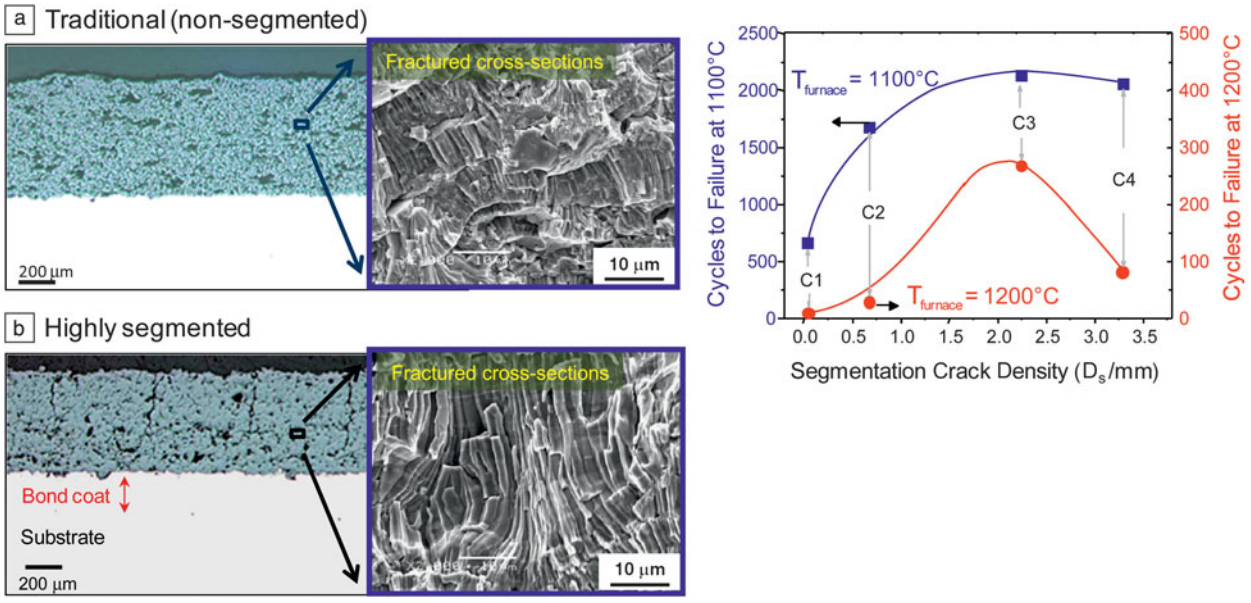

Figure 4. Metallographically prepared cross-sections of (a) traditional (non-segmented) and (b) highly segmented thermal-barrier coatings (TBCs) produced at low and high substrate temperatures, respectively, with enlarged scanning electron microscopy images obtained from fractured sections of the coatings. On the right are plots of thermal cycle life of TBCs tested at 1100 and 1200°C as a function of segmentation crack density. C1 to C4 correspond to different plasma spray conditions with increasingly higher substrate temperatures during spraying.[20]

portions of the lamellar interfaces are not bonded.[23] This results in a significantly thicker TBC being needed to impart similar heat resistance.

Suspension and solution plasma spraying of ceramics

Thermal spray processes usually involve the injection of a powder feedstock into a flame or a plasma jet. In the case of the conventional APS process, the powder particles must have a diameter in the range of 10–100 µm in order to be flowable (favored by smaller particles) and also capable of impact deposition (requires inertial mass). This limitation in the feedstock particle size leads to limitations in terms of expanding process capabilities. With APS, it is difficult to obtain nanostructured coatings with a very fine microstructure and/or to manufacture very thin coatings (below approx. 10 µm in thickness), as at least several lamellae piled up on each other are necessary to form a coating.

Suspensions and solutions have long been considered as alternative feedstock for plasma spray.[9,24,25] This area received much more attention in recent years through the desire to both use nanostructured materials as well as to fabricate nanostructured coatings. In this approach, submicron particles are agglomerated within a liquid suspension to allow their introduction into high pressure thermal plasma jets. Referred to as suspension plasma spraying (SPS), this relatively novel process is very promising for the manufacture of nanostructured coatings for a large range of applications.

The use of such suspensions or solutions in the case of TBC deposition leads to the generation of hybrid microstructures that combine the low conductivity of APS TBCs resulting from through-thickness layering with the ability to produce vertical separations (segmented cracks) imparting in-plane compliance.[26,27] In some respects, this technique combines the advantages of traditional APS, segmented crack structures, and EBPVD attributes, and overcomes some of the limitations of segmented crack TBCs.

To produce SPS coatings, fine particles of the oxide materials are dispersed in a solvent such as ethanol with a solid fraction commonly in the range of 5–30 wt%, and the formulated suspension is directly injected into a typical APS thermal plasma jet (**Figure 5**). Liquid injection can be realized as a coherent stream or as atomized droplets.[26] When entering the plasma jet, the liquid is subjected to fragmentation due to the plasma jet shear effects, yielding even smaller suspension droplets.[27] The solvent is rapidly vaporized, and the particles located in a single droplet form an agglomerate. The obtained solid agglomerates are accelerated and melted in the plasma jet, transforming into ceramic molten droplets, and eventually impacted onto the substrate surface. The deposited splats have very small dimensions (diameters from 0.2–6 µm and thicknesses of 20–300 nm[28]) compared to typical APS splats having thicknesses of about 2–5 µm. As a result, SPS coatings have an increased number of lamellae and interfaces and present significantly finer microstructures, resulting in coatings with significantly lower thermal conductivities than conventional APS coatings.[29]

The processing conditions for SPS are drastically different than those of APS in two ways: First, the powder carrier is no longer a gas but a liquid whose interaction with hot gases is

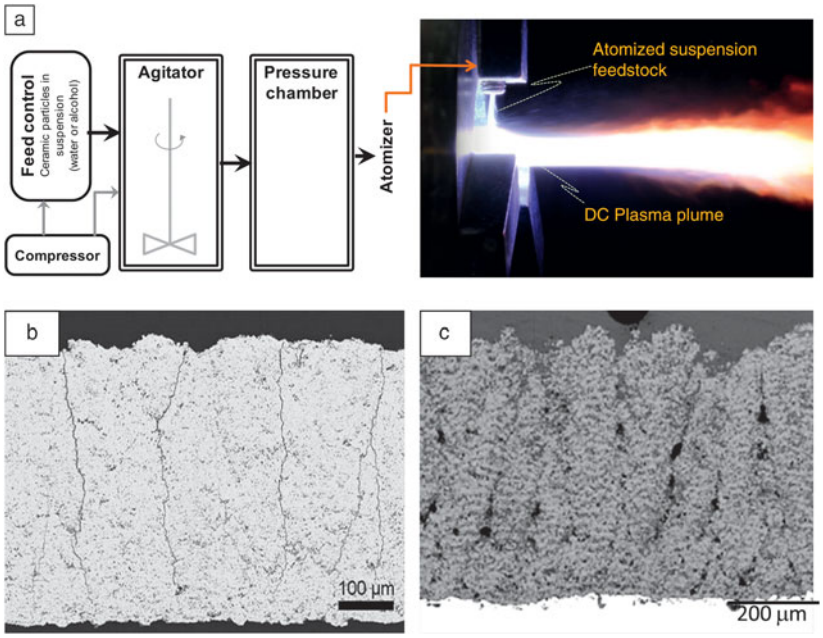

Figure 5. Illustrative and pictorial description of the suspension plasma spraying process for deposition of thermal-barrier coatings along with examples of deposited microstructures displaying segmentation cracking resulting from high temperature processing (>600°C). (a) Key components of a suspension feeding system and associated injection in the thermal plasma torch. Two variants of the microstructures are shown, (b) similar to an atmospheric plasma spray segmented crack structure, while (c) is closer to the electron-beam physical vapor deposition structures displaying both vertical separations as well as a feathery inner structure within the columns. Adapted from References 27 and 31.

more complex than that of a gas, and second, submicrometer- or nanometer-sized particles, contained in suspensions or those formed in-flight in solution, have very low inertia and can only reach the substrate in a melted state if the spray distance is short (from one-half to one-fifth of that of conventional coatings). This results in very strong heat fluxes to the coating under formation, with corresponding microstructural implications. SPS coatings do not have the lamellar structure of conventional APS, but present a mostly granular nanostructure.

Figure 5 provides an illustrative description of the process along with examples of microstructures. As in standard coatings, SPS coatings show areas of (a) good and (b) poor inter-splat bonding. But what is common to both cases is the presence of periodic vertical separations. These separations are a result of the elevated processing temperatures in SPS and are in some ways similar to segmented APS TBCs.

Another closely related SPS process employs liquid precursors rather than suspensions. The solution precursor plasma spray (SPPS) utilizes molecularly mixed solutions, for example aqueous solutions of yttrium and zirconium salts targeted to achieve the standard 7% yttria composition of YSZ.[25] The precursor is introduced into the spray torch via atomization of the liquid in a manner similar to the SPS process, and the resultant liquid undergoes a series of substeps within the plasma flame, including evaporation, breakup of the droplet, gelation, pyrolysis, and sintering prior to impact on to the substrate. The deposit formed is comprised of very fine agglomerates devoid of the typical splat boundaries and cracks, and, due to the high deposition temperature, also results in vertical segmentation cracks. SPPS coatings, also due to the fine architecture (many more interfaces), show simultaneously good compliance and low conductivity. As a result, these coatings typically offer enhanced durability compared to traditional APS coatings.

Innovative future concepts: Plasma spray physical vapor deposition

PSPVD is a novel extension to vacuum plasma spray technology allowing for vapor generation within the thermal plasma followed by deposition onto a hot substrate in ways akin to PVD but at higher rates.[11,31,32] Originally developed as a very low pressure plasma spray (VLPPS), the goal was depositing uniform and thin coatings with large area coverage based on plasma spraying. At typical pressures of 50–200 Pa, the characteristics of the plasma jet change compared to conventional low pressure plasma spraying processes operating at 5–20 kPa, increasing in length from a few 100 mm to 1.5 m. At appropriate parameters, it is even possible to evaporate powder

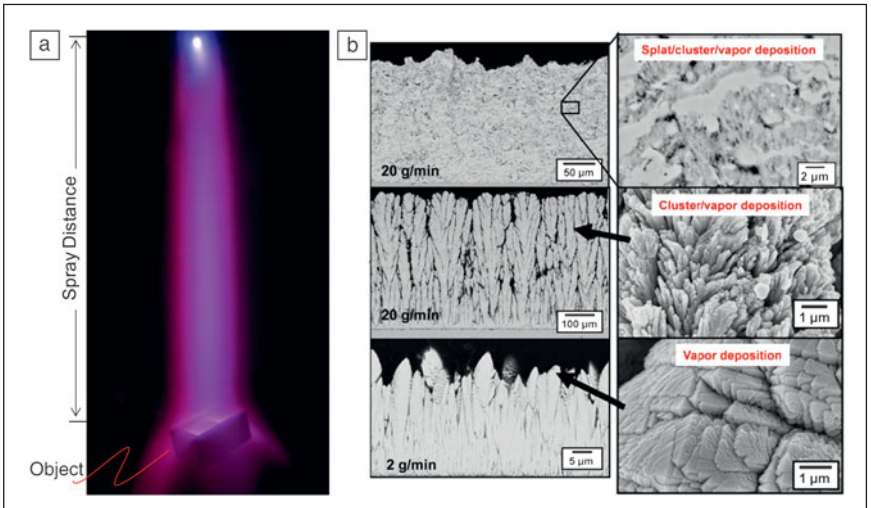

Figure 6. (a) Photograph of a plasma spray physical vapor deposition (PSPVD) plume coating a part (plume length ~1 m) and (b) scanning electron microscopy images of PSPVD microstructures from splat/cluster deposition all the way to vapor deposition obtained at different deposition rates. Adapted with permission from Reference 29. ©2011 Forschungszentrum Jülich GmbH. Process photo courtesy of Sulzer Metco.

feedstock material, achieving advanced microstructures and non-line of sight deposition (e.g., for TBCs). Thin and dense ceramic coatings as well as columnar-structured strain-tolerant coatings with low thermal conductivity can be achieved.[5] Under certain process conditions, it is possible to use VLPPS to obtain structures very similar to that of EBPVD, hence these conditions are termed PSPVD. **Figure 6** shows examples of microstructures obtained from the VLPPS process at different deposition rates ranging from splat/cluster deposition all the way to vapor deposition. PSPVD has the advantage of coating non-line of sight objects, such as complex shaped vane doublets at a relatively higher rate. The process is currently being investigated by turbine companies for potential commercialization.

Summary and concluding remarks

The integration of thermal-barrier coatings (TBCs) into modern propulsion and energy-generating turbine systems has allowed both performance enhancement and life extension of advanced superalloy components. Their widespread use has created a large industrial manufacturing base for advanced ceramic deposition technologies, such as plasma spray and EBPVD. Advanced TBCs are now moving from life extension to prime reliance (i.e., they are essential to component life and engine operation), requiring insertion of process science and control in manufacturing. Given the complexity in terms of structure, defects, and layering, the interplay between scientific research and technology will continue to evolve. To some extent, the ease of TBC processing is enabled due to the utilization of YSZ. Both yttria and zirconia have similar vapor pressures, melting points, and thermophysical characteristics, and as such chemical complications from rapid heating, melting, and evaporation are not significant. However, industry is moving toward more complex compositions (e.g., multicomponent stabilization based Y, Yb, and Gd), as well as pyrochlore structures based on zirconates ($La_2Zr_2O_7$, $Gd_2Zr_2O_7$) to meet new performance requirements such as erosion resistance, molten glass attack (CMAS), as well as increased heat flux.[33–35]

An additional issue for consideration is the stability of the as-deposited defected microstructure and their crystal phases during sustained thermal exposure. In the case of YSZ, at temperatures above 1000°C, the porosity and splat interfaces tend to sinter, causing a loss of compliance and an increase in conductivity. The extent of sintering is microstructure dependent and controlled via processing parameters.[36] Similarly, both APS and EBPVD YSZ coatings are comprised of a metastable tetragonal prime (t') structure, which is generally stable up to 1200°C. Under sustained exposure above 1200°C, the t' phase is susceptible to decomposition into cubic and tetragonal forms, with the latter ultimately transforming into monoclinic upon cooling.[37] The t' phase is also known to be of significantly higher toughness than other phases due to ferroelastic switching events, which not only depend on composition but also on metastability.[38] Thus, emergence of new compositions is closely tied to process-related microstructural and phase attributes. It is clear that future development of TBCs will involve integration among processing science, phase/microstructure control, and linkage to performance. Research is under way in all of these areas, driven by the need for reliable multifunctional coating systems.

Acknowledgments

We are grateful to Dr. Gopal Dwivedi of Stony Brook University for his assistance in integrating the figures for this article.

References

1. A. Kulkarni, Z. Wang, T. Nakamura, S. Sampath, A. Goland, H. Herman, J. Allen, J. Ilavsky, G. Long, J. Frahm, R.W. Steinbrech, *Acta Mater.* **51**, 2457 (2003).
2. A. Flores Renteria, B. Saruhan, U. Schulz, H.-J. Raetzer-Scheibe, J. Haug, A. Wiedenmann, *Surf. Coat. Technol.* **201**, 2611 (2006).
3. A.G. Evans, D.R. Mumm, J.W. Hutchinson, G.H. Meier, F.S. Pettit, *Prog. Mater. Sci.* **46** (5) 505 (2001).
4. Y. Liu, T. Nakamura, G. Dwivedi, A. Valarezo, S. Sampath, *J. Am. Ceram. Soc.* **91** (12), 4036 (2008).
5. Y. Liu, T. Nakamura, V. Srinivasan, A. Vaidya, A. Gouldstone, S. Sampath, *Acta Mater.* **55**, 4667 (2007).
6. C.A. Johnson, J.A. Ruud, R. Bruce, D. Wortman, *Surf. Coat. Technol.* **108**, 80 (1998).
7. T.A. Taylor, US Patent 5, 073, 433 (1989).
8. D.M. Gray, Y.C. Lau, C.A. Johnson, M.P. Boron, W.A. Nelson, US Patent 5,830,586 (1996).
9. P. Fauchais, G. Montavon, *J. Therm. Spray Technol.* **19** (1–2), 226 (2010).
10. D.D. Hass, H.N.G. Wadley, US Patent Appl. 2008/0131611 A1 (2008).
11. K. Von Niessen, M. Gindrat, *J. Therm. Spray Technol.* **20** (4), 736 (2011).
12. U. Schulz, B. Saruhan, K. Fritscher, C. Leyens, *Int. J. Appl. Ceram. Technol.* **1**, 302 (2004).
13. A. Flores Renteria, B. Saruhan, J. Ilavsky, A.J. Allen, *Surf. Coat. Tech.* **201** (8) 4781 (2007).
14. U. Schulz, S.G. Terry, C.G. Levi, *Mater. Sci. Eng. A* **360**, 319 (2003).
15. A. Vaidya, V. Srinivasan, T. Streibl, M. Friis, W. Chi, S. Sampath, *Mater. Sci. Eng., A* **497**, 239 (2008).
16. S. Kuroda, T.W. Clyne, *Thin Solid Films* **200** (1), 49 (1991).
17. T. Nakamura, Y. Liu, *Int. J. Solids Struct.* **44** (6), 1990 (2007).
18. W. Chi, S. Sampath, H. Wang, *J. Am. Ceram. Soc.* **91** (8), 2636 (2008).
19. G. Dwivedi, T. Nakamura, S. Sampath, *J. Am. Ceram. Soc.* **94**, 104 (2011).
20. H.B. Guo, H. Murakami, S. Kuroda, *Mater. Trans.* **47** (42), 308 (2006).
21. H.B. Guo, R. Vaßen, D. Stöver, *Surf. Coat. Technol.* **186** (3), 353 (2004).
22. K. Ito, H. Kuriki, M. Watanabe, S. Kuroda, M. Enoki, *Mater. Trans.* **53**, 671 (2012).
23. A. Kulkarni, A. Goland, H. Herman, A. Allen, J. Ilavsky, G. Long, C. Johnson, J. Ruud, *J. Am. Ceram. Soc.* **87** (7), 1294 (2004).
24. J. Karthikeyan, C.C. Berndt, J. Tikkanen, S. Reddy, H. Herman, *Mater. Sci. Eng., A* **238** (2), 275 (1997).
25. T. Bhatia, A. Ozturk, L. Xie, E. Jordan, B. Cetegen, M. Gell, X. Ma, N. Padture, *J. Mater. Res.* **17**, 2363 (2002).
26. R. Rampon, C. Filiatre, G. Bertrand, *J. Therm. Spray Technol.* **17** (1), 105 (2008).
27. C. Delbos, J. Fazilleau, V. Rat, J.F. Coudert, P. Fauchais, B. Pateyron, *Plasma Chem. Plasma Process.* **26** (4), 393 (2006).
28. H. Kassner, R. Siegert, D. Hathiramani, R. Vassen, D. Stoever, *J. Therm. Spray Technol.* **17** (1), 115 (2008).
29. H. Kaßner, A. Stuke, M. Rödig, R. Vaßen, D. Stöver, *Ceramic Engineering and Science Proceedings* **29** (4) 147 (2009).
30. A. Guignard, G. Mauer, R. Vaßen, D. Stöver, *J. Therm. Spray Technol.* **21**, 416 (2012).
31. A. Guignard, doctoral thesis, Ruhr University, Bochum, Germany (2012).
32. A. Hospach, G. Mauer, R. Vassen, D. Stover, *J. Therm. Spray Technol.* **20** (1–2), 116 (2011).
33. D. Zhu, R. Miller, *Int. J. Appl. Ceram. Technol.* **1**, 86 (2004).
34. R. Vassen, X. Cao, F. Tietz, D. Basu, D. Stöver, *J. Am. Ceram. Soc.* **83** (8), 2023 (2000).
35. M. Jarligo, D.E. Mack, R. Vassen, D. Stöver, *J. Therm. Spray Technol.* **18** (2), 187 (2009).
36. Y. Tan, J. Longtin, S. Sampath, H. Wang, *J. Am. Ceram. Soc.* **92** (3), 710 (2009).
37. R.A. Miller, J.L. Smialek, R.G. Garilick, in *Science and Technology of Zirconia I*, A.H. Heuer, L.W. Hobbs, Eds. (American Ceramic Society, Columbus, OH, 1981), p. 241.
38. C. Mercer, J.R. Williams, D.R. Clarke, A.G. Evans, *Proc. R. Soc.* **463** (2081), 1393 (2007). □

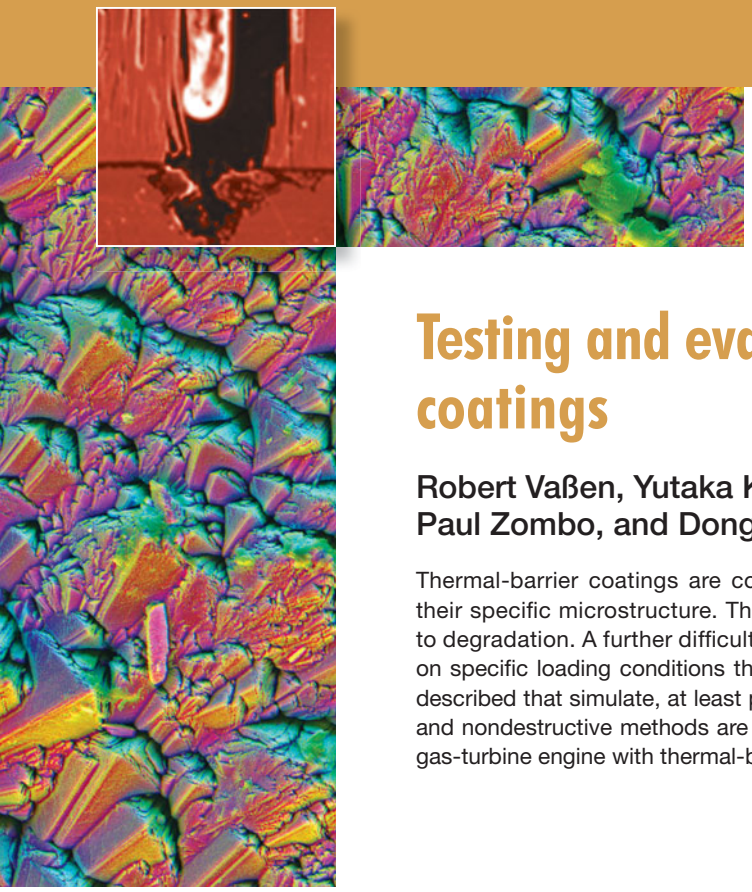

Testing and evaluation of thermal-barrier coatings

Robert Vaßen, Yutaka Kagawa, Ramesh Subramanian, Paul Zombo, and Dongming Zhu

Thermal-barrier coatings are complex systems with properties that largely depend on their specific microstructure. Their properties change during operation, typically leading to degradation. A further difficulty arises from the fact that this degradation also depends on specific loading conditions that can be rather complex. Different laboratory setups are described that simulate, at least partially, the actual loading conditions. In addition, sensing and nondestructive methods are described that are targeted toward reliable operation of a gas-turbine engine with thermal-barrier coated components.

Introduction

Testing thermal-barrier coating (TBC) systems and evaluating their performance in service presents major challenges. First and foremost, the conditions under which they operate are often extremely harsh, combining high temperatures, steep temperature gradients, fast temperature transients, high pressures, and additional mechanical loading, as well as oxidative and corrosive environments. These are difficult to reproduce in the laboratory. The coating system also changes with time and temperature as interdiffusion occurs, microstructures evolve, and the properties of the constituent multilayer materials change. For instance, the oxide topcoat sinters,[1,12] increasing both its thermal conductivity and elastic modulus, but the rate of sintering depends on its purity. Furthermore, the properties that need to be evaluated are rarely those of the constituent bulk materials themselves. For instance, while the intrinsic fracture toughness of the ceramic topcoat—typically made of 7 wt% yttria-stabilized zirconia (7YSZ)—is important, it is the toughness that a delamination crack experiences as it extends in or near the interface with the thermally grown oxide (TGO) that directly influences the lifetime under thermal cycling conditions. As coatings become prime-reliant, meaning that they can be implemented into the design of the engine with reliable performance criteria, it is also essential to develop sensors and nondestructive evaluation methods to monitor TBC temperatures, the extent of sub-critical delamination in service, as well as identifying manufacturing flaws, while also creating an artificial intelligence supervisory system that can be implemented in the field to provide feedback to the manufacturing and design sectors for product improvement. Several sensor approaches are being explored, including infrared imaging, Raman spectroscopy, thermography, impedance spectroscopy, acoustic emission, and luminescence sensing.[2–7]

Mechanical properties

One of the fundamental problems in discussing and evaluating the mechanical properties of coatings is establishing what the appropriate value of a particular property should be and at what microstructural scale it should be determined. This is especially true of the oxide topcoat since considerable variability and uncertainty arise from the porous nature of the coating as well as its anisotropy and microstructural evolution at elevated temperatures. For simple properties, such as the overall thermal expansion mismatch stresses on thermal cycling and the available elastic strain energy release rate, the macroscopic biaxial Young's modulus, such as determined by a macroscopic mechanical test, is generally adequate, recognizing that it can be expected to be different under tension than compression. In contrast, the local modulus obtained by nanoindentation, for instance, pertains to the modulus of the intrinsic material

Robert Vaßen, Institute of Energy and Climate Research, Forschungszentrum Jülich GmbH, Germany; r.vassen@fz-juelich.de
Yutaka Kagawa, Research Center for Advanced Science and Technology, The University of Tokyo, Japan; kagawa@rcast.u-tokyo.ac.jp
Ramesh Subramanian, Siemens Energy Inc., Orlando, FL; Ramesh.Subramanian@siemens.com
Paul Zombo, Engine and Component Diagnostics, Siemens Energy Inc., Orlando, FL; Paul.Zombo@siemens.com
Dongming Zhu, Durability and Protective Coatings Branch, Structures and Materials Division, NASA Glenn Research Center, Cleveland, OH; dongming.zhu@nasa.gov
DOI: 10.1557/mrs.2012.235

and local stiffness but not to the generation of average thermal cycling induced stresses. The same issue pertains to distinguishing macroscopic and local thermal conductivity. For this reason, there is intense interest in using local information, such as that obtained from nanoindentation, together with tomographic images to predict overall properties using object-oriented finite element (OOF) methods, such as the OOF tool available on the National Institute of Standards and Technology web page.[8]

While this is a very promising methodology, it is less suited to understanding or predicting crack growth, since it does not depend on just the average mechanical properties. For small crack lengths, crack growth rates are mainly controlled by intrinsic fracture toughness. For YSZ, this property is unusually high for an oxide and has recently been attributed to ferroelastic domain switching.[9] Understanding the toughening processes in YSZ also provides guidance for the selection and design of new TBC materials with enhanced toughness levels. One of the surprising results of recent measurements has been that fracture resistance for long cracks in TBCs, for instance those associated with coating delamination, is at least four times higher than the intrinsic toughness, as can be seen in **Figure 1** comparing the maximum value for short (inter-splat) cracks and the mean for long cracks. While it has always been recognized that microstructure must play a role in the fracture of TBCs, the magnitude of the toughening enhancement, on the order of 150 N m^{-1},[10] and extent of the R-curve (rising toughness with increasing crack extension) is considerably larger than anticipated. The origin of the R-curve in plasma-sprayed and electron-beam physical vapor deposited (EBPVD) TBCs is now known to differ in detail but is essentially due to local crack deflections resulting in a tortuous crack path forming microstructural heterogeneities whose relative motion during crack propagation results in friction. Details on crack path and toughening mechanisms are discussed in References 10 and 11.

Thermal gradient testing

Testing coatings under extreme temperature gradients and heat flux conditions approximating actual engine operation poses special challenges. One approach has been to use a high-power CO_2 laser rig,[13] such as implemented at the NASA Glenn Research Center,[14] and the other is to use a flame rig configuration in which heat is applied to one side of a coating by an oxygen/hydrocarbon gas flame.[15] In both cases, the samples are cooled from the back side with a high-pressure compressed air jet. While these configurations are less suitable for testing complex shaped blades and vanes, these new testing platforms can be used to evaluate fundamental coating properties such as rates of sintering, thermal cycle lifetimes, thermal conductivities, and to monitor damage evolution under high-flux conditions of planar TBC systems, such as coated superalloy buttons. These configurations also allow for the introduction of particulates (sand, ash), water, and salt during testing, as shown in **Figure 2**[16] to evaluate the degradation they may cause. At high surface temperature, or with particulate addition, this type of testing typically results in subsequent chipping of surface layers due to the thermal gradient present (see the article by Levi et al. in this issue). Actual coating failure modes identified from engine testing or from service operation are usually complex, largely depending on excursions from standard engine operating conditions, and processed coating composition, architecture, and microstructures. Nevertheless, once a particular failure mode has been identified, the tests can be used to evaluate coatings under similar conditions.

Since the initial development of the steady-state CO_2 laser (wavelength 10.6 μm) test facility at NASA Glenn Research Center and its application to measuring the sintering of coatings and thermal conductivity for instance,[17–19] its capabilities have subsequently been extended. Among the most recent is evaluating interface crack propagation under extreme heat flux and cyclic loading conditions,[20] such as might occur during repeated aircraft takeoff. **Figure 3** shows the test results at this

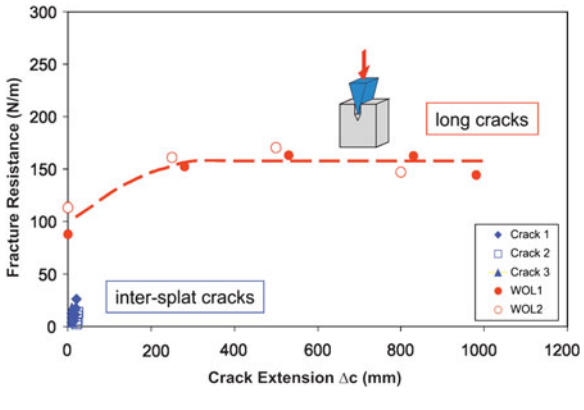

Figure 1. Crack resistance of inter-splat cracks (formed between individual deposition splats during cooling) and R-curve from extension of long delamination cracks in wedge opening loading (WOL).

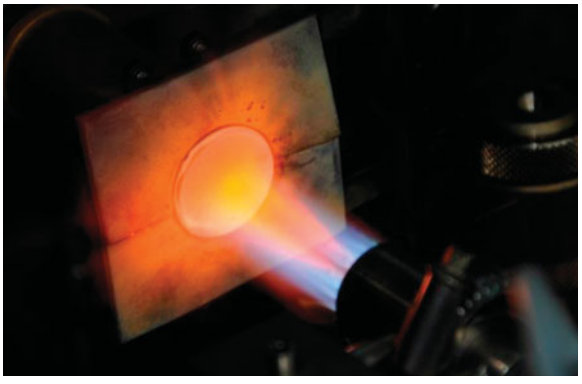

Figure 2. Photograph of the Jülich gas burner rig heating a disk-shaped thermal-barrier coating sample with back-side compressed air cooling. In the central part of the flame, a solution of calcium-magnesium alumino-silicates is injected to spray onto the hot surface.

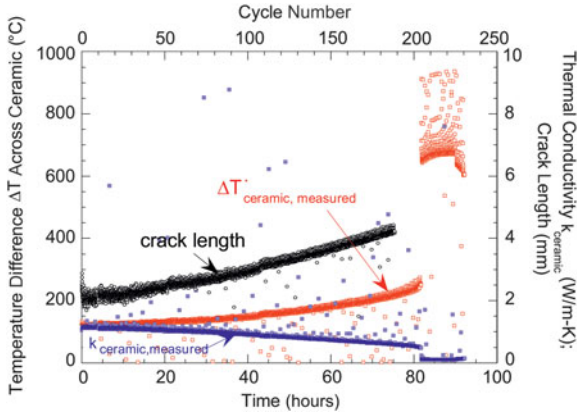

Figure 3. Laser heat flux thermal gradient cyclic test results of a 127-μm-thick, precracked thermal-barrier coating specimen subject to 20 min heating and 4 min cooling thermal cycling. The initial circular crack was 2 mm in diameter. The effective thermal conductivity clearly correlates with the crack propagation until the coating spalled after 200 cycles.

facility of a 127-μm-thick, precracked TBC specimen, with the crack introduced at the TBC/bond-coat interface. The initial ceramic surface temperature was set at approximately 1287°C and 20-min heating/cooling cycles with 60–100 W cm^{-2} heat flux were applied. The coating surface temperature increased continuously as the crack propagated, whereas the metal backside temperature remained relatively constant. The apparent coating thermal conductivity, calculated from the known laser heat flux, decreased as the delamination crack grew until the test was interrupted by spallation of the coating after about 200 cycles. The crack propagation process was also monitored independently by a high sensitivity video camera for calibrating the crack propagation with cycles. From these data, the crack propagation rate (*da/dN)* and the laser thermal transient stress associated stress intensity factor amplitude (ΔK) (the crack propagation driving force on the coating) for the plasma sprayed 7–8YSZ were also determined.[20] The results show slower thermal fatigue crack propagation rates compared to monolithic ceramics, indicative of additional R-curve toughening effects due to the roughness and plasticity at or near the ceramic/metal interface.

Thermomechanical fatigue

As with other high-temperature materials, including superalloys, thermomechanical fatigue (TMF) can adversely influence coating durability.[21–24] The origin of TMF is creep and plastic deformation in each of the component layers in the TBC system driven by the coefficient of thermal expansion (CTE) mismatch, especially the CTE mismatch between the bond coat, the superalloy, and the topcoat under thermal gradient conditions, as well as mechanical loads, such as centrifugal force. Testing under TMF conditions is essential, but the wide variety of possible in-phase mechanical and temperature loadings and out-of-phase loading conditions as well as realistic thermal gradient conditions makes this a demanding materials engineering task that is only now being addressed. Even so, there have been surprises. One is that contrary to initial expectation, compressive deformation is the major form of damage in strain-controlled in-phase and stress-controlled out-of-phase modes.[25] Another is that cracks can nucleate in the bond coat at high-temperatures and propagate into the superalloy.

Figure 4 illustrates characteristic damage accumulation behavior in EBPVD TBC systems in an in-phase stress-controlled TMF test mode.[26,27] The temperature of the substrate is kept at a constant 1000°C, while the TBC surface is heated to 1150°C and cooled again over 960s cycles. An uniaxial tensile load of 1.8 kN (60 MPa) is applied to the specimen while the TBC surface is heated. Evolution of strain with time and numbers of loading cycles under in-phase TMF test conditions are consistent with the creep behavior of superalloys (Figure 4a). Ratcheting behavior,[27] where the materials are left permanently deformed after each cycle, is superimposed on the creep behavior, as illustrated in Figure 4b. This behavior is consistent with most of the applied load being supported by the superalloy substrate. However, the creep behavior of the EBPVD TBC layer is interesting: at 1150°C, the layer can deform up to about 8% tensile strain without evidence of visible cracking.[28] With increasing tensile creep strain, cracking of the TBC layer initiates, and, ultimately, multiple fragmentation occurs, as seen in Figure 4c–d. It is found that the cracks in the TBC layer do not propagate through the entire thickness, and the crack spacing of the TBC layer (Figure 4d) is much smaller than that predicted using continuum mechanics.[27] In addition, TMF tests on samples with a center-hole clearly demonstrate that cracking is related to tensile stress/strain concentrations.[27] Following cracking of the TBC layer, void formation in the bond coat below the cracks can occur, and new oxide forms in the exposed alloy. The width of the cracks in the TBC layer typically has a wide distribution, and the cracks below wider TBC layer cracks propagate deeper into the bond-coat layer (Figure 4c and 4f). The evidence suggests that there is a sequence of cracking in the TBC oxide. After cracking of the TBC, the life of the system is similar to that of the bare superalloy. Another form of damage is large area delamination where the bond coat and superalloy are locally exposed to higher temperatures (Figure 4g). Anisotropic growth and stress distribution in the TGO layer (Figure 4h–i) are also observed and analyzed.[25,29]

Sensing and non-destructive evaluation

Luminescence sensing

Concurrent with developments in testing the mechanical properties of TBC systems, there have been explorations of new sensing approaches. For instance, as the temperatures at the TBC surface and at the TGO are critical parameters, there has been an emphasis on non-contact methods of measuring temperature at these locations. One method that has shown particular promise is luminescence sensing based on the dependence of photoluminescence lifetime on temperature. Luminescence is also used to monitor delamination by detecting the interface

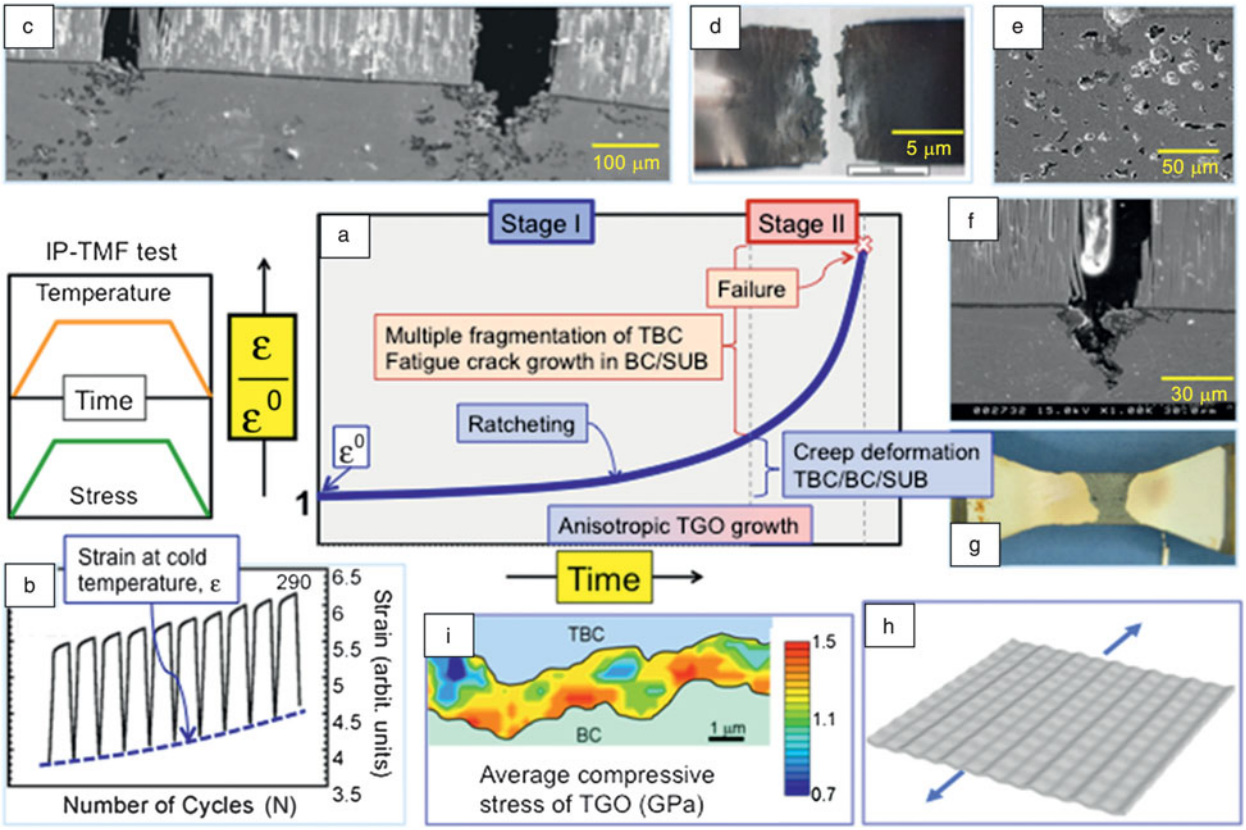

Figure 4. Examples of typical behavior and damage in an electron-beam physical vapor deposited thermal-barrier coating (TBC) system during in-phase thermomechanical fatigue (IP-TMF) testing mode: (a) Creep curve of normalized average strain $\varepsilon/\varepsilon^0$, where ε^0 is strain at first loading. SUB, substrate; BC, bond-coat layer. (b) Ratcheting behavior of the TBC system shown by the increasing strain at low temperature after each loading cycle. Scanning electron microscopy (SEM) images (c–f) show (c) TBC layer cracking (image of a polished section, parallel to loading axis), (d) macroscopic appearance of multiple fragmentation of TBC layer, (e) void formation in the BC layer, and (f) fatigue crack growth and new thermally grown oxide (TGO) formation in the BC layer. (g) Delamination of TBC layer, (h) illustration of anisotropic TGO morphology (arrow, loading direction), and (i) an example of stress distribution in the TGO layer.

temperature changes and interface luminescence reflectivity.[30–33] In this method, luminescent rare-earth ions are incorporated into the crystal structure of the YSZ coating during deposition of the EBPVD coating so that they are localized, for instance, at the ceramic topcoat/TGO interface and then again at the topcoat surface. During high temperature testing, they are stimulated by a pulsed laser, and the decay of the excited luminescence is monitored. In addition to being a non-contact method, the rare-earth dopant can also be localized to a smaller depth than the optical penetration depth in optical pyrometry, giving superior depth resolution.

This temperature sensing methodology has recently been demonstrated using EBPVD 7YSZ TBCs[30,33,34] with an integrated luminescence sensing layer composed of europium doped YSZ at the TBC/bond-coat interface. The experimental setup is illustrated in **Figure 5**a.[30] A solid-state frequency doubled YAG:Nd laser emitting at 532 nm illuminates the center of the coating surface, while the high heat flux CO_2 laser is used for heating the specimens under large thermal gradients. A sapphire light pipe is positioned to collect the excited luminescence signal during the testing. Figure 5b shows the luminescence sensor measured real-time interface temperature under various heat flux conditions, demonstrating the ability to collect luminescence from a thin embedded sensor layer in TBC systems under high temperature thermal gradients.

Infrared imaging

The key to extending the use of TBCs is assessing damage, especially sub-critical coating delamination, prior to coating failure. In particular, early detection of TBC damage also enables a part to be replaced and, possibly, repaired. The majority of non-destructive methods for this type of monitoring utilize spectral variations in the optical properties of YSZ. For instance, at 10.6 μm, the wavelength of CO_2 lasers, YSZ is heavily absorbing, but it is translucent in the visible and near infrared (IR). One approach is to image local separations between the coating and alloy based on variations in reflectivity of thermal waves launched by pulse heating of the coating surface. The larger effusivity at the delamination than at the interface between the TBC and the underlying alloy locally causes a greater thermal reflectivity and hence higher image contrast, enabling an image to be formed of large delaminations. In the visible, YSZ is

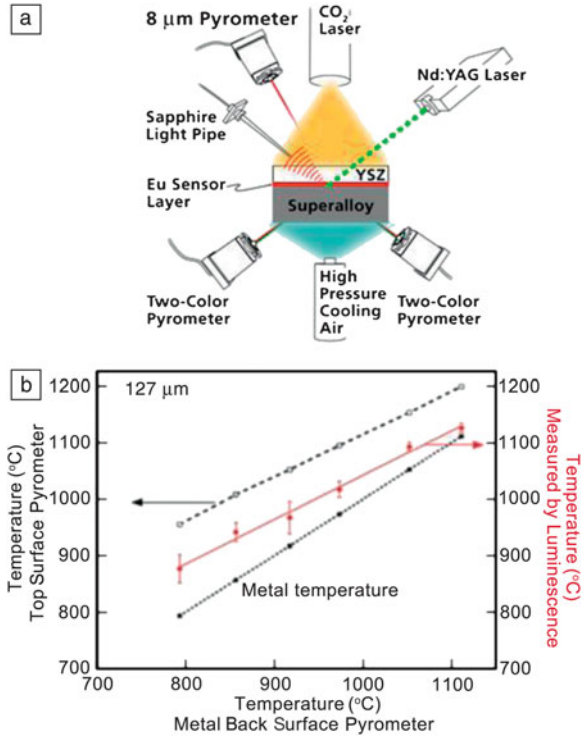

Figure 5. (a) Experimental setup for measuring the thermal-barrier coating (TBC)/metal interface temperature through the TBC by Eu luminescence under laser high heat flux thermal gradient tests.[30] (b) TBC interface temperature measured as a function of TBC surface and metal back surface temperatures with various heat fluxes, for two electron beam physical vapor deposited coating thicknesses. A good correlation of the sensor measurements with the heat flux measurements has been observed with an embedded Eu-YSZ sensor at high temperature.[30,34]

transparent but highly scattering. However, in the mid-IR, the scattering is reduced, enabling optical imaging of delaminations in both EBPVD and plasma-sprayed TBCs.[35]

Recently, it has also been demonstrated that with advances in IR focal plane array cameras, it is now possible to perform real-time, online near-IR monitoring of rotating blades during engine operation. This offers the prospect of increasing gas turbine operational reliability, especially by minimizing engine shutdown or outage time. In addition, with a link to component computer aided design (CAD) models, thermal design models can be validated by *in situ* temperature measurements. This is expected to enable better diagnosis and prognostics of component integrity for more advanced engine operation.

As the technology of focal plane imaging has become more sophisticated, the number, types, and pixels of array detectors have greatly increased. Together with more selective filtering capabilities, these detectors can more efficiently be matched to specific applications, improving measurement performance. When used with complex algorithms to provide real-time linearization and compensation of the detector output, higher precision temperature measurements become feasible. For instance, measuring the temperatures of high speed rotating components using focal plane technology requires very short integration (<3 ms) or the ability to have photons fill the focal plane to form a snapshot in microseconds and even nanoseconds, thus creating qualitative spatial detail of the rotating blade. In effect, every imaging pixel is a pyrometer. In a recent Siemens implementation, a telescopic lens system is used to image a portion of the blades onto a focal plane array over the spectral range of 0.9 μm to 1.6 μm, avoiding characteristic emissions from combustion from gas species, such as CO_2 and H_2O, while also maximizing the sensitivity of the array to the peak of the black body radiation from the blades.

Radiation reaching the detector includes contributions from three sources: (1) radiation emitted from the surface of the turbine component being imaged, (2) reflected radiation included from particulates in the gas stream, as well as (3) radiation emitted from hot gases and particles in the field of view. A methodology was developed to overcome these hurdles and perform the surface temperature measurements. **Figure 6** illustrates features that can be seen during engine operation using state-of-the-art focal plane arrays with advanced software imaging (see Figure 1 in the introductory article for an image of turbine blades). These include (a) TBC spallation on the leading edge of the blade as seen by the dark edge of the TBC, (b) local heating due to rubbing between two components—bright feature near rub, (c) local cooling at a blade platform—dark due to cooling air leakage, (d) platform TBC delamination, observed as bright/dark line corresponding to a buckled TBC, (e) overlapping cooling holes on the blade, where the dark cooling streams are not giving good coverage, and (f) a platform TBC crack observed as a faint bright line, verified by the visual picture shown in the inset in Figure 6f.

One exciting development in inspection methods is combining thermal imaging with ultrasonics. The concept is to induce vibrations in a component or an array of blades, for instance, with an ultrasonic source and use a highly sensitive focal plane array to image the locations of frictional heating.[36] This has recently been implemented, for instance, in the Siemens acoustic thermography system, SIEMAT, for the detection of cracks and kissing (detached) bonds in parts. Its attributes include high sensitivity to tight interfaces, the ability to see defects through coatings, and the ability to inspect components with minimal preparation.[37,38] Post-processing algorithms are then used to assist in the identification of defects.

Summary and outlook

It is abundantly clear that testing and evaluation of thermal-barrier coatings (TBCs) is extremely challenging, yet TBC progress depends critically on our ability to test, evaluate, and monitor TBCs under conditions relevant to engine operation. New methods for measuring mechanical properties of TBCs will need to be developed with a deep understanding of TBC failure mechanisms. Thermomechanical fatigue and thermal gradient testing under realistic engine conditions are also needed to more accurately simulate TBC failure that is

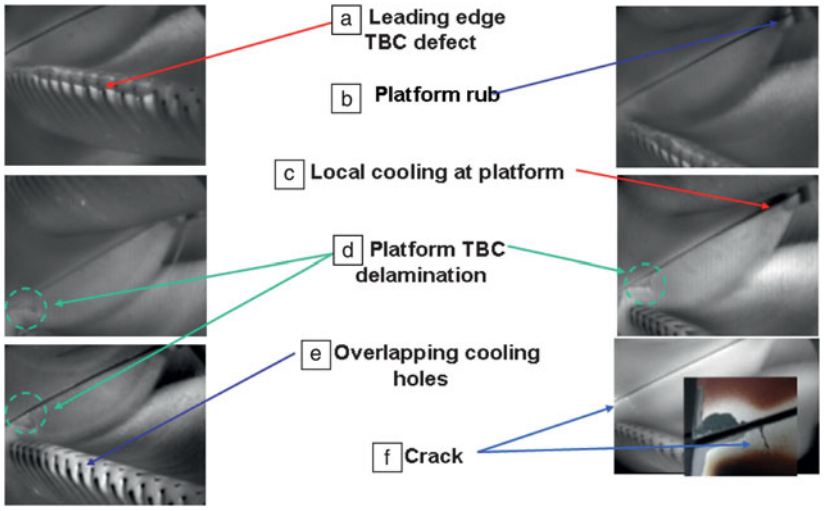

Figure 6. Example of turbine features that can be observed by an infrared camera during engine operation at 3600 rpm with gas path temperatures higher than 1200°C. Pictures are "still" frames of rotating blades. (a) Thermal-barrier coating (TBC) spallation on the leading edge of the blade as seen by the dark edge of the TBC; (b) local heating due to rubbing between two components—bright feature near rub; (c) local cooling at a blade platform—dark due to cooling air leakage; (d) platform TBC delamination, observed as bright/dark line corresponding to a buckled TBC; (e) overlapping cooling holes, where the dark cooling streams are not giving good coverage; and (f) platform TBC crack observed as a faint bright line.

representative of what happens in operating engines. Sensing, nondestructive evaluation, and *in situ* monitoring of TBC health are critical for the intelligent operation of engines with maximum utilization of TBCs and to avoid catastrophic failure.

References

1. D. Zhu, R.A. Miller, *Surf. Coat. Technol.* **108–109**, 114 (1998).
2. F. Yu, T.D. Bennett, *J. Appl. Phys.* **98**, 103501 (2005).
3. K.W. Schlichting, K. Vaidyanathan, Y.H. Sohn, E.H. Jordan, M. Gell, N.P. Padture, *Mater. Sci. Eng., A* **291**, 68 (2000).
4. A.L. Heyes, J.P. Feist, X. Chen, Z. Mutasim, J.R. Nicholls, *J. Eng. Gas Turbines Power* **130**, 061301 (2008).
5. S. Song, P. Xiao, *Mater. Sci. Eng., B* **97**, 46 (2003).
6. D. Renusch, M. Schütze, *Surf. Coat. Technol.* **202**, 740 (2007).
7. P.G. Bison, S. Marinetti, E. Grinzato, V.P. Vavilov, F. Cernuschi, D. Robba, *Proc. SPIE* **5073**, 318 (2003).
8. www.nist.gov/mml/ctcms/oof/index.cfm.
9. C. Mercer, J.R. Williams, D.R. Clarke, A.G. Evans, *Proc. R. Soc. London, Ser. A* **463**, 1393 (2007).
10. J. Malzbender, T. Wakui, E. Wessel, R.W. Steinbrech, *Fract. Mech. Ceram.* **14**, 435 (2005).
11. M. Dononue, N.R. Philips, M.R. Begley, C.G. Levi, *Acta Mater.* (2012), in press.
12. R. Vaßen, N. Czech, W. Malléner, W. Stamm, D. Stöver, *Surf. Coat. Technol.* **141**, 135 (2001).
13. D. Zhu, R.A. Miller, *J. Mater. Res.* **14**, 146 (1999).
14. D. Zhu, R. A. Miller, *Surf. Coat. Technol.* **94**, 94 (1997).
15. F. Traeger, R. Vaßen, K.-H. Rauwald, D. Stöver, *Adv. Eng. Mater.* **5**, 429 (2003).
16. T. Steinke, D. Sebold, D.E. Mack, R. Vaßen, D. Stöver, *Surf. Coat. Technol.* **205**, 2287 (2010).
17. D. Zhu, R.A. Miller, *J. Therm. Spray Technol.* **9**, 175 (2000).
18. D. Zhu, R.A. Miller, B.A. Nagaraj, R.W. Bruce, *Surf. Coat. Technol.* **138**, 1 (2001).
19. D. Zhu, R.A. Miller, *MRS Bull.* **27**, 43 (2000).
20. D. Zhu, S.R. Choi, R.A. Miller, *Surf. Coat. Technol.* **188–189**, 146 (2004).
21. B. Baufeld, E. Tzimas, H. Mullejans, S. Peteves, J. Bressers, W. Stamm, *Mater. Sci. Eng., A* **315**, 231 (2001).
22. A. Peichl, T. Beck, O. Vohringer, *Surf. Coat. Technol.* **162**, 113 (2003).
23. E. Tzimas, H. Mullejans, S.D. Peteves, J. Bressers, W. Stamm, *Acta Mater.* **48**, 4699 (2000).
24. P.K. Wright, *Mater. Sci. Eng., A* **245**, 191 (1998).
25. R. Kitazawa, PhD Thesis, The University of Tokyo (2012).
26. R. Kitazawa, M. Tanaka, Y. Kagawa, Y.F. Liu, *Mater. Sci. Eng., B* **173**, 130 (2010).
27. M. Tanaka, C. Mercer, Y. Kagawa, A.G. Evans, *J. Am. Ceram. Soc.* **94**, 128 (2011).
28. M. Tanaka, Y.F. Liu, S.S. Kim, Y. Kagawa, *J. Mater. Res.* **23**, 2382 (2008).
29. D.S. Balint, S.-S. Kim, Y.-F. Liu, R. Kitazawa, Y. Kagawa, A.G. Evans, *Acta. Mater.* **59**, 5524 (2011).
30. M.M. Gentleman, J.I. Eldridge, D.M. Zhu, K.S. Murphy, D.R. Clarke, *Surf. Coat. Technol.* **201**, 3937 (2006).
31. M.D. Chambers, D.R. Clarke, *Annu. Rev. Mater. Res.* **39**, 325 (2009).
32. A. Rabhiou, J. Feist, A. Kempf, S. Skinner, A. Heyes, *Sens. Actuators, A* **169**, 18 (2011).
33. J.I. Eldridge, D. Zhu, D.E. Wolfe, *Ceram. Eng. Sci. Proc.* **32**, 3 (2011).
34. M.M. Gentleman, PhD thesis, University of California, Santa Barbara (2007).
35. J.I. Eldridge, C.M. Spuckler, R.E. Martin, *Intl. J. Appl. Ceram. Technol.* **3**, 94 (2006).
36. X. Han, V. Loggins, Z. Zeng, L.D. Favro, R.L. Thomas, *Appl. Phys. Lett.* **85**, 1332 (2004).
37. C. Homma, M. Rothenfusser, J. Baumann, R. Shannon, *Proc. Rev. Prog. Quantum NDE, AIP*, **820**, 566 (2006).
38. M. Rothenfusser, C. Homma, *Proc. Rev. Prog. Quantum NDE, AIP*, **760**, 624 (2005). □

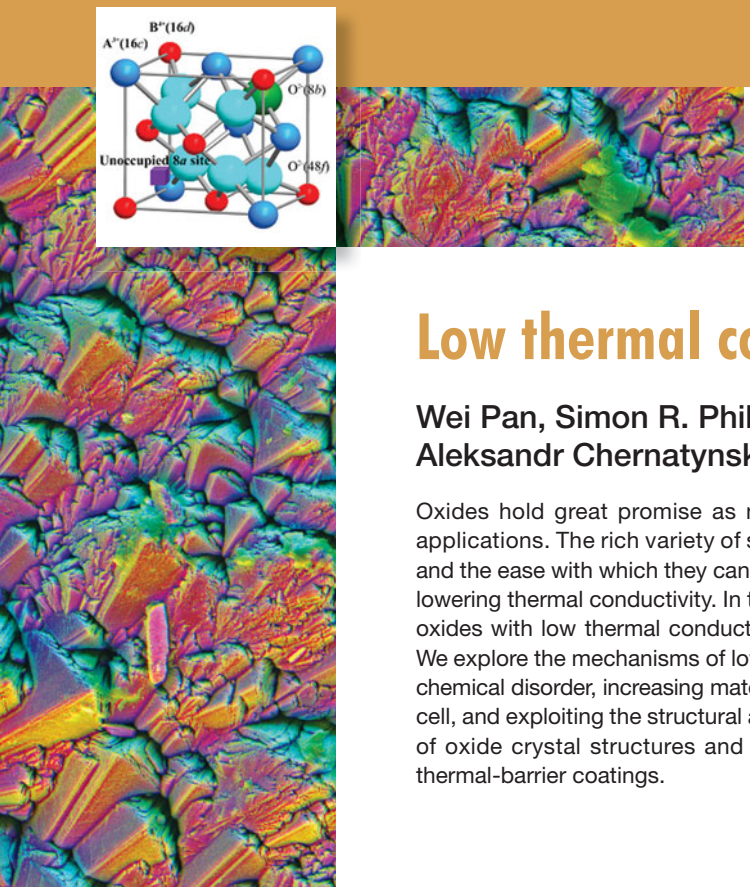

Low thermal conductivity oxides

Wei Pan, Simon R. Phillpot, Chunlei Wan, Aleksandr Chernatynskiy, and Zhixue Qu

Oxides hold great promise as new and improved materials for thermal-barrier coating applications. The rich variety of structures and compositions of the materials in this class, and the ease with which they can be doped, allow the exploration of various mechanisms for lowering thermal conductivity. In this article, we review recent progress in identifying specific oxides with low thermal conductivity from both theoretical and experimental perspectives. We explore the mechanisms of lowering thermal conductivity, such as introducing structural/chemical disorder, increasing material density, increasing the number of atoms in the primitive cell, and exploiting the structural anisotropy. We conclude that further systematic exploration of oxide crystal structures and chemistries are likely to result in even further improved thermal-barrier coatings.

Introduction

The need for thermal-barrier coating (TBC) materials with lower thermal conductivity than the currently used 7% yttria-stabilized zirconia (7YSZ) composition that can also operate in the strongly oxidative environment of combustion gases has stimulated a worldwide effort to identify new oxide compositions (see the introductory article in this issue). It has also stimulated a better understanding of the factors that determine low thermal conductivity in crystalline solids at high temperatures. Although TBC materials must satisfy a wide range of requirements, the primary performance metric is their thermal conductivity at operating temperatures of 1250°C and above. Depending on the processing technology and conditions, the thermal conductivity of 7YSZ lies in the range of 1.2–1.8 W m^{-1} K^{-1}; we are therefore most interested in materials with thermal conductivities below ~1 W m^{-1} K^{-1}. For the foreseeable future, the operating temperatures are still not high enough for appreciable radiative heat transfer unless the coating material contains ions that absorb in the infrared.[1] As this article will describe, an impressive number of new oxide materials have been identified in the last decade that have conductivities lower than 7YSZ; the thermal conductivities of the emerging ceramics for TBC are summarized in **Figure 1**a–b. There are good reasons to believe that the continued search, combining crystal chemistry principles and simulation, will identify others. Unless otherwise noted, all the conductivity values presented are for fully dense materials without porosity, since porosity can significantly reduce the measured conductivity. Indeed, porosity is deliberately introduced into TBCs to decrease the thermal conductivity as well as increase strain compliance. We provide an overview of recently identified low thermal conductivity oxides and discuss the mechanisms involved in the minimization of the thermal conductivity.

Yttria-stabilized zirconia

The most widely used TBC material is YSZ, zirconia containing 6–8 wt% Y_2O_3 (equivalent to about 3.4–4.5 mol%), which is produced in a metastable tetragonal phase (t').[2] Alloying zirconia with yttria is necessary to avoid the disruptive monoclinic to tetragonal phase transformation that would otherwise cause mechanical breakdown of the zirconia; however, it also reduces the thermal conductivity by creating point defects that scatter phonons. The introduction of Y^{3+} as an aliovalent dopant on the Zr^{4+} site is compensated by vacant oxygen sites. Interestingly, because of the similarity in atomic mass between the Y^{3+} and Zr^{4+} ions, the oxygen vacancies are primarily responsible for reducing thermal conductivity.

A physical picture of thermal transport in solids is given by propagating lattice waves, known as phonons. Scattering of these waves off of each other, as well as off of the defects in

Wei Pan, State Key Lab of New Ceramics and Fine Processing, Tsinghua University, Beijing, China; panw@mail.tsinghua.edu.cn
Simon R. Phillpot, Department of Materials Science and Engineering, University of Florida, Gainesville, FL; sphil@mse.ufl.edu
Chunlei Wan, Graduate School of Engineering, Nagoya University, Nagoya, Japan; chunlei.wan@gmail.com
Aleksandr Chernatynskiy, Department of Materials Science and Engineering, University of Florida, Gainesville, FL; avtche01@gmail.com
Zhixue Qu, College of Materials Science and Engineering, Beijing University of Technology, Beijing, China; quzhixue@bjut.edu.cn
DOI: 10.1557/mrs.2012.234

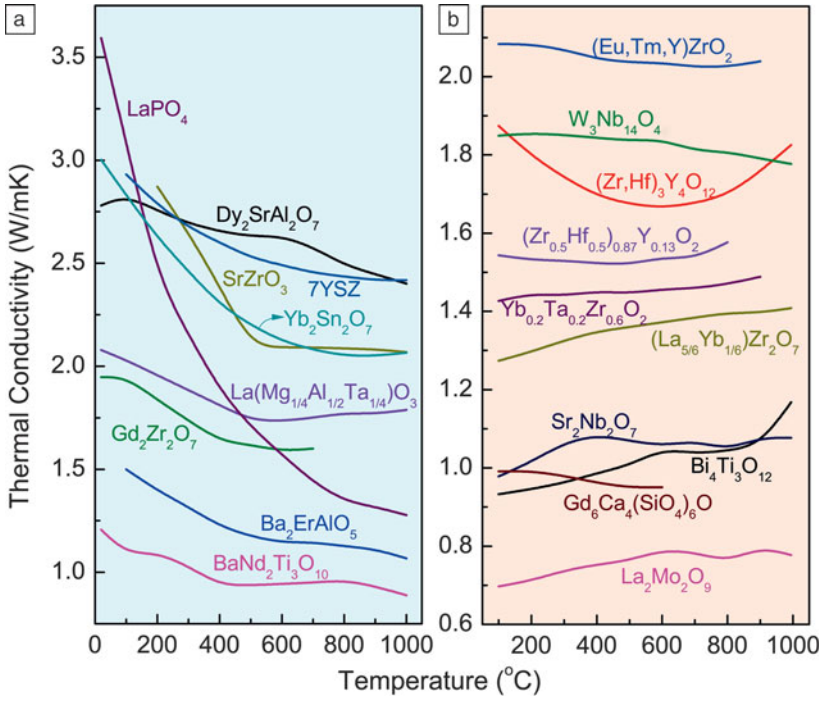

Figure 1. (a) Thermal conductivity summary of the emerging ceramics for thermal-barrier coatings, whose conductivities vary with temperature, including 7YSZ,[23] $Gd_2Zr_2O_7$,[22] $Yb_2Sn_2O_7$,[21] $SrZrO_3$,[29] $La(Mg_{1/4}Al_{1/2}Ta_{1/4})O_3$,[31] Ba_2ErAlO_5,[32] $Dy_2SrAl_2O_7$,[33] $BaNd_2Ti_3O_{10}$, and $LaPO_4$;[38] (b) temperature-independent thermal conductivities of ceramics, including $Yb_{0.2}Ta_{0.2}Zr_{0.6}O_2$,[13] $(La_{5/6}Yb_{1/6})Zr_2O_7$,[27] $Gd_6Ca_4(SiO_4)_6O$,[40] $La_2Mo_2O_9$,[23] $Bi_4Ti_3O_{12}$,[35] $(Zr,Hf)_3Y_4O_{12}$,[23] $(Eu,Tm,Y)ZrO_2$, $W_3Nb_{14}O_4$,[23] $Sr_2Nb_2O_7$, and $(Zr_{0.5}Hf_{0.5})_{0.87}Y_{0.13}O_2$.

the crystal lattice, impedes energy flow and pronounces itself as a thermal resistivity. Although models for the reduction in thermal conductivity from point defects based on this physical picture describe the basic mechanisms well,[3] molecular dynamics simulations reveal a more complex situation in YSZ. Interestingly, the physics is very similar in off-stoichiometric fluorite-structured UO_2, the dominant fuel system for nuclear fission reactors.[4,5] These studies show that with increasing defect concentration, the thermal conductivity transitions from that characteristic of a crystalline material to that characteristic of an amorphous solid.[6] This transition can be described in terms of the structure of the vibrational modes of the system. These can be classified as propagons (normal phonon modes that are delocalized with well-defined momentum and polarization), diffusons (delocalized like phonons, but no longer possessing well-defined polarizations), and locons (strongly localized modes). While the vibrational modes in a crystalline solid are essentially all propagons, the vibrations in amorphous materials contain diffusons (~93% of all modes in a-Si); these modes are far less efficient heat carriers. In both YSZ and UO_2, propagon modes only appear at the low-frequency end of the spectrum (<2 THz), while locons are concentrated at the high end (>26 THz). In the case of YSZ, complete transition to amorphous-like heat transport dominated by the diffusons takes place at about 24 YSZ (24% yttria): further increase of the Y_2O_3 content does not affect the structure of the vibrational spectrum. These molecular dynamics simulations indicate that more detailed exploration of the different forms of phonons in other complex oxides should be especially insightful.

The limitation in using YSZ at much higher temperatures than currently used is that the metastable tetragonal (t') phase partitions by diffusion into the equilibrium tetragonal (t) and cubic phases (c) at high temperatures; the former of which will transform into a monoclinic phase (m) during cooling, resulting in disintegration of the coating. This is a slow process, taking more than 100 hr at temperatures in excess of 1350°C before monoclinic zirconia is detectable.[7] To slow down this transformation and also lower the thermal conductivity, stabilizers other than yttria have been sought. Stabilization with rare-earth oxides, such as Gd_2O_3, Yb_2O_3, and Nd_2O_3, results in lower thermal conductivities than that of YSZ[8,9] as a result of larger mass difference between the dopant and zirconia. However, with the exception of Yb_2O_3, these ions actually decrease the resistance to destabilization of the t' phase.[10]

Co-doping zirconia with two or more oxides, one a trivalent oxide such as Y_2O_3 and the other a pentavalent oxide such as Nb_2O_5 or Ta_2O_5, has been shown to reduce the thermal conductivity.[11,12] Of particular interest is the compositional range over which the concentrations of trivalent and pentavalent ions are equal. In this range, a stable non-transformable tetragonal zirconia can form, with thermal conductivity almost half that of the conventional YSZ, despite the absence of oxygen vacancies.[11–13] Moreover, yttria can be replaced by other heavier rare-earth oxides, which can further reduce the thermal conductivity to 1.4 W m^{-1} K^{-1} at 900°C for Yb-Ta co-doped zirconia.[13,14]

A further route to optimizing the performance involves the addition of paired dopants, such as Nd_2O_3 (or Gd_2O_3) and Yb_2O_3 (and/or Sc_2O_3), into the ZrO_2-Y_2O_3 system, which segregate into 5–100 nm defect clusters and can reduce the thermal conductivity by about 20–40%, compared with the baseline ZrO_2-Y_2O_3 ceramics.[15–17] Meanwhile, these thermodynamically immobile defect clusters can significantly enhance the sintering resistance of the coating at high temperatures.

Pyrochlore materials

Increasing the complexity of the crystal structure tends to reduce the thermal conductivity due to the increasing number of optical phonons that tend not to contribute substantially to the thermal conductivity. This is primarily due to typically small group velocities of the optical phonons as compared to acoustic phonons. Additionally, increasing the number of optical states also increases the number of available phonon-phonon interactions, further reducing thermal conductivity.

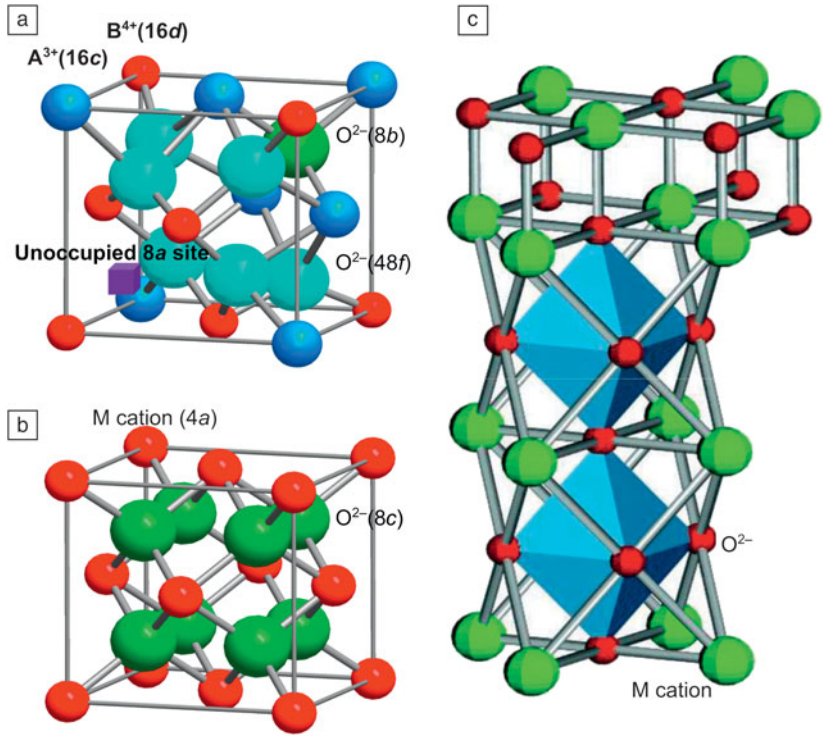

Figure 2. (a) A 1/8 unit cell of the $A_2B_2O_7$-type pyrochlore structure that can be adopted by low thermal conductivity rare-earth zirconates (A = rare earth element, B = Zr), indicating lattice sites and the unoccupied oxygen position. (b) The defect fluorite structure that can be induced in heavier rare-earth zirconates or by heat treatment of pyrochlore-type $Gd_2Zr_2O_7$ and shows similar thermal conductivities to the pyrochlores. In this structure, the cations are completely disordered, and the occupancy for each anion site is 0.875.[33] (c) An example of a perovskite-structured oxide: The layered Ruddlesden–Popper phase of Sr-Ti-O.[34] The oxygen octahedra of the two perovskite unit cells are outlined in blue, and the single rock salt layer is shown at the top.

The $A_2B_2O_7$-pyrochlore structure is one of a number of more complex crystal structures based on the fluorite structure of zirconia. It has a unit cell consisting of eight fluorite-like subcells, each of which contains one vacant oxygen site defect (the subcell of the pyrochlore structure is shown in **Figure 2a**). Both the presence of vacant sites and the larger unit cell should lower the thermal conductivity. Indeed, pyrochlore compounds of rare earth zirconates (where A= rare-earth element and B = Zr) exhibit extremely low thermal conductivity, ranging from ~1.1–1.7 W m^{-1} K^{-1} at temperatures between 700°C and 1200°C for A = La, Eu, Sm, Nd, and Gd.[18] The stability of the pyrochlore structure is sensitive to the ratio of the A and B cation radii.[19] Thermal conductivity simulations have been performed on the large family of pyrochlores with A = La, Pr, Nd, Sm, Eu, Gd, Y, Er, or Lu and B = Ti, Mo, Sn, Zr, or Pb.[20] **Figure 3** presents the resultant map of the thermal conductivity as a function of the A and B ionic radii. Of particular note is that increasing the B-cation radii consistently reduces thermal conductivity, whereas the A cation size has less of an effect. As yet, there is insufficient experimental data to confirm the details of this property map.[21] Large rare-earth ions in $Ln_2Zr_2O_7$ (Ln = La, Nd, Sm, Gd) can lead to a stable pyrochlore structure up to at least 1500°C.[22] $Gd_2Zr_2O_7$ can also take on a defected fluorite structure (Figure 2b) if suitably heat-treated, but the thermal conductivity was found to be the same as its pyrochlore counterpart.[22] It is interesting to note that a different defective fluorite structure, the delta-phase, is formed with smaller rare-earth ions, such as Dy, Er, Yb, and Y, and that these too have thermal conductivity similar to those of pyrochlores.[23,24]

The expectation that doping and alloying will reduce thermal conductivity is borne out experimentally. Some success has been achieved, at least up to ~800°C, as exemplified by $La_2Zr_2O_7$, which when doped with 30 at.% Gd displays a decrease in thermal conductivity from ~1.55 W m^{-1} K^{-1} to ~0.9 W m^{-1} K^{-1}.[25] In addition to lowering the thermal conductivity due to alloy scattering, doping can change the pyrochlore structure itself in ways that affect the thermal conductivity.[26] For example, in the $(Sm_{1-x}Yb_x)_2Zr_2O_7$ series, there is a transition from pyrochlore to a more disordered fluorite state when the x value lies between 1/6 and 1/3, at which there is also a dip in the thermal conductivity.[26] By contrast, in $(La_{1-x}Yb_x)_2Zr_2O_7$, the Yb^{3+} was found to "rattle" (undergo very large localized thermal vibration) at the 16 c-site, which could lead to a glass-like thermal conductivity.[27] Among the mentioned pyrochlores, some oxides such as $Sm_2Zr_2O_7$, $Gd_2Zr_2O_7$, and their composites may become the potential materials for TBCs, owing to the better comprehensive mechanical and thermal performances.

Perovskite-structured oxides

The ABO_3-type perovskites are another class of material that show both a large number of options for the A and B

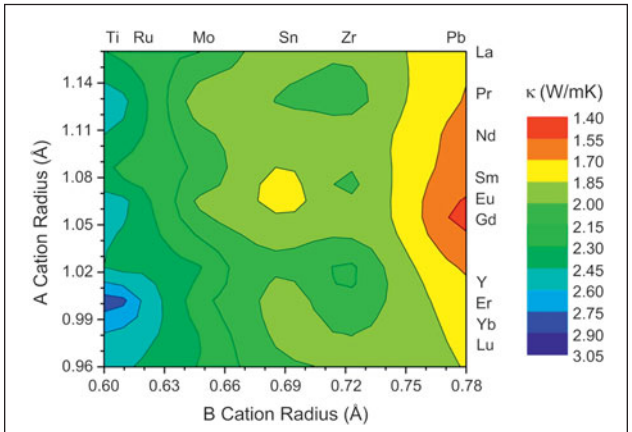

Figure 3. Contour map of thermal conductivity (κ) determined at T = 1473 K by simulation, as a function of ionic radii of the A and B ions for pyrochlore $A_2B_2O_7$.[20]

cations, and display a large number of structural variants.[28] They therefore seem to be good candidates for engineering the thermal conductivity. Pure ABO_3 perovskites containing high atomic mass ions exhibit low thermal conductivities, for example, 2.1 W m^{-1} K^{-1} for $SrZrO_3$[29] and 3.4 W m^{-1} K^{-1} for $BaZrO_3$[18] at 1000°C on account of the structural rigidity of corner-shared octahedra.[29] However, following the strategy that was so successful for fluorite, Yb_2O_3 has been doped onto the B site of $SrZrO_3$, leading to a 20% reduction in the thermal conductivity over the temperature range of 200–1200°C.[30] Moreover, increasing the doping level can lead to new complex perovskite structures. For example, $Ba(Mg_{1/3}Ta_{2/3})O_3$ has a melting temperature of ~3000°C and is considered among the most refractory of all oxides;[15] its thermal conductivity reaches 2.5 W m^{-1} K^{-1} at 1100°C. Likewise, the $La(Al_{1/4}Mg_{1/2}Ta_{1/4})O_3$ complex perovskite system shows a low value of thermal conductivity (~2 W m^{-1} K^{-1}) and high coefficient of thermal expansion (~11.9 × 10^{-6} K^{-1}), which is a promising combination for TBC applications. However, TBCs made of these complex perovskites show short thermal cycling life, possibly due to their low toughness and consequent weak thermal shock resistance.[31]

Bearing a similar relationship to the perovskite structure as the pyrochlore structure does to fluorite, Ba_2LnAlO_5 (Ln = lanthanide element), in which one-sixth of the oxygen sites in the perovskite structure are vacant, has a thermal conductivity of only 1.1 W m^{-1} K^{-1} at 1000°C.[32] Again following the strategy of increasing the size of the unit cell and increasing the number of atoms per unit cell, thereby increasing the number of optical phonons and reducing the thermal conductivity, the perovskite structure can also be a building block for complex superlattice structures. The thermal conductivities of Ruddlesden–Popper (RP) structures of $Ln_2SrAl_2O_7$[33] and $Sr_{n+1}Ti_nO_{3n+1}$[34] (**Figure 2**c), the Aurivillius phases[35] of $Bi_4Ti_3O_{12}$, and the Dion–Jacobson phases of $BaLa_2Ti_3O_{10}$[36] have been studied, all producing thermal conductivities of 1–2 W m^{-1} K^{-1}, which are substantially lower than the typical value of 2.5 W m^{-1} K^{-1} for 7YSZ. As shown in Figure 2c, the RP structure consists of n (n = 1, 2,...) layers of perovskite structured material separated by a rock salt structured layer; the Aurivillius and Dion–Jacobson phases show analogous layered perovskite structures.

Lanthanide orthophosphates and silicates

The lanthanide orthophosphates ($LnPO_4$) are another set of compounds with low thermal conductivities.[37] The orthophosphates can take on either a monazite or xenotime crystal structure, depending on the ionic size of the lanthanide ions. Monazite $LnPO_4$ (Ln = La-Gd) is expected to show a distinctly lower thermal conductivity than the xenotime structure compounds due to its lower crystal symmetry and weaker bonds.[23,38] The anisotropy of thermal conductivity of the most studied monazite compound $LaPO_4$ is also noticeable, due to the non-cubic crystal structure.[39] However, the characteristics of the line compound (small deviations from the stoichiometry can significantly change the solidus temperature, thereby making it hard to apply the plasma spraying process to make coatings) and poor adherence to the bond-coat layer (between the TBC and the superalloy) limits the applications of $LaPO_4$ as a TBC.[37]

Based on their large unit cell and complex structures, the rare-earth silicates (**Figure 4**) can be expected to yield low thermal conductivity values. Among these, apatite structured $Gd_8Ca_2(SiO_4)_6O_2$ has attracted particular attention;[40] it exhibits an extremely low and temperature-independent thermal conductivity of about 1.4 W m^{-1} K^{-1} for almost fully dense samples. Another interesting feature of this compound is that the composition can be systematically altered by adjusting the relative proportions of alkaline earth cations and rare-earth ions to introduce different populations of oxygen vacancies, cation vacancies, and oxygen interstitials, resulting in even lower thermal conductivities for defect-containing compositions (**Figure 5**).[40]

Thermal expansion coefficient

While thermal conductivity is the key performance metric for potential TBC materials, it is also essential that they be thermomechanically compatible with both the superalloy that they coat and the intermediate bonding layers (see the introductory article in this issue). The thermal expansion coefficient of YSZ is 10.7 × 10^{-6} K^{-1} from room temperature to 1273 K,[41] while those of the typical superalloy substrate and bond coat (NiCrAlY) are 16 × 10^{-6} K^{-1} and 17.5 × 10^{-6} K^{-1}, respectively, for the same temperature range.[41] This mismatch can lead to high thermal stresses that have the potential to promote coating failure. Although YSZ coatings can last tens of thousands of hours and multiple cycling without failing, it is still believed

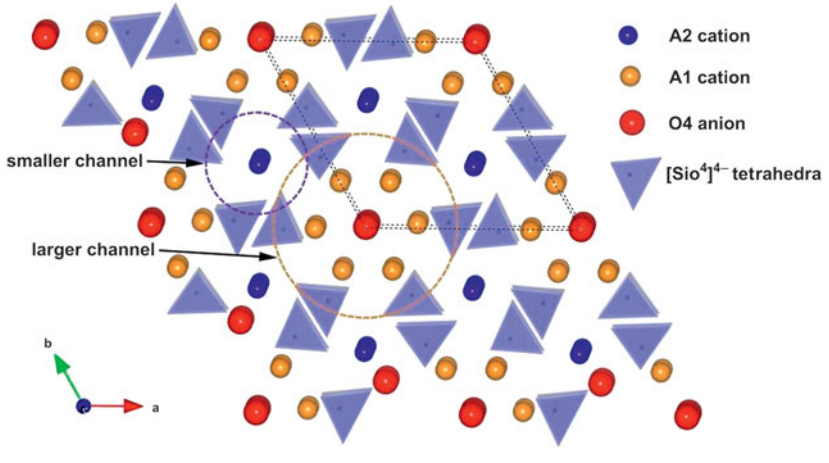

Figure 4. View of the crystal structure of the stoichiometric rare-earth apatites $A_{10}(SiO_4)_6O_{2+\delta}$, along the [001] axis, and the location of the two types of cation sites, A1 and A2, as well as the oxygen sites, O4.[40] The complexity and large unit cell of this structure is believed to give rise to low thermal conductivity in materials such as $Gd_8Ca_2(SiO_4)_6O_2$.

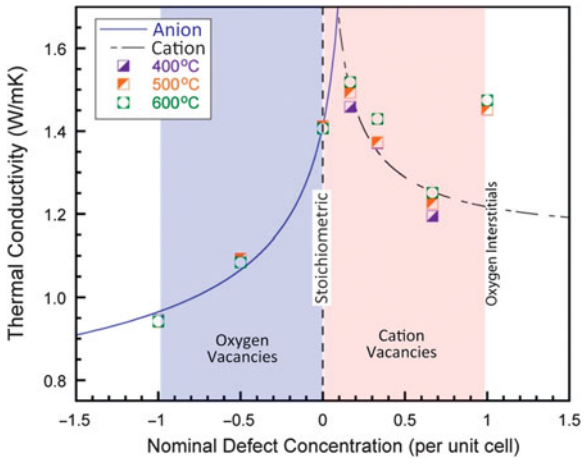

Figure 5. Thermal conductivity of rare-earth apatites in the range 400–600°C as a function of nominal defect concentration per unit cell. One defect per unit cell corresponds to a concentration of 2.5 at.%.[40] The thermal conductivities agree well with the trend predicted by the simple defect scattering model, in which the thermal conductivities are proportional to the inverse square root of the anion and cation vacancy concentrations.

that enhancement of the thermal expansion coefficients of TBCs could minimize this mismatch and thereby further improve the thermal cycling lifetime of TBCs. Ceria (CeO_2), which has a high thermal expansion coefficient and relatively low thermal conductivity, has been found to improve the thermal expansion behavior of zirconia-based ceramics. For example, Sodeoka et al.[42] observed that the average thermal expansion coefficient of pure zirconia over the range of 25–800°C increases to $12.5 \times 10^{-6}\ K^{-1}$ with the addition of CeO_2. Moreover, Cao et al.[43] proposed lanthanum-cerium oxide ($La_2Ce_2O_7$) as a potential TBC material; it has a thermal expansion coefficient as high as about $13 \times 10^{-6}\ K^{-1}$ at elevated temperature, though it displays a sharp decrease between 180°C and 300°C. The thermal expansion coefficient of pyrochlore-type $Sm_2Zr_2O_7$ can be improved from $10.8 \times 10^{-6}\ K^{-1}$ [22] to $11.9 \times 10^{-6}\ K^{-1}$ [44] with 7.5 mol% doping of MgO, as the relatively smaller Mg^{2+} can easily get into the interstitial site of the crystal, thereby weakening the bonds of ZrO_6 octahedra. These successes notwithstanding, there remains a substantial gap between the thermal expansion coefficients of TBC materials and the bond coat and alloy.

Conclusions and outlook

The fluorite system provides a blueprint for a successful design strategy of starting with a crystal structure that can accommodate a large number of different chemical species and making it chemically and structurally more complex, has proven fruitful in developing low thermal conductivity materials for possible thermal-barrier coating (TBC) applications. This strategy is now being used in the context of perovskite materials, particularly through layering. The rich complexities of other oxide crystal systems remain largely unexplored for TBC applications. To move beyond an Edisonian approach to these materials, a more detailed fundamental understanding of thermal transport mechanisms is still required. Moreover, to truly accelerate the development of new TBCs, an integrated strategy of design for thermal management, thermomechanical, and chemical stability is required. This remains a challenge for the TBC community.

Acknowledgments

The work described has been supported, in part, by several agencies. The work of W.P., C.W., and Z.Q. was supported by the National Natural Science Foundation of China (Grant No. 51072088, 50990302) as well as through the US National Science Foundation through a World Materials Network grant. SRP and AC are subcontractors of the US Government under DOE Contract No. DE-AC07–05ID14517, under the Energy Frontier Research Center (Office of Science, Office of Basic Energy Science, FWP 1356). The US Government retains a worldwide license to publish or reproduce the published form of this manuscript, or allow others to do so, for US Government purposes.

References

1. R. Siegel, C.M. Spuckler, *Mater. Sci. Eng., A* **245**, 150 (1998).
2. S. Stecura, "Optimization of the NiCrAl-Y/ZrO_2-Y_2O_3 Thermal Barrier System" (NASA Tech. memo, Cleveland, 1985).
3. J. Callaway, H.C. von Baeyer, *Phys. Rev.* **120** (4), 1149 (1960).
4. P.K. Schelling, S.R. Phillpot, *J. Am. Ceram. Soc.* **84** (12), 2997 (2001).
5. T. Watanabe, S.G. Srivilliputhur, P.K. Schelling, J.S. Tulenko, S.B. Sinnott, S.R. Phillpot, *J. Am. Ceram. Soc.* **92** (4), 850 (2009).
6. P.B. Allen, J.L. Feldman, S.R. Bickham, *Philos. Mag. B* **79** (11–12), 1715 (1999).
7. V. Lughi, D.R. Clarke, *Surf. Coat. Technol.* **200** (5–6), 1287 (2005).
8. J. Feng, X.R. Ren, X. Wang, R. Zhou, W. Pan, *Scripta Mater.* **66** (1), 41 (2012).
9. M.N. Rahaman, J.R. Gross, R.E. Dutton, H. Wang, *Acta Mater.* **54** (6), 1615 (2006).
10. C.G. Levi, *Curr. Opin. Solid State Mater. Sci.* **8** (1), 77 (2004).
11. S. Raghavan, H. Wang, R.B. Dinwiddie, W.D. Porter, R. Vaβen, D. Stöver, M.J. Mayo, *J. Am. Ceram. Soc.* **87** (3), 431 (2004).
12. S. Raghavan, H. Wang, W.D. Porter, R.B. Dinwiddie, M.J. Mayo, *Acta Mater.* **49** (1), 169 (2001).
13. Y. Shen, R.M. Leckie, C.G. Levi, D.R. Clarke, *Acta Mater.* **58** (13), 4424 (2010).
14. X.W. Song, M. Xie, R. Mu, F. Zhou, G. Jia, S. An, *Acta Mater.* **59** (10), 3895 (2011).
15. M.O. Jarligo, D.E. Mack, G. Mauer, R. Vaβen, D. Stöver, *J. Therm. Spray Technol.* **19** (1–2), 303 (2010).
16. R. Vaβen, M.O. Jarligo, T. Steinke, D.E. Mack, D. Stöver, *Surf. Coat. Technol.* **205** (4), 938 (2010).
17. D.M. Zhu, R.A. Miller, *Int. J. Appl. Ceram. Technol.* **1** (1), 86 (2004).
18. R. Vaβen, X.Q. Cao, F. Tietz, D. Basu, D. Stöver, *J. Am. Ceram. Soc.* **83** (8), 2023 (2000).
19. B.J. Wuensch, K.W. Eberman, *J. Miner.* **52**, 19 (2000).
20. P.K. Schelling, S.R. Phillpot, R.W. Grimes, *Philos. Mag. Lett.* **84** (2), 127 (2004).
21. Z. Qu, C. Wan, W. Pan, *Acta Mater.* **60** (6–7), 2939 (2012).
22. J. Wu, X.Z. Wei, N.P. Padture, P.G. Klemens, M. Gell, E. Garcia, P. Miranzo, M.I. Osendi, *J. Am. Ceram. Soc.* **85** (12), 3031 (2002).
23. M.R. Winter, D.R. Clarke, *J. Am. Ceram. Soc.* **90** (2), 533 (2007).
24. Q. Xu, W. Pan, J. Wang, C. Wan, L. Qi, H. Miao, K. Mori, T. Torigoe, *J. Am. Ceram. Soc.* **89** (1), 340 (2006).
25. H. Lehmann, D. Pitzer, G. Pracht, R. Vaβen, D. Stöver, *J. Am. Ceram. Soc.* **86** (8), 1338 (2003).
26. C.L. Wan, Z.X. Qu, A. Du, W. Pan, *J. Am. Ceram. Soc.* **94** (2), 592 (2011).
27. C.L. Wan, W. Zhang, Y. Wang, Z.X. Qu, A. Du, R. Wu, W. Pan, *Acta Mater.* **58** (18), 6166 (2010).
28. R.H. Mitchell, *Perovskites: Modern and Ancient* (Almaz Press, Thunder Bay, 2002).
29. W. Ma, D.E. Mack, R. Vaβen, D. Stöver, *J. Am. Ceram. Soc.* **91** (8), 2630 (2008).
30. W. Ma, M.O. Jarligo, D. Pitzer, J. Malzbender, R. Vaβen, D. Stöver, *J. Therm. Spray Technol.* **17** (5–6), 831 (2008).

31. M.O. Jarligo, D.E. Mack, R. Vaβen, D. Stöver, *J. Therm. Spray Technol.* **18** (2), 187 (2009).
32. C. Wan, Z. Qu, Y. He, D. Luan, W. Pan, *Phys. Rev. Lett.* **101** (8), 085901 (2008).
33. C.L. Wan, T.D. Sparks, W. Pan, D.R. Clarke, R. David, *J. Am. Ceram. Soc.* **93** (5), 1457 (2010).
34. A. Chernatynskiy, R.W. Grimes, M.A. Zurbuchen, D.R. Clarke, S.R. Phillpot, *Appl. Phys. Lett.* **95** (16) (2009).
35. Y. Shen, D.R. Clarke, P.A. Fuierer, *Appl. Phys. Lett.* **93** (10) (2008).
36. H. Guo, H. Zhang, G. Ma, S. Gong, *Surf. Coat. Technol.* **204** (5), 691 (2009).
37. X.Q. Cao, R. Vaβen, D. Stöver, *J. Eur. Ceram. Soc.* **24** (1), 1 (2004).
38. A.B. Du, C.L. Wan, Z. Qu, W. Pan, *J. Am. Ceram. Soc.* **92** (11), 2687 (2009).
39. A.B. Du, C.L. Wan, Z. Qu, R. Wu, W. Pan, *J. Am. Ceram. Soc.* **93** (9), 2822 (2010).
40. Z.X. Qu, T.D. Sparks, W. Pan, D.R. Clarke, *Acta Mater.* **59** (10), 3841 (2011).
41. R. Vaβen, G. Kerkhof, D. Stöver, *Mater. Sci. Eng., A* **303** (1–2), 100 (2001).
42. S. Sodeoka, M. Suzuki, K. Ueno. H. Sakuramoto, T. Shibata, M. Ando, *J. Therm. Spray Technol.* **6** (3), 361 (1997).
43. X.Q. Cao, R. Vaβen, W. Fischer, F. Tietz, W. Jungen, D. Stöve, *Adv. Mater.* **15** (17), 1438 (2003).
44. Z.X. Qu, C.L. Wan, W. Pan, *Chem. Mater.* **19** (20), 4913 (2007). □

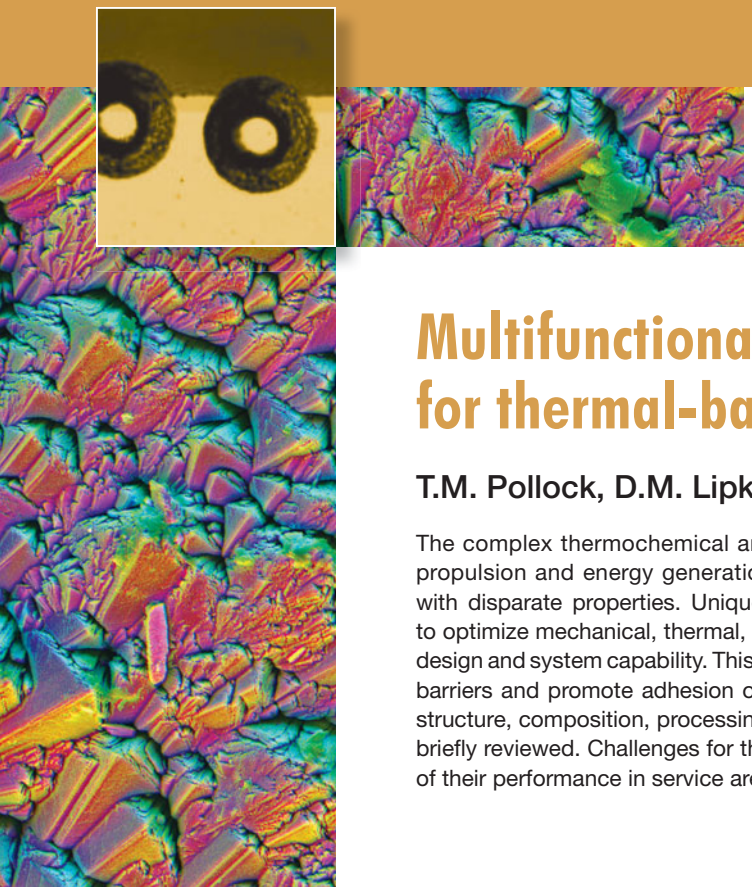

Multifunctional coating interlayers for thermal-barrier systems

T.M. Pollock, D.M. Lipkin, and K.J. Hemker

The complex thermochemical and thermomechanical environments in high temperature propulsion and energy generation systems often demand the use of suites of materials with disparate properties. Unique combinations of materials that simultaneously function to optimize mechanical, thermal, and environmental properties can enable breakthroughs in design and system capability. This article focuses on interlayers that function as environmental barriers and promote adhesion of the ceramic thermal barriers to metallic substrates. The structure, composition, processing, and performance of major classes of bond coatings are briefly reviewed. Challenges for the development of new coating systems and for prediction of their performance in service are addressed.

Introduction

Thermal-barrier systems are an excellent example of multilayered, multifunctional material assemblies that have enabled substantial improvements in the performance and efficiency of gas turbine engines. The combination of a metallic substrate, an intermetallic (or mixed metallic and intermetallic) interlayer, and a low conductivity ceramic topcoat permits the system to operate near, or even above, the melting point of the substrate in a highly oxidizing combustion environment.[1–7]

Intermetallic coatings have long been a central requirement for high temperature operation of propulsion and power generation systems. In early applications in aero- and land-based turbines (before ceramic thermal barriers were developed), environmental coatings typically served a single function. Aluminide-type coatings based on NiAl and NiCoCrAl-family coatings became the standard systems for oxidation protection, while diffusion chromides and overlay CoNiCrAl materials were used to protect against hot corrosion.[1,6] As turbine operating temperatures have increased, fuels have become cleaner, substrate alloys have evolved to refractory-rich nickel-based single crystals, and environmental coatings have become (by necessity) multifunctional. In current turbine components (see Figure 1 in the introductory article for a depiction of a gas turbine), a single coating deposited on a turbine blade may be expected to:[1–9]

- Resist Type II hot corrosion in cooler sections (e.g., in blade shanks).
- Resist Type I hot corrosion in intermediate-temperature regions (e.g., below the blade platform and in cooler sections of airfoils).
- Resist high-temperature oxidation in the hottest sections (e.g., blade tips, platforms, and airfoils).
- Maintain adhesion to the thermal-barrier coating (TBC).
- Provide environmental protection in the event of TBC spallation.
- Minimize interdiffusion and limit transformations at the interface with the nickel-based substrate.

The challenges of developing intermetallic bond coatings that will reliably perform in present and future engineering systems are addressed in this article. A perspective on presently available bond coating systems and their functionality is given first. The suite of processing approaches for interlayer synthesis and challenges in controlling structure and composition are then addressed. Aspects of the bond coating that limit system performance are reviewed. New experimental and characterization tools and computational design approaches are highlighted, along with future prospects for discovery of new materials combinations and for prediction of their performance in complex thermo-chemical-mechanical environments.

T.M. Pollock, Materials Department, University of California, Santa Barbara; Pollock@engineering.ucsb.edu
D.M. Lipkin, GE Global Research, Fairfield, CT; lipkin@ge.com
K.J. Hemker, Department of Mechanical Engineering, Whiting School of Engineering, The Johns Hopkins University; hemker@jhu.edu
DOI: 10.1557/mrs.2012.238

Structure, functionality, and classes of bond coatings

The intermetallic bond coat exists as an intermediate layer between the metallic substrate (typically a nickel-based superalloy) and the ceramic top coating (typically yttria-stabilized zirconia). The thickness of the bond-coat layer is typically between 30–100 μm, varying in thickness as a function of processing approach and service time. The bond coating is chemically complex due to the need to optimize a broad set of thermomechanical and thermochemical properties.

Given that bond coatings are deposited on Ni-based substrates and upon high temperature exposure from surface films of either chromia or alumina, the Ni-Al-Cr ternary diagram at 1100°C, **Figure 1**, is relevant. In the ternary compositional space, phases that exist include the B2 β phase with approximately equal levels of Ni and Al, the fcc γ-Ni and γ-Al phases, the $L1_2$ γ′–Ni_3Al phase, and the A2 α-Cr phase. These phases are often present in as-deposited coatings. Bond coatings can be broadly classified by these major phase constituents.[1,2,7] Coatings comprised primarily of the B2 β phase are typically referred to as "nickel aluminide" coatings, and if they additionally contain platinum are classified as "platinum aluminides." A combination of the β and γ′ phases forms the basis of "MCrAlY" coatings, where the "M" often refers to Ni, Co, or a combination of both. Several emerging coating systems contain a γ′ phase with some level of γ–Ni present.

The high temperature processing paths for application of the coatings, discussed in more detail in the next section, inevitably include interdiffusion with the substrate, resulting in an interdiffusion zone that may contain several additional refractory-rich phases. Moreover, the bond-coat structure evolves by interdiffusion during high temperature exposure, potentially resulting in further phase transformations and/or migration of elements that are detrimental to system performance (**Figure 2**). Calculated phase diagrams for higher order multicomponent systems can be useful for avoiding the formation of brittle intermetallic phases in this zone and for designing thermal treatments that follow coating application. Given the operating environments for these coatings, control of both the thermodynamic and kinetic properties is essential.

The bond coating must serve as an environmental barrier for the substrate due to the fact that the outer, low conductivity ceramic is permeable to oxygen. Consequently, the ability to form a dense, protective oxide in the operating environment is one of the primary requirements of the bond coating. Most of the intermetallics presently employed as bond coatings contain a sufficiently high level of aluminum to promote the formation of a dense α-Al_2O_3 layer at the surface of the bond coat adjacent to the TBC, which has a relatively slow growth rate and is resistant to degradation by any corrosive species that reach the surface through the thermal barrier, or subsequent to spallation of the ceramic thermal barrier.[2–9] The thin oxide layer is typically referred to as the thermally grown oxide (TGO). Given the high temperature operating requirements, it is essential that the TGO be thermodynamically compatible with the ceramic thermal barrier. To achieve the protective requirements, the bond coating must serve as a chemical reservoir for TGO formation, as well as a diffusion barrier or diffusion sink for any deleterious refractory elements from the superalloy substrate that may degrade the bond-coat properties or the bond coat—TGO interface adhesion.[10–14] While the TGO provides the coating system with an oxidation benefit, this thin interlayer may also endure large thermal and growth stresses that challenge the durability of the layered TBC system when exposed to severe thermal transients characteristic of turbine airfoils, as discussed in more detail later.

To be effective over the life span of the turbine component for which the bond coating is intended to protect the substrate, it must also be thermochemically and thermomechanically compatible with the substrate so as to prevent—or at least limit—debits to the mechanical properties of the load-bearing components. At present, coatings are still not relied upon to provide load-bearing capability, though this may be on the horizon for the next generation of coatings. In addition to their functional requirements, the coatings must be applied using processes that are cost effective, capable of providing the required thickness and chemical homogeneity, and compatible with other processes or thermal operations required for component fabrication. These requirements drive the development of new coating compositions, architectures, and the processes to fabricate them, discussed in the following section.

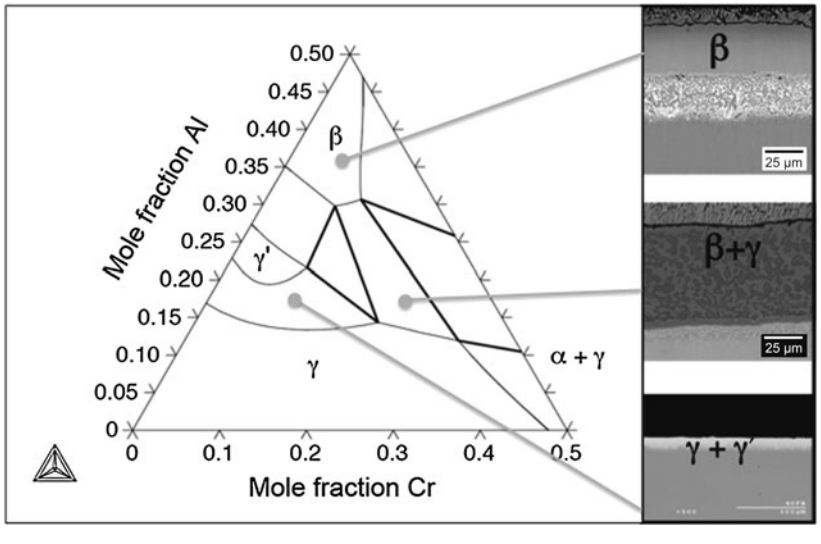

Figure 1. Ternary Ni-Al-Cr phase diagram predicted by the Calphad method, and approximate compositions of three different bond coating classes shown in scanning electron micrographs on the right. Shifts in the amounts of Al, Cr, and Ni in these coatings permit changes in the predominant phase.

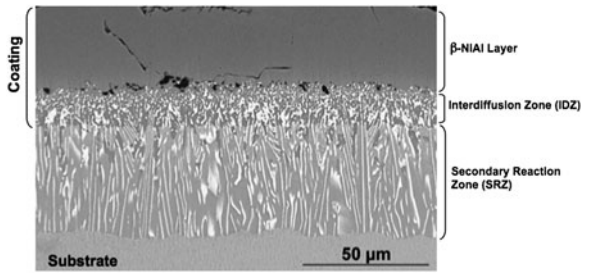

Figure 2. Interdiffusion-induced cellular transformation that results in detrimental intermetallic phases in a secondary reaction zone as a result of deposition of a NiAl coating on a Ni-5.9Al-5.6Ru-7.9Ta-7.4Re-2.9W-2.3Co-6.6Cr (wt%) substrate. This zone continues to grow into the substrate.

Coating application: A multiplicity of processing paths

As coating compositions have evolved to keep up with the functional demands of engineering components, so too have the processes for depositing them. While coating compositions can be optimized solely on their chemical and microstructural characteristics, it is essential to have a coating process capable of uniformly covering the complex geometries of the turbine components and compatible with all subsequent manufacturing processes, such as TBC deposition, heat treatments used to establish braze joints, and any heat treatments used to establish the desired substrate properties. The challenge of delivering ever-increasing coating functionality while maintaining robust and cost-effective manufacturing processes has led to a multiplicity of coating processes, which may be broadly classified into two categories: diffusion coatings and overlays.

Diffusion coatings

Diffusion coatings, particularly aluminide coatings, are the product of interdiffusion between the superalloy component and an aluminum source (donor). The simplest of these processes, and the earliest to be industrially implemented, is pack cementation,[15] schematically illustrated in **Figure 3**a. Components to be aluminized are embedded into a mixture of the aluminum source, an inert matrix (typically alumina sand), and a halide salt activator (e.g., AlF_3 or NH_4F). The aluminum sources can be elemental aluminum or aluminum-containing alloys, such as CrAl, CoAl, or NiAl. Alloy donors are used to increase the donor melting temperature and define the chemical activity of aluminum, allowing the coating microstructures to be tuned for improved performance. The pack is located in a retort and heated to temperatures in the range 650–1200°C in a non-oxidizing atmosphere, such as argon or hydrogen. On heating, the halide activator transports aluminum from the donor to the surface of the target component, where it decomposes, releasing aluminum to diffuse into the alloy and cycling the halide back to the donor to pick up more aluminum. At temperatures above ~1050°C and with packs having low-aluminum activity donors, NiAl coatings form via predominantly outward diffusion of the nickel from the substrate. These coatings are typically single-phase and have Al:Ni ratios less than unity. For pack aluminizing at temperatures below ~1000°C, and especially when the packs have high-activity donors (e.g., metallic aluminum), coatings grow by predominantly inward diffusion of aluminum.

Aluminizing processes employing long-range vapor-phase transport of the aluminum source have also been developed, eliminating the need to place components directly in the pack. These processes are generally categorized as vapor-phase aluminizing (VPA) and chemical vapor deposition (CVD). In both cases, the components to be coated are placed in a high-temperature retort, and the aluminum-bearing vapors are transported to them by an inert gas.[16] This allows both external and internal surfaces to be coated. In VPA, the aluminum source, or donor alloy, is usually a refractory alloy of aluminum; examples include CrAl, CoAl, NiAl, and Ti_2AlC-TiAl (also known as Codep donor).[17,18] A halide salt (e.g., AlF_3, NH_4F, NaF, and mixtures thereof) is used as an activator to destabilize the native oxide and initiate vapor-phase transport transfer of aluminum.

In CVD aluminizing,[6] the aluminum source is injected into the heated retort as a precursor gas in a non-oxidizing carrier gas. The precursor can be delivered directly from a tank source (e.g., as $AlCl_3$) or by passing anhydrous halide, such as HCl or HF, over an aluminum donor at a controlled temperature, pressure, and flow rate, so as to form the corresponding volatile halide salts (e.g., $AlCl_3$ or AlF_3). Because each process has some advantages (and limitations) over the other, both VPA and CVD continue to be employed in industrial applications.

Additional environmental performance benefits can be gained by incorporating other elements into the aluminide coating. Elements including Cr, Si, Hf, Zr, and Y have been incorporated into diffusion aluminide coatings to impart enhanced resistance against corrosion, cyclic oxidation resistance, or improvement in TBC retention.[15,19,20] One of the most widely adopted durability enhancements to the simple aluminide (on external surfaces only) is platinum-modified nickel

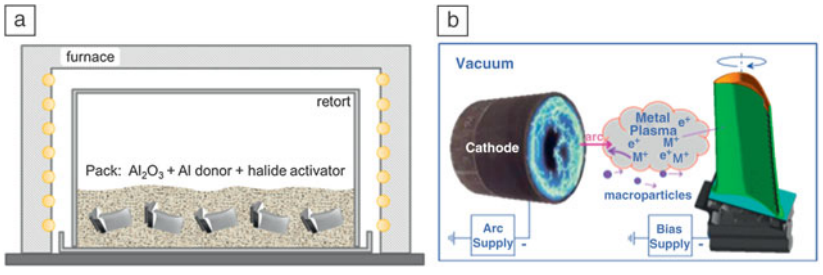

Figure 3. (a) Schematic of a pack cementation system, consisting of a high-temperature retort surrounded by a furnace. The parts are embedded in a pack consisting of an inert filler (typically alumina), donor (e.g., CrAl alloy), and halide activator (e.g., AlF_3). (b) Schematic of an ion plasma deposition process in which molten droplets and ionized vapor are ejected from a metal cathode to coat the part (shown in green).

aluminide.[21–24] These coatings are typically synthesized in a three-step process, consisting of electroplating 5–10 μm of platinum and an inert-atmosphere interdiffusion heat treatment, followed by a diffusion aluminizing process (pack or vapor phase), as described previously. In an additional variant of the platinum diffusion coatings, direct platinizing of the superalloy, without a subsequent aluminizing step, has also been demonstrated to improve the environmental resistance and TBC bond-coating performance of turbine alloys.[25–28]

While the processes for making simple and alloyed diffusion aluminides are widely used in the manufacture of turbine components, the degree to which their microstructures and thicknesses can be specified is limited by the phase equilibrium and diffusion kinetics inherent to the reactant-superalloy system. Whereas diffusion aluminides are still the standard for all internal coatings, external coatings are therefore also applied using overlay processes, as described later.

Overlay coatings

Overlay coatings provide the flexibility of tailoring the composition of complex, multi-component systems without the compositional and thickness constraints inherent to the diffusion coatings. Because thermal spray deposition processes have been most broadly applied to environmental and bond coatings, these are described first.

Simple MCrAl-family coatings can be deposited by a number of processes, producing varying degrees of coating density and process-induced oxidation.[29] As interest in the incorporation of reactive element additions (e.g., Hf, Y, Zr, and Si) into the MCrAl-based coatings has increased, inert-atmosphere processes have been employed to prevent tying up these elements with oxygen during deposition. Physical vapor deposition in vacuum, namely electron-beam physical vapor deposition (EBPVD), can deposit high-quality MCrAls with reactive element additions.[30] While EBPVD and other physical vapor deposition processes have several appealing features, including their ability to deposit clean, dense coatings containing highly reactive elements, these processes involve costly equipment and maintenance and throughput-limiting sample exchange protocols. As a result, low-pressure plasma spray (LPPS) has emerged as a lower-cost alternative and is broadly used.[31]

LPPS systems carry the burden of high cost associated with the accompanying vacuum chamber. In this regard, the emergence of atmospheric deposition processes, including inert-gas shrouded plasma spray[32,33] and high-velocity oxyfuel (HVOF),[34] has made the high-volume deposition of complex MCrAls with reactive elements routine.[35] The trend toward simultaneously reducing particle temperatures while increasing particle velocities has continued with the emergence of new processes, such as activated combustion high-velocity air fuel (HVAF)[34,36] and cold-gas dynamic spraying (cold spray).[37,38] These processes enable the atmospheric deposition of dense coatings with limited oxidation of the most reactive elements.

An emerging trend in process technologies is the hybridization of what used to be considered distinct deposition mechanisms in order to synergistically benefit from the advantages of multiple processes. Recent examples include very-low pressure plasma spray[39] and ion plasma deposition (Figure 3b).[40–42] These processes combine the benefits of droplet-based deposition (fast, clean, amenable to transferring multi-component chemistries) with those of physical vapor deposition (dense, adherent, chemically homogeneous). Yet another hybrid process that has been employed to improve the failure resistance of bond coatings is the over-aluminizing (by either overlay, pack diffusion, or out-of-pack diffusion processes) of MCrAl-family and NiAl-family coatings.[6] It is anticipated that these as well as new combinations of conventionally distinct processes will continue to be explored.

Coating properties and performance

Bond coatings are key to TBC system durability and require a complex combination of thermal, mechanical, and environmental properties to maintain adherence of the ceramic top layer. For example, bond-coat creep strength, thermal misfit with the superalloy substrate, and TGO growth strains strongly influence three major intrinsic failure modes: rumpling, edge delamination, and sustained peak low cycle fatigue (see Figure 1 in the Levi article in this issue).[43–45] A major challenge lies in the measurement and prediction of the physical and mechanical properties of the interlayers that compose the coating system to increase resistance to these failure modes and maximize system life. As described later, some of the relevant properties of the most common coating systems have been measured. Unfortunately, property measurement is rarely incorporated as a tool for developing new generations of coatings. As described in the section on "New design and characterization tools," there are emerging characterization techniques that may permit more systematic development of coating systems.

With thermal excursions exceeding 1000°C, differences in the coefficients of thermal expansion (CTEs) of the coating relative to the superalloy substrate of only 1 μstrain °C^{-1} generates thermal stresses on the order of hundreds of MPa—stresses that are high enough to promote bond-coat plasticity at elevated temperatures and interfacial delamination upon cool down.[9] The CTEs of bulk materials are readily measured using a dilatometer, but measuring the CTE of thin films extracted from the various layers of a thermal-barrier system requires alternative techniques. Non-contact digital image correlation provides one route to measuring the CTE of thin films as a function of temperature; **Figure 4** compares CTE measurements for a standard diffusion aluminide bond coat with those for a standard commercial single crystal superalloy substrate, René N5. Differences in CTE of approximately 2 μstrain °C^{-1} are present at room temperature, but this difference varies over the temperature range of interest and reverses at high temperature. Comparison of the CTE for commercial MCrAlY bond coats and their substrates do not exhibit a reversal, but differences of 2 to 3 μstrain °C^{-1} are not uncommon and are generally exacerbated at the highest temperatures. To more closely match the expansion characteristics of the superalloy substrate, coatings

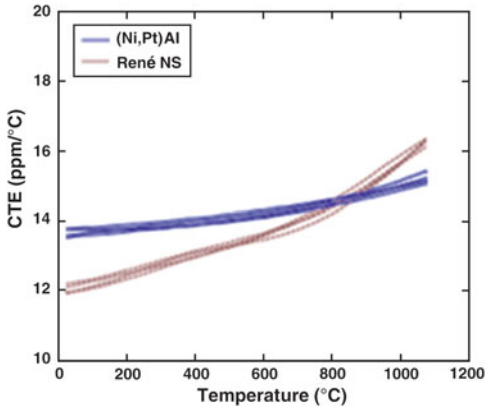

Figure 4. Coefficients of thermal expansion (CTEs) for a commercial diffusion aluminide (Ni,Pt)Al bond coat and its generation 3 René N5 Ni-based superalloy.

with the same phase constituents (γ′ and γ phases) with more optimal compositions for oxidation have been investigated.[46–48] Beyond CTE matching, these systems are desirable due to the lowered driving forces for interdiffusion. However, a drawback is the lower amount of Al available in the coating "reservoir" for TGO formation.

The mechanical properties of bond coatings have a significant influence on their durability in service. Diffusion aluminide coatings have been shown to have a ductile-brittle transition temperature (DBTT) of approximately 600°C. Below the DBTT, the bond coat is linearly elastic with a Young's modulus that depends on composition and is comparable with what has been reported for the β-NiAl phase. Above the DBTT, the ultimate tensile strength and creep response of the diffusion aluminide bond coat is extremely temperature dependent (**Figure 5**a). Strengths of 400 MPa have been measured at intermediate temperatures, but above 1000°C, the strength of commercial diffusion aluminide bond coats does not exceed 50 MPa. Attempts to improve the elevated temperature strength have been only minimally successful, with the greatest high temperature strength being associated with the development of ruthenium aluminide bond coats[49–51] (Figure 5a).

Overlay properties can vary much more widely than those of the diffusion coatings since the composition and microstructure can be more widely varied. Their properties have been somewhat better characterized, since it is possible to deposit very thick layers of the coating (albeit with some loss of similitude of microstructure) and machine conventionally sized test specimens. In general, the physical properties of overlay coatings are similar to those of conventional superalloys. The thermal expansion, particularly of coatings containing Co, tends to be greater than that of superalloys, which tends to increase thermal stresses in these coatings. MCrAlY coatings have been reported to be very strong at room temperature, but their elevated temperature strength is dramatically reduced. Micro-tensile tests of a commercial NiCoCrAlY coating demonstrate impressive room temperature properties with an ultimate tensile strength of 1.4 GPa and significant (>2%) ductility.[52] The strength of these coatings is, however, very temperature dependent and significantly lower than has been measured for diffusion aluminide coatings (Figure 5b).

During service, incorporation of Al into the TGO and continued interdiffusion between the coating and underlying substrate significantly reduces the Al content of the bond coating, which can result in the formation of metastable $L1_0$ martensite phase γ′-Ni_3Al, and eventually γ-Ni. The formation of the $L1_0$ martensite can have a dramatic effect on rumpling if the martensitic (diffusionless) transformation, and attendant volume change, occurs at intermediate temperatures, where the bond coat is easily plastically deformed. The martensite start temperature (M_s) is extremely sensitive to composition and the presence of Pt, which is a common addition to many commercial diffusion aluminide coatings.[53] Without Pt, the martensitic transformation occurs at temperatures well below the β–NiAl DBTT and is stored and recovered elastically. The addition of Pt raises the transformation temperature, which promotes plastic deformation of the bond coat.[54,55]

The TGO is also a key mechanical element of the multilayered system. The TGO undergoes thickening and elongation during the lifetime of the system. The thickening increases the strain energy density, while the elongation provides a driving force for coating failure via the rumpling mechanism.[54,55] TGO elongation results from new TGO forming on internal grain boundaries,[55–57] while thickening is caused by new TGO forming at the TGO/bond-coat interface. The elongation strain

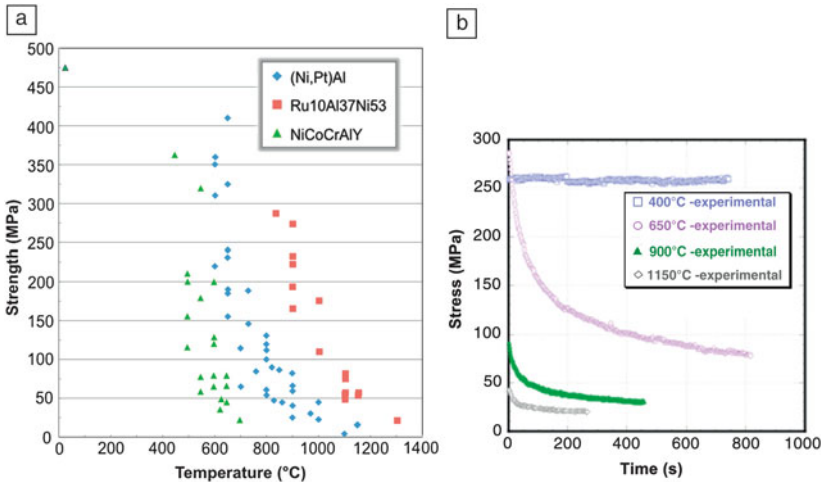

Figure 5. (a) The tensile strength of a NiCoCrAlY overlay bond coat, a platinum modified diffusion aluminide bond coat, and a developmental ruthenium aluminide alloy measured and plotted as a function of temperature. (b) Measured stress relaxations for a diffusion aluminide bond coat. The rate of relaxation above 600°C is impressive, but the relaxation data have been shown to follow conventional models for thermally activated power law creep.

causes the TGO to develop in-plane compression as it grows. At elevated temperatures, the magnitude of this growth stress is limited by the yield/creep strength of the coating.[9] The growth stresses also provide a key driving force for the sustained peak low cycle fatigue failure mechanism.[56,57] In this scenario, cracks form on the surface of the bond coating, and their faces subsequently oxidize during cycling. These cracks then propagate deep into the substrate by the same oxide elongation processes. The development of the growth stresses in the oxide and the dependence of these stresses on the chemistry of the bond coating are not well understood.

The interface between the TGO and the bond coating is important to the durability of the overall multilayered system. The interface between the TGO and the bond coat is susceptible to decohesion, and this is exacerbated by the segregation of deleterious impurity elements. The most deleterious segregant is S, which at less than 1/3 monolayer coverage causes the work-of-adhesion to be diminished by a factor 10.[58] Conversely, other elements, such as Pt, appear to increase the adhesion,[59,60] though the mechanism is still not well understood. Reactive elements such as Y and Hf also improve adhesion,[60,61] but again their distribution within the coating and at the interface and the mechanism(s) by which they improve adhesion require further fundamental study. In general, the chemical environment at the interfaces and its influence on interfacial toughness is still not well understood.

New design and characterization tools

Optimization of the composition and properties of each coating layer remains a major challenge. Calphad thermodynamic phase equilibria tools that provide insights to the thermodynamically stable phases that exist at elevated temperature as a function of composition (Figure 1) can be used to guide the design of new systems. However, since the superalloy substrate may contain 8–10 elements and the coating often contains an additional 3–6 elements, the thermodynamic assessments of all the potential phases are often not accurate enough to predict the structure of the coating. With regard to kinetics and the prediction of structure evolution, limited interdiffusion data in the relevant range of composition represents a major constraint. First principles computational techniques can now be employed to investigate atomic hop mechanisms in multicomponent systems. Combined with cluster expansions and Monte Carlo simulations, it is possible to predict macroscopic diffusion coefficients, including the large variations in diffusivity with departures from stoichiometry in NiAl.[62–65] Such approaches hold promise for the design of coatings that resist interdiffusion.

When incomplete information on phase equilibria and interdiffusion behavior exists, combinatorial experimental approaches are useful. **Figure 6**a shows 45 coating samples placed in an ion plasma deposition system among three cathodes, each of a different composition. The resultant distribution of Pd with a Cathode 1 composition of Ni-46Al-4Cr-12Pd (and other cathodes Pd-free) is shown in Figure 6b. In this manner, the influence of Pd in a B2 type coating can be explored over a wide range of composition within a single coating deposition cycle.

The mechanical properties of the coating layers have proven to be extremely difficult to measure experimentally, owing to their reduced dimensionality, propensity to interact and evolve with thermal cycling, and the need to measure these properties at both room and elevated temperatures. MEMS (microelectromechanical systems)-inspired techniques have led to the implementation of micro-tensile testing as a reliable means for elucidating the constitutive behavior of individual TBC layers. Freestanding bond coats can be prepared by chemically etching away the ceramic topcoat and TGO, scalping 500-μm slices of bond coat with a thin layer of superalloy from the underlying substrate with electro-discharge machining, and then lapping and polishing to remove the underlying superalloy.[45] Bow tie shaped micro-tensile specimens can be cut and individually ground and polished to a thickness of 20–50 μm with all unwanted layers (topcoat, TGO, and substrate) removed, **Figure 7**a. For measurement of mechanical properties, custom micro-tensile piezoelectric driven load frames have been developed, Figure 7a. Thermal and electrical isolation of the grips from the load frame allow for resistive heating. Young's modulus, yield, and ultimate tensile strengths and strain to failure have been measured from full micro-tensile stress-strain curves. Time-dependent creep properties can also be measured by loading in tension, fixing the grips, and recording the changes in stress and strain that occur as a function of time for characterization of power law creep constitutive relationships.[45]

Location specific measurements of room temperature mechanical response can also be measured using nanoindentation and micropillar compression testing, Figure 7b–c. These pillars may be machined within individual layers normal to the growth direction using focused ion beam systems[66] or by recently developed femtosecond laser micromachining

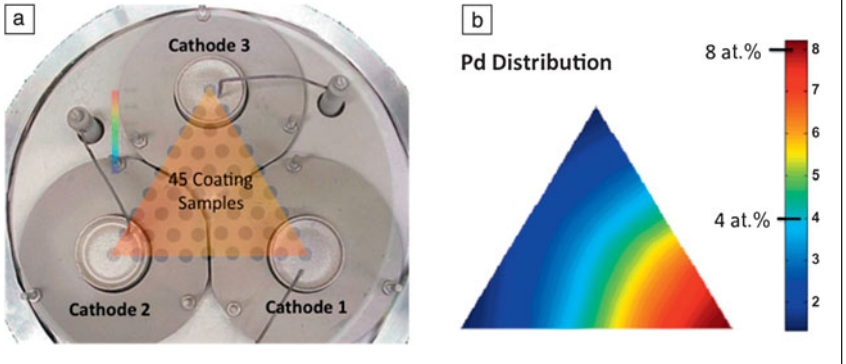

Figure 6. (a) Combinatorial matrix of 45 samples fabricated from three cathodes of different compositions in an ion plasma deposition system, and (b) the distribution of Pd across the set of 45 samples with Cathode 1 containing 12 at.% Pd and Cathodes 2 and 3 containing no Pd.

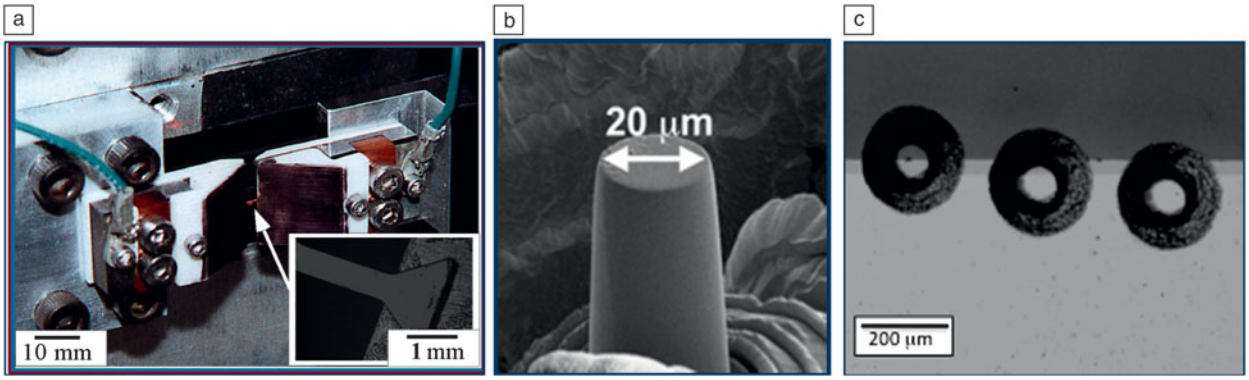

Figure 7. (a) Freestanding diffusion aluminide bond coat micro-tensile specimen mounted in a custom build load frame, resistively heated and ready for tensile testing, (b) micropillar machined with femtosecond laser, and (c) a series of micropillars machined across a coating interface.

methods.[67,68] A well-developed methodology of compressing these pillars with flat diamond microindentors[66] permits acquisition of room temperature properties of the coatings. With size-scale effects properly accounted for, these techniques provide location specific measures of modulus, hardness, and strength, but they are currently limited to room temperature measurement. Other location-specific measurements for properties such as thermal conductivity have also recently been developed.[69,70] Prospects for intermediate temperature testing are promising, but these techniques are far from being used at temperatures of 1000°C.

As mentioned previously, the TGO, typically alumina, is a key element of the multilayered system that must adhere to the bond coating to provide an environmental barrier and to maintain adherence of the ceramic topcoat. Optical spectroscopy tools offer non-contact, non-destructive evaluation of the state of the TGO during cycling.[71–75] Luminescence lines generated by laser illumination undergo a stress-induced frequency shift due to the presence of very small quantities of naturally occurring Cr^{3+} as an impurity. Analysis of the luminescence spectrum permits assessment of the stresses in the TGO, which are compressive and of the order of 100–400 MPa at elevated temperature and rise beyond 4 GPa at room temperature due to the CTE mismatch with the superalloy substrate.[57,77,78] With recently incorporated scanning capabilities, new piezospectroscopy tools can analyze the spatial variations in stress as well as assess subsurface damage that alters the stress state in the oxide.[73–76] An example of the spatial variation in stresses is shown for a platinum aluminide coating oxidized at 1093°C, **Figure 8**, where the compressive stresses in the oxide range from 3–7 GPa following cooling to room temperature. Synchrotron x-ray experiments have additionally been employed to observe the development and evolution of growth stresses *in situ* at elevated temperatures.[77,78]

Future challenges and opportunities

Building the infrastructure to design multicomponent bond coatings that perform in a predictable manner within the multilayered thermal-barrier coating (TBC) system remains a major challenge. The bond-coat element of the TBC system has traditionally been developed in isolation from the substrate and the ceramic topcoat with limited measurement of properties as a function of composition. This can lead to substantial debits in performance when combined with system elements. Emerging

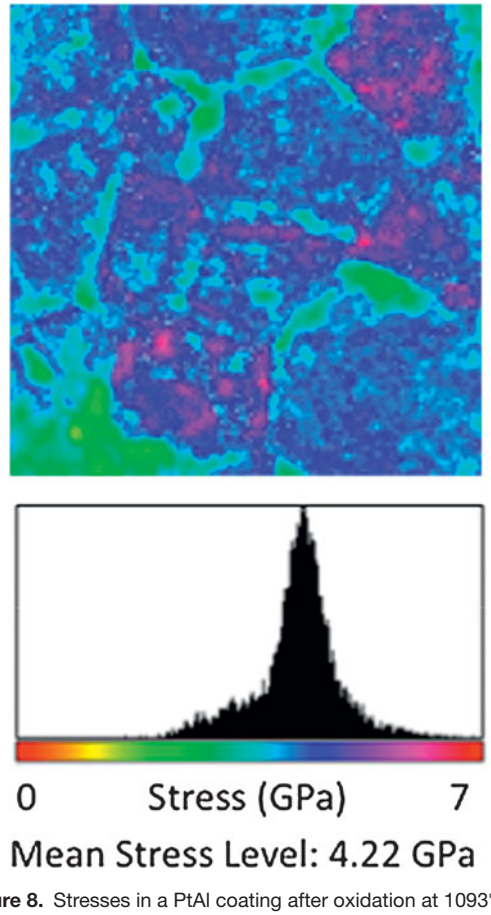

Figure 8. Stresses in a PtAl coating after oxidation at 1093°C /160 h and subsequent cooling to room temperature measured by confocal piezospectroscopy.

tools with improved capabilities for predicting and measuring properties, some described in the previous sections and some yet to be developed, will contribute positively to this challenge. The properties of interfaces within the system remain as a barrier to predicting system performance.

The drive toward higher-efficiency (i.e., hotter-running, more highly stressed) engines, unconventional propulsion fuels, and reduced reliance on exotic materials will motivate these new tools for optimizing system performance as well as new coatings with the following characteristics:

- Multi-component coatings for turbine parts with internal passages that are not amenable to line-of-sight overlay coating processes
- Multi-functional coatings capable of location-specific response
- Coatings that possess load-bearing capability, which are increasingly important as aero components move to thinner walls
- Coating processes that are amenable to field application (e.g., high-agility thermal spray processes that can be employed for localized repair)
- Reduced cost coatings that contain limited amounts of Pt and other costly/scarce materials that can be applied with low-capital processing equipment, flexible chemistry, and simplification of manufacturing processes (fewer process steps, scalable equipment, low maintenance).

Finally, with regard to system performance, experience with existing bond-coat/TBC systems has illustrated a competition between failure mechanisms that depend strongly on the plastic properties of the bond coat, the interface fracture toughness governing bond coat/TGO or TGO/TBC failure, and the fracture toughness of the ceramic topcoat.[2,8,9] In order to speed system development and deployment, simulations are needed to help anticipate such competitions and identify material combinations that balance multiple failure mechanisms. Conventional approaches to simulate interface and coating failure processes are not well suited to this task because they require explicit *a priori* definition of the failure mode, including multiple crack geometries, computation of the associated energy release rates, and the post-*priori* assessment of stability (by comparing driving forces to toughness). Coupled with the need to conduct simulations for a broad material parameter space, there is a critical need for an efficient alternative approach that reduces the number of simulations required to identify active failure mechanisms in terms of system properties. Parallel computing approaches are likely to advance these systems-based challenges.

Acknowledgments

T.P. is grateful for the support of an NSF-GOALI program DMR-11–05672.

References

1. R.C. Reed, *The Superalloys: Fundamentals and Applications* (Cambridge University Press, UK, 2006).
2. A.G. Evans, D.R. Clarke, C.G. Levi, *J. Eur. Ceram. Soc.* **28** (7), 1405 (2008).
3. S.M. Meier, D.K. Gupta, *Trans. ASME* **116**, 250 (1994).
4. U. Schulz, C. Leyens, K. Fritscher, M. Peters, B. Saruhan-Brings, O. Lavigne, M. Dorvaux, M. Poulain, R. Mévrel, M.L. Caliez, *Aerosp. Sci. Technol.* **7** (1), 73 (2003).
5. T. DeMasi-Marcin, D.K. Gupta, *Surf. Coat. Technol.* **68/69**, 1 (1994).
6. J.R. Nicholls, *MRS Bulletin* **28**, 659, (2003).
7. M.J. Stiger, N.M. Yanar, M. Topping, F.S. Pettit, G.H. Meier, *Z. Metallkd.* **90**, 1069 (1999).
8. P.K. Wright, A.G. Evans, *Curr. Opin. Solid State Mater. Sci.* **4**, 255 (1999).
9. A.G. Evans, D.R. Mumm, J.W. Hutchinson, G.H. Meier, F.S. Pettit, *Prog. Mater Sci.* **46**, 505 (2001).
10. R.T. Wu, K. Kawagishi, H. Harada, R.C. Reed, *Acta Mater.* **14**, 3622 (2008).
11. J.G. Smeggil, A.W. Funkenbush, N.S. Bornstein, *Metall. Trans. A* **17**, 923 (1986).
12. J.L. Smialek, in *Microscopy of Oxidation 3*, S.B. Newcomb, J.A. Little, Eds. (The Institute of Materials, London, UK, 1996), p. 127.
13. P.Y. Hou, *Oxid. Met.* **52**, 337 (1999).
14. I.G. Wright, B.A. Pint, W.Y. Lee, K.B. Alexander, K. Prüssner, in *High Temperature Surface Engineering* (The Institute of Materials, London, UK, 2000), p. 95.
15. G.W. Goward, L.W. Cannon, ASME Paper 87-GT-50 (ASME, New York, 1988).
16. G.M.C.A. Gauje, US Patent 3,486,927 (1969).
17. D.J. Levine, M.A. Levinstein, US Patent 3,540,878 (1970).
18. D.J. Levine, US Patent No. 3,598,638 (1971).
19. R.L. Wachtell, C.A. De Guisto, US Patent No. 3,073,015 (1963).
20. R. Bianco, R.A. Rapp, *J. Electrochem. Soc.* **140** (4), 1181 (1993).
21. R.G. Wing, I.R. McGill, *Platinum Met. Rev.* **25** (3), 94 (1981).
22. J.S. Smith, D.H. Boone, ASME Paper 90-GT-319 (ASME, 1990).
23. P.C. Patnaik, R. Thamburaj, T.S. Sudarshan, in *Surface Modification Technologies III*, T.S. Sudarshan, D.G. Bhat, Eds. (TMS, Warrendale, PA, 1990), p. 759.
24. T.E. Strangman, US Patent 5,514,482 (1996).
25. I.R. McGill, G.L. Selman, US Patent 4,399,199 (1983).
26. G.J. Tatlock, T.J. Hurd, *Oxid. Met.* **22**, 201 (1984).
27. B.A. Nagaraj, W.B. Connor, R.W. Jendrix, D.J. Wortman, L.W. Plemmons, US Patent 5,427,866 (1995).
28. D.S. Rickerby, S.R. Bell, R.G. Wing, US Patent 5,667,663 (1997).
29. S. Sampath, X.Y. Jiang, J. Matejicek, L. Prchlik, A. Kulkarni, A. Vaidya, *Mater. Sci. Eng., A* **364**, 216 (2004).
30. D.H. Boone, S. Shen, R. McKoon, *Thin Solid Films* **64** (2), 299 (1979).
31. S. Shankar, D.E. Koenig, L.E. Dardi, *J. Met.* **33** (10), 13 (1981).
32. J.E. Jackson, US Patent No. 3,470,347 (1969).
33. T.A. Taylor, M.P. Overs, B.J. Gill, R.C. Tucker, *J. Vac. Sci. Technol., A* **3** (6), 2526 (1985).
34. J.A. Browning, US Patent 5,120,582 (1992).
35. L. Russo, M. Dorfman, in *Proceedings of the International Thermal Spray Conference*, A. Ohmori, Ed. (High-Temperature Society of Japan, 2002), p. 1179.
36. V. Baranovski, A. Verstak, US Patent 6,245,390 (2001).
37. T. Stoltenhoff, H. Kreye, H.J. Richter, *J. Therm. Spray Technol.* **11** (4), 542 (2002).
38. Y. Ichikawa, K. Sakaguchi, K. Ogawa, T. Shoji, S. Barradas, M. Jeandin, M. Boustie, in *Thermal Spray 2007: Global Coating Solutions*, B.R. Marple, M.M. Hyland, Y.-C. Lau, C.-J. Li, R.S. Lima, G. Montavon, Eds. (ASM International, Materials Park, OH, 2007), p. 54.
39. M.F. Smith, A.C. Hall, J.D. Fleetwood, P. Meyer, *Coatings* **1**, 117 (2011).
40. E.N. Kablov, S.A. Muboyadzhyan, S.A. Budinovskii, A.N. Lutsenko, *Russ. Metall.* **5**, 364 (2007).
41. J. Vetter, O. Knotek, J. Brand, W. Beele, *Surf. Coat. Technol.* **68–69**, 27 (1994); O. Knotek, E. Lugscheider, F. Löffler, W. Beele, C. Barimani, *Surf. Coat. Technol.* **74–75**, 118(1995).
42. J.-C. Zhao, D.M. Lipkin, US Patent 6,964,791 (2005).
43. D.S. Balint, J.W. Hutchinson, *Acta Mater.* **51**, 3965 (2003).
44. D.S. Balint, J.W. Hutchinson, *J. Mech. Phys. Solids* **53**, 949 (2005).
45. D. Pan, M.W. Chen, P.K. Wright, K.J. Hemker, *Acta Mater.* **51**, 2205 (2003).
46. I. Takeshi, B. Gleeson, *J. Jpn. Inst. Met.* **71**, 34 (2007).
47. A. Sato, H. Harada, K. Kawagishi, *Metall. Mater. Trans. A* **37**, 790 (2006).
48. K. Kawagishi, H. Harada, A. Sato, K. Matsumoto, *Superalloys* 76 (2008).
49. B. Tryon, F. Cao, K.S. Murphy, C.G. Levi, T.M. Pollock, *JOM* **58**, 53 (2006).
50. B. Tryon, Q. Feng, R. Wellman, K. Murphy, J. Yang, C. Levi, J. Nicholls, T.M. Pollock, *Metall. Mater. Trans. A* **37**, 3347 (2006).
51. F. Cao, T.M. Pollock, *Metall. Mater. Trans. A* **39**, 39 (2008).
52. K.J. Hemker, B.G. Mendis, C. Eberl, *Mater. Sci. Eng., A* **483–484**, 727 (2008).
53. M.W. Chen, M.L. Glynn, R.T. Ott, T.C. Hufnagel, K.J. Hemker, *Acta Mater.* **51**, 4279 (2003).
54. A.M. Karlsson, J.W. Hutchinson, A.G. Evans, *Mater. Sci. Eng., A* **351**, 24 (2003).
55. D.R. Mumm, A.G. Evans, I.T. Spitsberg, *Acta Mater.* **49**, 2329 (2001).

56. A. Suzuki, M.F.X. Gigliotti, B.T. Hazel, D.G. Konitzer, T.M. Pollock, *Metall. Mater. Trans. A* **41**, 948 (2010).
57. A.G. Evans, M.Y. He, A. Suzuki, M. Gigliotti, B. Hazel, T.M. Pollock, *Acta Mater.* **57**, 2969 (2009).
58. W. Zhang, J.R. Smith, X.-G. Wang, A.G. Evans, *Phys. Rev. B* **67** (245414), 1 (2003).
59. B.A. Pint, I.G. Wright, W.Y. Lee, Y. Zhang, K. Prüßner, K.B. Alexander, *Mater. Sci. Eng., A* **245**, 201 (1998).
60. B. Pint, J.A. Haynes, T.M. Besmann, *Surf. Coat. Technol.* **204**, 3287 (2010).
61. J.L. Smialek, in *Proc. Electrochemical Society: Symposium on High Temperature Corrosion and Materials Chemistry*, P.Y. Hou, M.J. McNallan, R. Oltra, E.J. Opila, D.A. Shores, Eds. (Electrochemical Society, Pennington, NJ, 1998), pp. 211–220.
62. Q. Xu, A. Van der Ven, *Acta Mater.* **59**, 1095 (2011).
63. A. Van der Ven, J.C. Thomas, Q. Xu, J. Bhattacharya, *Math. Comput. Simul.* **80** (7), 1393 (2010).
64. Q. Xu, A. Van der Ven, *Phys. Rev. B* **81**, 064303 (2010).
65. Q. Xu, A. Van der Ven, Intermetallics **17** (5), 319 (2009).
66. M.D. Uchic, D.M. Dimiduk, J.N. Florando, W.D. Nix, *Science* **305**, 986 (2004).
67. Q. Feng, Y.N. Picard, H. Liu, S.M. Yalisove, G. Mourou, T.M. Pollock, *Scripta Mater.* **53**, 511 (2005).
68. S. Ma, B. Tryon, J.P. McDonald, S.M. Yalisove, T.M. Pollock, *Metall. Mater. Trans. A* **38**, 2153 (2007).
69. X. Zheng, D.G. Cahill, R. Weaver, J.-C. Zhao, *J. Appl. Phys.* **104**, 073509 (2008).
70. J.-C. Zhao, *Prog. Mater Sci.* **51**, 557 (2006).
71. S.H. Margueron, D.R. Clarke, *Acta Mater.* **54**, 5551 (2006).
72. D.R. Clarke, D.J. Gardiner, *Int. J. Mater. Res.* **98**, 8 (2007).
73. V.K. Tolpygo, D.R. Clarke, K.S. Murphy, *Surf. Coat. Technol.* **188–189**, 62 (2004).
74. D.R. Clarke, *Curr. Opin. Solid State Mater. Sci.* **6**, 237 (2002).
75. V. Sergo, D.R. Clarke, *J. Am. Ceram. Soc.* **81**, 3237 (1998).
76. V.K. Tolpygo, J.R. Dryden, D.R. Clarke, *Acta Mater.* **46**, 927 (1998).
77. P.Y. Hou, A.P. Paullikas, B.W. Veal, *Mater. Sci. Forum* **522–523**, 433 (2006).
78. D. Hovis, L. Hu, A. Reddy, A.H. Heuer, A.P. Paullikas, B.W. Veal, *Int. J. Mater. Res.* **98**, 12 (2007). □

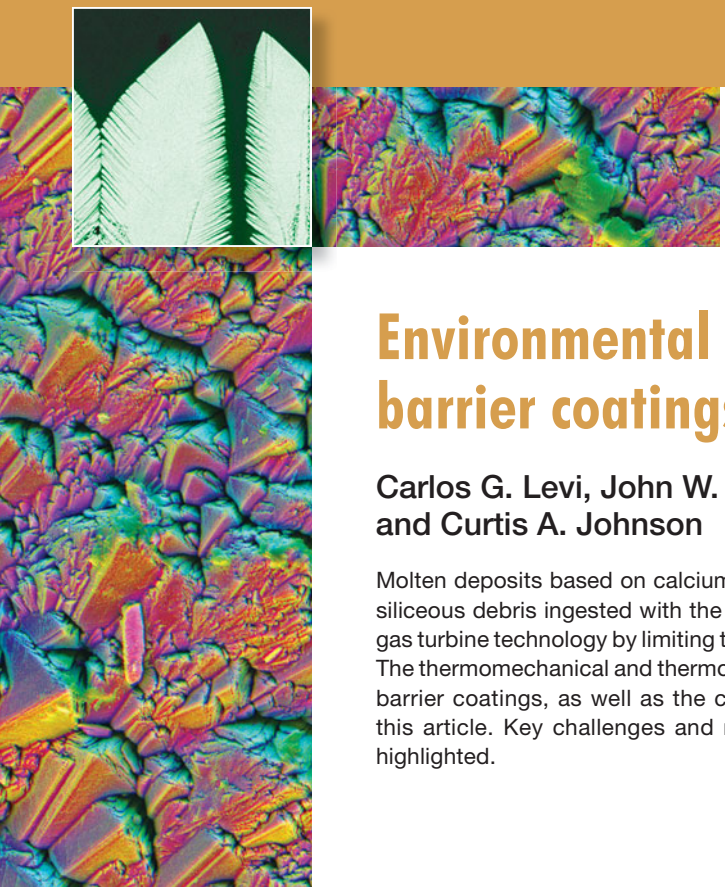

Environmental degradation of thermal-barrier coatings by molten deposits

Carlos G. Levi, John W. Hutchinson, Marie-Hélène Vidal-Sétif, and Curtis A. Johnson

Molten deposits based on calcium-magnesium alumino-silicates (CMAS), originating from siliceous debris ingested with the intake air, represent a fundamental threat to progress in gas turbine technology by limiting the operating surface temperature of coated components. The thermomechanical and thermochemical aspects of the CMAS interactions with thermal-barrier coatings, as well as the current status of mitigating strategies, are discussed in this article. Key challenges and research needs for developing adequate solutions are highlighted.

Introduction

The degradation of thermal-barrier coatings (TBCs) by molten deposits resulting from a combination of impurities introduced with the intake air and/or the fuel has been a concern since the introduction of these material systems in gas turbines. Corrosion by molten salts, especially alkaline sulfate-vanadate mixtures, was of early interest owing to (1) their potential for de-stabilization of the non-transformable, metastable tetragonal yttria-stabilized zirconia (*t'*-YSZ)[1–3] commonly used as a topcoat material and (2) their possible infiltration toward the thermally grown oxide (TGO) because their melting point is below the temperature of the TGO/TBC interface (see the Introductory article in this issue for a more detailed description of TBC structure). The latter could have two consequences, one related to a chemical attack of the TGO/bond coat,[4] and the other associated with freezing of the salt within the TBC on cooling and the ensuing loss of strain tolerance.[5] Phenomenological models have been developed to assess the effects of sulfate infiltration on coating life,[6] and promising materials solutions have been proposed.[7–9] However, currently adopted solutions rely primarily on fuel quality control.

As noted elsewhere in this issue, coatings are now enabling to the design of advanced gas turbines, whether based on metallic or ceramic components, with current goals calling for material surface temperatures ≥1500°C.[10] While low melting temperature salts remain a problem in some TBC applications, they do not constitute a fundamental barrier to increased performance, because the projected elevation in gas temperature would be above the dew point of most sulfate/vanadate salts. In contrast, the severe threat of silicate deposits at higher temperature operation was recognized quite early.[11–13] The problem arises from the ingestion of siliceous debris (airborne dust, sand, ash) that adheres to the surfaces in the hot gas path (combustors, airfoils, shrouds) and at peak temperatures of the engine cycle (e.g., take-off or landing) yields glassy melts based on calcium-magnesium alumino-silicates (CMAS). The glass wets all coating materials of interest and can (1) penetrate the TBC void spaces that accommodate the strain incompatibility with the metallic substrate and/or (2) chemically dissolve the coating material, usually followed by precipitation of a modified oxide.[12–16] Because all prospective TBCs have to be porous/segmented to render them strain-tolerant and most silicate deposits melt around 1200°C,[12,13,17,18] any increases in operating temperature needed to enhance turbine efficiency would require finding solutions to the CMAS problem. These deposits and the associated degradation of TBCs are therefore the primary focus of this article.

This article is organized into three main sections. The first section discusses the thermomechanical problem and the associated driving forces. The second addresses thermochemical

Carlos G. Levi, Materials Department, University of California, Santa Barbara; levic@engineering.ucsb.edu
John W. Hutchinson, School of Engineering and Applied Sciences, Harvard University; Hutchinson@husm.harvard.edu
Marie-Hélène Vidal-Sétif, Department of Metallic Materials and Structures, Onera, French Aerospace Lab; marie-helene.vidal-setif@onera.fr
Curtis A. Johnson, GE Global Research and Center for Thermal Spray Research, Stony Brook University; johnsonca@nycap.rr.com
DOI: 10.1557/mrs.2012.230

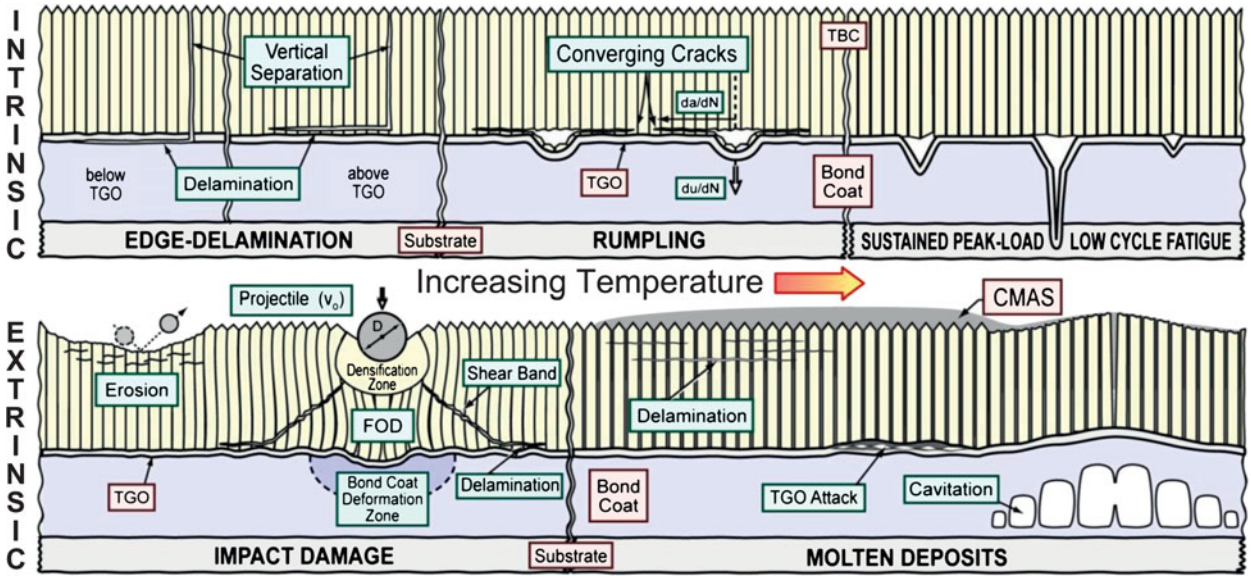

Figure 1. Extended menu of failure mechanisms typical of current thermal-barrier coatings (TBCs).[19] Three general modes of CMAS damage (lower right), characteristic of higher temperature operation, have been identified so far. One involves delamination cracks propagating through the TBC, another leads to chemical attack of the thermally grown oxide (TGO) with concomitant loss of adherence, and a third results from creep cavitation of the bond coat below a heavily penetrated TBC. FOD, foreign object damage; da/dN, crack growth per cycle; du/dN, inward displacement of TGO per cycle.

issues, which lead to opportunities for mitigation. The third deals with the experimental evaluation of the mitigation approaches. It finishes with a brief outlook on critical research needs.

Thermomechanical aspects

CMAS related damage mechanisms and field evidence

The TBC failure mechanisms identified to date are illustrated in **Figure 1**. While the role of CMAS is viewed primarily in terms of stiffening of the top *t'*-YSZ coat leading to shallow or deep delaminations,[13,20,21] recent work has shown that CMAS contact with the TGO results in chemical interactions and subsequent delamination along the TGO[22] or may promote creep cavitation in the bond coat wherein the delamination crack path would propagate within the metal, rather than the ceramic layers.[23] As turbine temperatures continue to increase, existing mechanisms will be aggravated, and new forms of damage may arise. Moreover, CMAS infiltration leads not only to stiffening of the coating, but also to degradation of the insulating properties of the TBC,[24,25] which may aggravate other intrinsic but nominally unrelated forms of degradation (e.g., rumpling[26]). The challenge of coating life prediction thus acquires new dimensions in the presence of CMAS.

An example of CMAS damage on current airfoils is depicted in **Figure 2** (left side) corresponding to state-of-the-art *t'*-YSZ TBCs in a commercial aircraft engine. While the thermal history cannot be ascertained, it is known that the engine operated short flights (i.e., frequent cycles with substantial hot periods) in dusty environments.[27] The distress is quite evident, extending beyond TBC loss to affect the TGO and bond coat, in some places exposing the base metal. (The coating on the right side of Figure 2 is discussed later in the text.)

Delamination damage due to CMAS has been studied in both commercial and military aircraft engines and exhibits common features in coatings produced by electron-beam physical vapor deposition (EBPVD)[20] as well as dense, vertically cracked TBCs produced by atmospheric plasma spray (APS).[21] In areas where the coating was cracked but not yet lost, the level

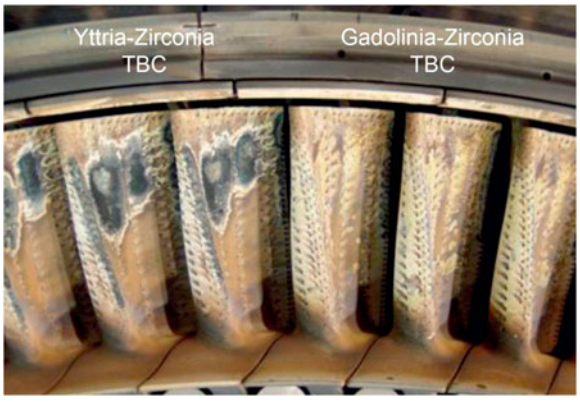

Figure 2. Comparison of typical distress experienced by conventional thermal-barrier coatings (TBCs) based on 7–8% yttria-stabilized zirconia with an advanced TBC based on $Gd_xZr_{1-x}O_{2-x/2}$ pyrochlore, where $x \approx 0.5$. The airfoils were part of an engine test in actual aircraft operation.[26] Courtesy of M.J. Maloney, Pratt & Whitney.

of CMAS penetration was about one-half of the total thickness, but deeper penetrations have been found in other airfoils. The driving forces behind these failures are now examined briefly.

Understanding the driving force for thermo-mechanical failure

Release of the elastic strain energy stored in the coating supplies the underlying driving force for the delamination and spalling of TBC coatings.[28] The major source of this elastic energy is the thermal expansion mismatch between the coating and the metal substrate that occurs upon cooling. To facilitate understanding of the origin of this elastic energy, the following discussion will focus first on isothermal cooling of the TBC/substrate system and then consider more representative scenarios involving a thermal gradient through the system in the hot state and transient cooling.

Stress in the coatings is relaxed by creep at high temperatures, and, thus, a reasonable working assumption is that the coating stresses are zero at the hottest operating state. Cool-down is relatively rapid, such that in most instances, one may assume that thermoelastic behavior applies with no further creep relaxation. Clear insights into the coating stress and elastic energy emerge from a model that views the substrate as thick and at uniform temperature.[28] The substrate constrains bending, which is taken to vanish in the model and imposes an in-plane biaxial strain change, $-\alpha_s \Delta T_{sub}$, on the coating. Here, α_s is the thermal expansion coefficient of the substrate and, during cooling, $\Delta T_{sub} = T^0_{sub} - T_{sub}$ is the temperature drop of the substrate from its temperature in the hot state, T^0_{sub}. For simplicity, the coefficients of thermal expansion will be taken to be temperature-independent. In the hot state, a steady-state temperature distribution exists with T^0_{sur} at the coating surface and T^0_{sub} at its interface with the substrate. The temperature drop of the coating surface relative to the substrate is denoted by $\Delta T_{sur/sub} = \left(T^0_{sur} - T_{sur}\right) - \Delta T_{sub}$.

Consider a single layer uniform coating with Young's modulus, E_c, Poisson's ratio, ν_c, coefficient of thermal expansion, α_c, and thickness, h_c. At any stage during cool-down, idealize the temperature distribution in the coating to be linear according to

$$\Delta T(y) = \Delta T_{sub} + (y/h_C)\Delta T_{sur/sub}, \quad (1)$$

with y as the through-thickness coordinate measured from the interface. At any stage during cool-down, the state of stress in the layer is equibiaxial, in-plane, given by

$$\sigma(y) = \frac{E_C}{1-\nu_C}\left(-\Delta\alpha_C \Delta T_{sub} + (y/h_C)\alpha_C \Delta T_{sur/sub}\right). \quad (2)$$

This equation reveals that cooling of the coating relative to the substrate generates tensile stress depending on the full coefficient of thermal expansion of the coating, while cooling of the substrate imposes stress on the coating depending on the thermal expansion mismatch, $\Delta\alpha_c = \alpha_S - \alpha_c$. The elastic energy per area in the coating associated with these thermal stresses, available for release of the coating from the substrate under plane strain conditions, is

$$U = \frac{E_C h_C (1+\nu_C)}{2(1-\nu_C)}\left\{(\Delta\alpha_C \Delta T_{sub})^2 - (\Delta\alpha_C \Delta T_{sub})(\alpha_C \Delta T_{sur/sub}) + \frac{1}{3}(\alpha_C \Delta T_{sur/sub})^2\right\}. \quad (3)$$

The interaction term, $(\Delta\alpha_C \Delta T_{sub})(\alpha_C \Delta T_{sur/sub})$, is important, and it arises because the compressive coating stress driven by cooling of the substrate, ΔT_{sub}, can be offset by the tensile stress associated with cooling of the coating surface relative to the substrate, $\Delta T_{sur/sub}$. For the calculations shown here, $\alpha_C = 11 \times 10^{-6}\ C^{-1}$, $\alpha_S = 13 \times 10^{-6}\ C^{-1}$, and the coating's Poisson's ratio is $\nu_c = 0.2$.

The elastic energy/unit area given by Equation 3 is plotted in normalized form ($U/E_c h_c$) in **Figure 3**. Two limiting scenarios are insightful. The first applies when the coating and substrate have a uniform temperature both in the hot state and while cooled (i.e., ΔT_{sub} increases while $\Delta T_{sur/sub} = 0$). This is representative of furnace cycle tests involving isothermal holds and relatively slow-cooling. Given that U scales with h_c and considering a typical in-plane modulus absent CMAS penetration, $E_c = 30$ GPa, a "thin" 200 μm TBC illustrative of aero-engine blades would build up an elastic energy of ~11 J·m^{-2} on cooling from $T^0_{sub} = 800$°C, whereas a "thick" 1-mm coating that might be found in power generation components would reach ~58 J·m^{-2} under the same conditions. Whether failure would occur depends, of course, on the coating toughness under the pertinent crack propagation mode, which is not well characterized for these systems.

Consider now the case where the TBC is stiffened by complete penetration of CMAS, elevating the Young's modulus to at least that of typical glasses (i.e., $E_c = 90$ GPa). (Higher values are likely given that most of the coating is dense *t'*-YSZ, with $E_{YSZ} \approx 200$ GPa.) The elastic energy accumulated in the same thermal excursion for the representative "thin" and "thick" coatings cited previously would then go up by a factor of 3, to ~35 and ~173 J·m^{-2}, respectively. This simple result gives the clearest insight into the role CMAS plays in debilitating a TBC by degrading its in-plane compliance. CMAS infiltration also alters other properties of the coating such as the coefficient of thermal expansion and the thermal conductivity,[24,25] but from the vantage point of delamination, the major effect is the boost in the coating modulus. While CMAS seldom infiltrates all the way to the coating/substrate interface, as assumed in computing Figure 3 with a single value of E_c, its effect on the elastic energy in the coating is self-evident. In particular, a coating with an ample reserve against delamination may experience a factor-of-two increase in elastic energy/area due to thermal stresses when partially infiltrated by CMAS.[21,28]

The second scenario of interest in Figure 3 is one wherein the substrate temperature remains relatively unaffected, $\Delta T_{sub} \approx 0$, but the coating surface temperature drops rapidly relative to the substrate, $\Delta T_{sur/sub} > 0$. This may occur, for example, if cool

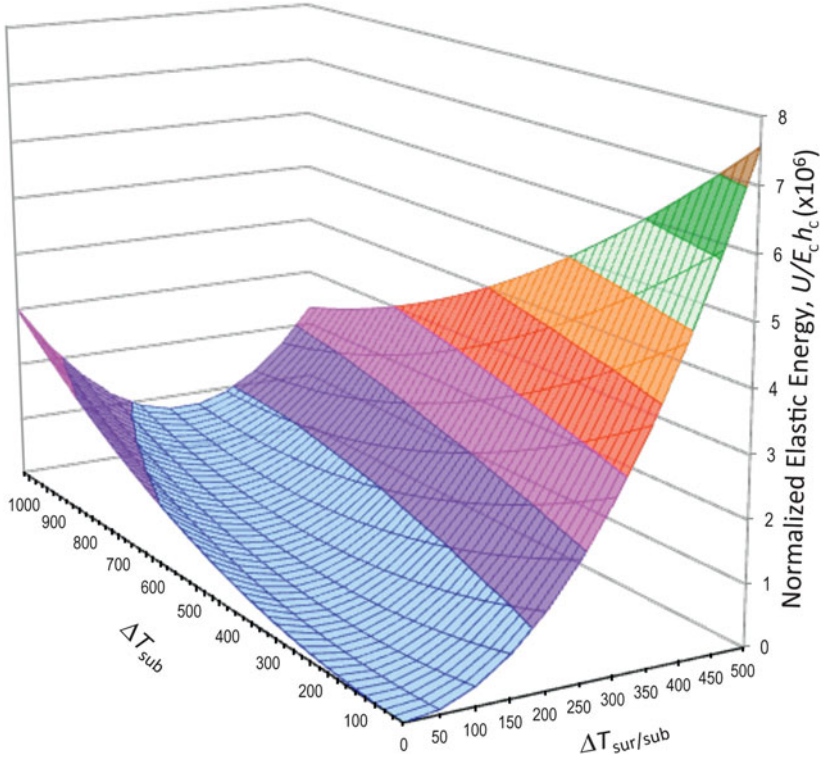

Figure 3. Normalized elastic energy/area in the coating ($U/E_c h_c$) calculated from Equation 3 and available for release under plane strain conditions due to thermal stress induced by cooling from an initially high temperature. ΔT_{sub} and $\Delta T_{sur/sub}$ are the temperature drops of the substrate and of the coating surface relative to the substrate, respectively, and the properties of the coating/substrate system are as defined in the text. Note that any value of U would scale with the coating modulus E_c (e.g., due to stiffening by calcium-magnesium alumino-silicate penetration) and with the coating thickness, h_c. Also note that cooling paths wherein $\Delta T_{sur/sub}$ and ΔT_{sub} change simultaneously may result in much lower strain energy buildup.

gas suddenly impinges on the coating owing to an unexpected flameout of an engine. As seen in Equation 2, the thermal stress in the coating is now proportional to $\alpha_c \Delta T_{sur/sub}$, and it develops primarily from self-constraint of the coating to thermal contraction as its surface cools faster than the region closer to the substrate. The trend in elastic energy/area that arises from this contribution corresponds to the trace of the $U/E_c h_c$ surface in Figure 3 with the plane $\Delta T_{sub} \approx 0$. If a rapid cooling event occurs with $\Delta T_{sur/sub}$ as large as 400°C, the elastic energy in the coating in the early stage of cool-down could exceed that at the final cool-down (cf. the "quench" scenario in Figure 8c). It is also evident from Figure 3 that the buildup of elastic energy can be ameliorated when both ΔT_{sub} and $\Delta T_{sur/sub}$ define a path along the valley in the $U/E_c h_c$ surface (cf. the "slow cool" scenario in Figure 8c).

Numerous thermal scenarios beyond those presented previously must be considered to assess the ability of a TBC to resist delamination.[29] To set the foundation for the discussion of thermal gradient tests (see the section on Assessing the mitigation strategy), a rapid cooling scenario will be illustrated for a system having a superalloy substrate 3.5 mm thick coated by a representative *t'*-YSZ layer with $h_c = 1$ mm. The initial steady-state temperatures of the coating surface and the underside of the substrate are $T^0_{sur} = 1300$°C (above the melting point of most typical CMAS deposits) and 800°C, respectively, with $T^0_{sub} = 830$°C at the coating/substrate interface. Starting at time $t = 0$, forced cooling air at 35°C is switched on, impinging on the coating surface, with nominally stagnant air at 35°C on the underside of the substrate. (This would not be typical of engine operation but is of interest in laboratory tests.) The transient temperature history shown in **Figure 4**a has been computed using heat transfer coefficients representative of forced air cooling at the coating surface and radiative cooling with natural convection at the underside.[29] In this figure, ΔT_{sub} is identified with the temperature drop at the interface, and $\Delta T_{sur/sub}$ is the temperature drop of the coating surface relative to that at the interface. Within the first several seconds, $\Delta T_{sur/sub}$ peaks at ~650°C, while ΔT_{sub} remains relatively small. As the cooling progresses, the approach to the asymptotic limits in Figure 4a reflect cooling of the substrate to room temperature and the contribution of the initial temperature gradient across the coating to $\Delta T_{sur/sub}$.

Transient histories of elastic energy/area in the coating, U, based on the transient temperature drops in Figure 4a, are plotted in Figure 4b for a uniform coating 1 mm thick and for a 1 mm coating having an upper layer of thickness 0.25 mm penetrated by CMAS. α_c, α_c, and ν_c are as specified. The lower curve for the uniform coating with no CMAS was computed using Equation 3. The upper curve was computed with an equation similar to 3, but more complicated, for a bilayer coating. For simplicity, the CMAS layer was assumed to have solidified as soon as cooling commenced, with the coating surface at 1300°C. In addition, only E_c was assumed to have been altered by CMAS; the thermal properties are assumed to remain the same as those of the unpenetrated coating.

The evolution of U in Figure 4b reveals that a TBC will experience a peak in elastic energy in the early stage of a rapid cool-down, within about 2 s for a 1 mm thick coating. More importantly, CMAS penetration in the upper quarter of the coating would double this peak energy. In the presence of an initial thermal gradient, the 1 mm coating is most susceptible to delamination under rapid cooling when the elastic energy due to the thermal stress peaks. Under this scenario, the energy/area in the cold state is much less than the early stage peak. This is partly due to the fact that the tensile stress in the cold state, due to the initial temperature gradient contribution to $\Delta T_{sur/sub}$, is offset by the compressive stress induced by the thermal expansion mismatch with the substrate.

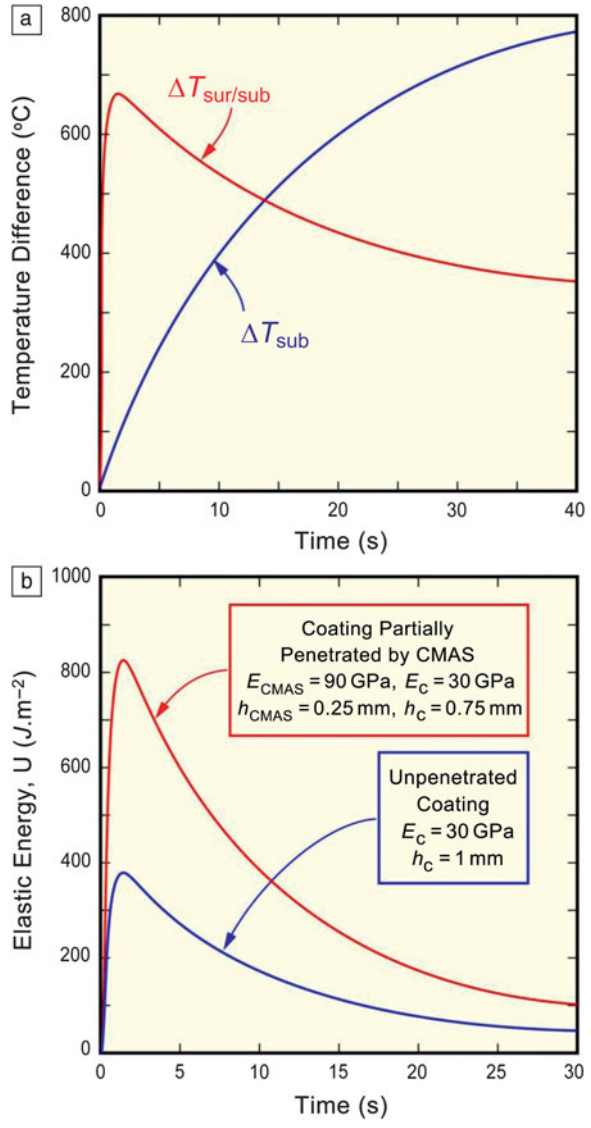

Figure 4. Transient temperature drops of the substrate (ΔT_{sub}) and of the coating surface relative to the substrate interface ($\Delta T_{sur/sub}$) (a) and associated transient elastic energy/area of the coating (b) for a sudden cooling event in which ambient air (35°C) impinging on the surface of the coating is switched on at $t = 0$. $T^0_{sur} = 1300$°C and $T^0_{sub} = 830$°C.

Coating design for resistance to delamination requires analysis of other thermal scenarios with due consideration given to the role of CMAS, as evident from the earlier discussion. A simplified model has been used here to reveal trends. More accurate calculations are required to account for details such as the full temperature distribution, bending of the substrate, and the crystallization/glass-transition temperature of the CMAS. Moreover, the energy release rate and mode mix associated with delamination cracking can be computed accurately with enhanced models. The trends for the energy release rate follow those for the stored elastic energy/area, *U,* quite closely.

Thermochemical aspects

Notwithstanding the predominantly thermomechanical origin of the CMAS-related TBC failures, substantial effort has been invested toward understanding the thermochemical interactions with *t'*-YSZ (e.g.,[12–14,26,30–33]). However, *t'*-YSZ is unlikely to meet the long-term requirements for advanced engines even when CMAS is not a concern, because of inherent limitations in its phase stability above ~1200°C.[34–36] Conversely, understanding the chemical interactions is essential for developing alternate coatings, since CMAS nominally attacks all oxides of interest for thermal (and environmental) barriers. Materials that may outperform *t'*-YSZ in a CMAS environment already exist, as illustrated in Figure 2,[37] but with penalties in critical properties such as toughness (see the Pan et al. article in this issue).[38] This section briefly addresses the salient issues regarding the nature of the deposits, the lessons learned from *t'*-YSZ, and the experiences with proposed mitigation strategies.

Sources and composition of silicate deposits

A key challenge in understanding thermochemical interactions and developing a foundation for life prediction models is the uncertainty in the amount and chemical composition of the molten glass formed on the coating surface. In general, compositions of actual engine deposits are significantly different from the common sources of siliceous minerals (**Figure 5**). The rationale is that only the finer particles (<10 μm) ingested with the intake air contribute to the deposit buildup.[17,39] Moreover, the deposits contain oxides originating from the engine components, presumably by erosion (e.g., NiO, TiO_2, ZrO_2).[13,26] It has also been shown that the composition of melts infiltrating the TBC are not necessarily the same as those of the deposits, suggesting partial melting of the latter. The infiltrated CMAS were reported to have similar compositions for a wide variety of deposits, loadings, and severity of exposure.[13] However, the diversity of reaction products with the *t'*-YSZ, discussed later, suggests that the CMAS compositions may vary more widely than originally suggested.

The mechanism and rate of deposit buildup remain under debate. One might anticipate that the siliceous "dust" melts in flight through the combustor and deposits as droplets. Examination of some airfoil deposits, however, reveals agglomerates of solid particulates, implying that melting might occur *in situ*, probably during the hotter stages of the engine cycle, but the details are obscure. The rate of accumulation also varies over the surface of an airfoil, concentrating on the hotter areas of the higher pressure side and, to some extent, on the leading edge, with little or no deposits on the suction side.[26,33,39]

Experiences with t'-YSZ

The primary mechanism of interaction between a molten silicate glass and an oxide is that of dissolution and, upon saturation, re-precipitation of one or more crystalline phases closer to equilibrium with the melt,[14] cf. **Figure 6**. When penetration is extensive, as in *t'*-YSZ under isothermal exposure above the CMAS melting point (cf. Figure 7 in the Introductory article),

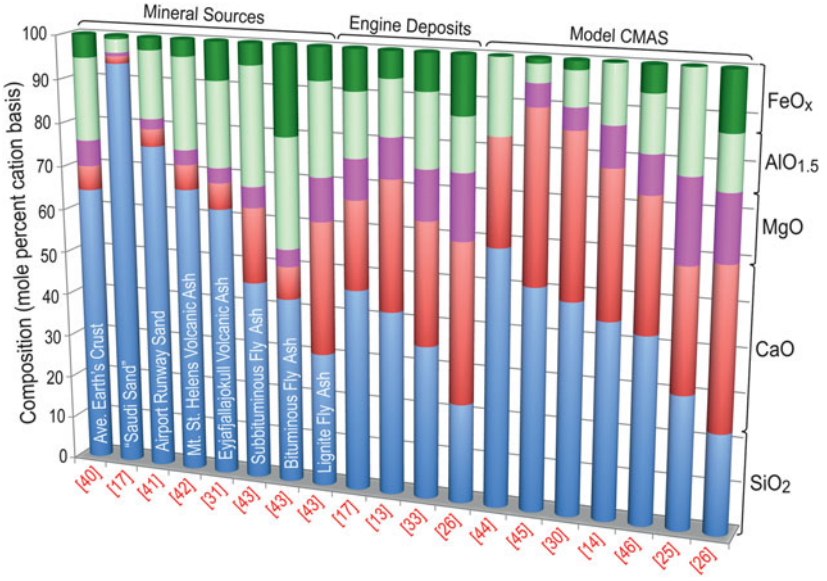

Figure 5. Concentration of predominant oxides in the composition of calcium-magnesium alumino-silicates, grouped by examples of sources of siliceous debris, compositions reported for actual deposits in engines, and model compositions used in laboratory investigations of the problem. (Small additions in some model compositions are not included.) Within each group, the compositions are listed from left to right in order of descending SiO_2 content, except for the average composition of the earth's crust that serves as a reference. Reference citations are listed along the bottom of the image.

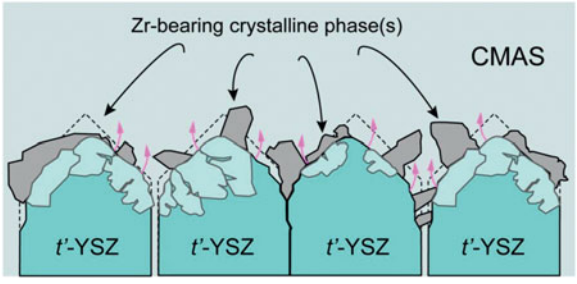

Figure 6. Schematic illustration of the dissolution-reprecipitation mechanism in yttria-stabilized zirconia, wherein the coating material dissolves in the molten glass and reprecipitates as one or more compositionally modified crystalline phases. Some of the phases may form at high temperature, whereas others may precipitate upon cooling.

the extent of interaction can be significantly different within the pore spaces, where the melt volume is small relative to the TBC, compared with the surface, where the relative proportion of melt is much larger. Laboratory approaches aiming to replicate the interaction in service range from those using materials sampled from the field,[12,13,31] to the use of "synthetic CMAS" similar in composition to the deposit (see References 32 and 47), to studies using simplified compositions with only a few oxides.[14,44,49]

In a baseline study, *t'*-YSZ (EBPVD) dissolved isothermally in a model CMAS melt with (Ca+Mg):Si ≈ 0.93 (1300°C/4h) and reprecipitated either Y-lean ZrO_2, transformable to monoclinic on cooling, or fully stabilized Y-rich cubic ZrO_2, depending on the alumina content of the melt.[14] Similar observations were made on APS *t'*-YSZ exposed to a more complex CMAS with (Ca+Mg):Si ≈ 0.86 (1121°C/24h).[30] In contrast, a simpler CAS melt with Ca:Si ≈ 0.41 and similar Al (1200°C/4h) yielded $Ca_2ZrSi_4O_{12}$.[49] A complex "synthetic volcanic ash" with an even lower (Ca+Mg):Si ≈ 0.15 (1200°C/1h) was reported to form $ZrSiO_4$ (zircon) at the interface, whereas a lignite fly ash with a much higher (Ca+Mg):Si ≈ 1.1 produced predominantly tetragonal YSZ.[31] In most of these experiments, the residual CMAS was largely amorphous upon cooling, although crystalline silicates were found in some cases. Observations in field specimens were at least qualitatively consistent with these simulated exposures, with no evidence that the reaction products played a significant role in mitigating penetration and the ensuing stiffening. In one peculiar service airfoil, where $CaSO_4$ was found to have infiltrated the TBC prior to CMAS exposure, there was no detectable reaction within the spaces in the columnar *t'*-YSZ structure, but $CaZrO_3$ was found on top of the column tips.[26] The latter reacted with the overlying silicate melt, presumably deposited later, to yield a complex garnet phase (kimzeyite) with composition $Ca_3(Zr,Mg,Ti)_2(Fe,Al,Si)_3O_{12}$. One might speculate that this reaction layer has potential for CMAS mitigation, but at the expense of infiltrating the TBC with solid $CaSO_4$, which would compromise the strain tolerance of the coating. While the coating survived in this case, this does not appear to be a practical solution in the long term.

Mitigation strategies

Numerous CMAS mitigation strategies for YSZ have been proposed in the literature,[46,50,51] but the persistence of the problem suggests they have not been as effective as expected. Most current approaches are based on manipulating the chemical reaction between the TBC and the melt to accomplish two goals simultaneously: (1) "immobilize" the melt by capturing its main constituents into crystalline phases, most obviously silicates, and (2) generating enough volume of precipitated products to fill the pore spaces and block access of any residual melt to the remaining TBC. The implications are that (1) the chemical reaction should yield stable crystalline products in excess of the simple reprecipitation of the Zr-rich phases, since those are essentially replacing the dissolved material, and (2) the kinetics of both the dissolution and reprecipitation processes must be competitive with the infiltration kinetics (i.e., the reaction must be quite fast).

Two broad strategies based on reactivity can be distinguished. One is based on alumina as the key reactant, which combines with CaO and SiO_2 to form anorthite, $CaAl_2Si_2O_8$. The seemingly most successful approach in this category involves the incorporation of alumina in metastable solid solution in

YSZ, with a small amount of TiO_2 to catalyze the crystallization process.[30,47] Because the volume of alumina required for effective mitigation is well beyond its equilibrium solubility in ZrO_2, the approach exploits the ability of solution precursor plasma spray[52] to generate the desired coatings (see the Sampath et al. article in this issue for a description of this technique).

The second mitigation strategy is based on rare-earth (RE) zirconates, exemplified by $Gd_2Zr_2O_7$ (GZO).[31,53,54] This is the material showing no significant distress on the right-hand side of Figure 2. The merit of the approach relies on the dissolution of $RE_2Zr_2O_7$ to precipitate a $Zr(RE,Ca)O_x$ fluorite phase combined with a highly stable apatite silicate with nominal composition $Ca_2RE_8(SiO_4)_6O_2$, where RE can be Y or one of the lanthanides from La to Yb.[54] The mechanism is illustrated in **Figure 7** and proceeds as follows: (a) the glass melt rapidly wets the inner surfaces of the columns, with some features of the interaction suggesting intriguing topography effects on melt spreading; (b) re-precipitation of fluorite starts soon thereafter, concurrent with that of apatite (faceted crystals) in the narrower spaces, indicating that dissolution was already occurring at the shortest time; (c) generalized precipitation of apatite and fluorite, filling first the narrower gaps wherein supersaturation is achieved earlier; (d) gaps are sealed, and the column surface is covered with a nominally dense layer of reaction product, which acts as a diffusion barrier; and (e) after the gaps are sealed (reflected in the ghost structures projecting from the voided column gaps underneath), reaction continues at a much slower rate consuming the column tips. The CMAS used in these experiments had Ca:Si ≈ 0.73, whereas the apatite product has Ca:Si = 0.33, implying that the melt should be preferentially depleted in Si upon reaction, with concomitant reduction in melt volume. Recent experiments have shown that similarly favorable reactions take place with other zirconates.[44,48]

To the best of the authors' knowledge, Gd-zirconate has now been in operation in engines for several years after the successful experience depicted in Figure 2. RE zirconates generally offer lower thermal conductivity and enhanced sintering resistance relative to *t'*-YSZ, although some concerns remain about their lower toughness.[55] Alternate compositions, including those based on other zirconates, as well as on alumina+titania additions, remain under investigation.

Assessing the mitigation strategy

Developing and optimizing a mitigation strategy requires insight into two major topics, namely the comparative kinetics of the infiltration, dissolution, and reprecipitation processes, and the mechanical robustness of the stiffened layers generated by the CMAS/TBC reactions. Thermal analysis coupled with microstructural observations can be used to assess the activity of the reaction.[57] Notably, recent measurements on the ZrO_2-Nd_2O_3 system[44] have determined that the dissolution rate of the oxide depends on the RE concentration, confirming that the pyrochlore structure zirconate not only promotes the precipitation of apatite, but also the rapid dissolution of the TBC, both needed to compete with the infiltration kinetics. It is also worth noting the potential effects of the initial state of the CMAS reactant. Pre-melted amorphous CMAS has homogeneity advantages but also leads to uncertainty in the behavior upon heating, since some compositions crystallize

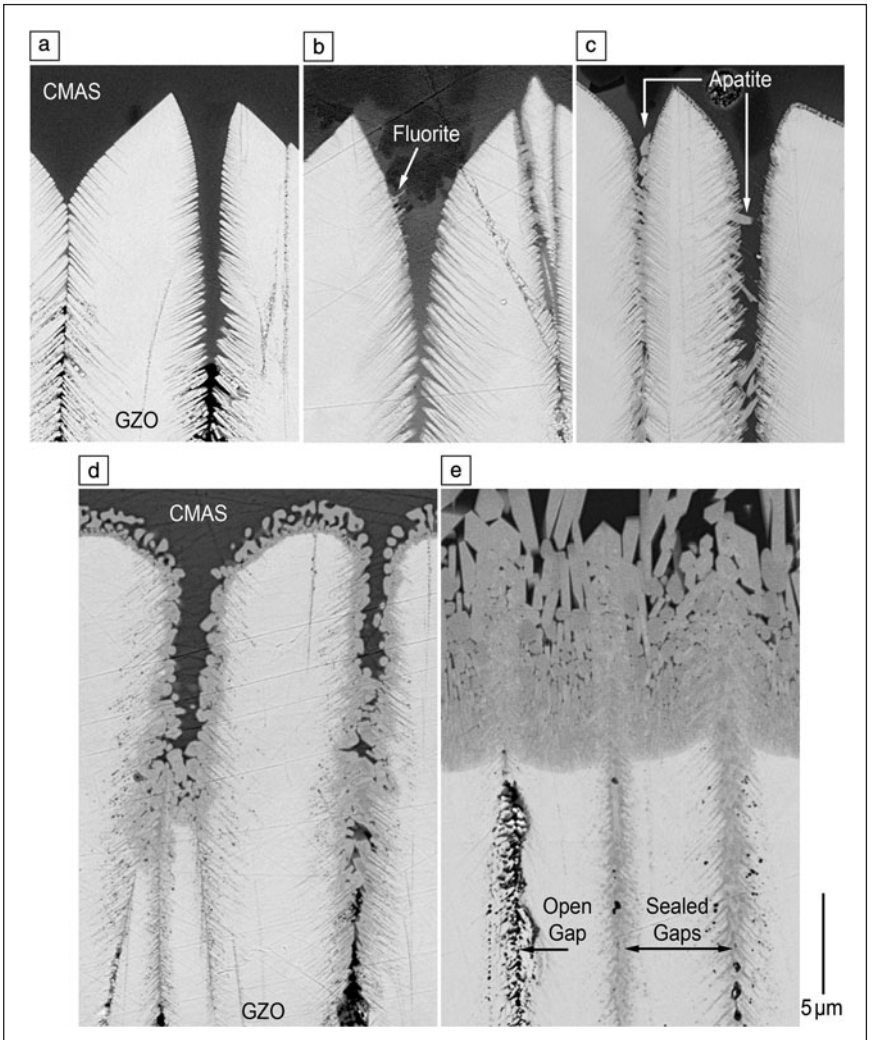

Figure 7. Illustration of the sequence of events that leads to the sealing of the intercolumnar gaps owing to the chemical interaction of calcium-magnesium aluminosilicates (CMAS) with a Gd zirconate electron beam physical vapor deposition coating (see the Introductory article of this issue). The top images represent the early stages of the reaction and were generated using amorphous CMAS heated rapidly to 1150°C for (a) 10s, (b) 20s, and (c) 30s. The bottom specimens were longer time exposures using initially crystalline CMAS (d) 4 min above the melting point and immediately cooled down, and (e) 4h at 1300°C. Images courtesy of S. Krämer.

and then melt, whereas others soften gradually, complicating the interpretation of the heat evolution history.[57]

Thermomechanical assessment of CMAS infiltrated/reacted systems is still in its infancy. Thermal gradient tests are essential since "isothermal" furnace cycle tests can lead to misleading results, and tests at 1300°C and above would compromise superalloy substrates. Jet engine thermal shock (JETS) tests[50,56] are often used to assess the performance of TBCs under thermal gradients and have been extended to CMAS testing (see the Vaβen et al. article in this issue). Burner rigs have also been modified to enable the injection of CMAS precursor solutions through the flame[45] and are used successfully for testing plasma spray $ZrYAlTiO_x$ coatings.[58] In both cases, the temperatures in the front and back of the specimen are measured during the cycle and used to calculate the evolution of the strain energy.[28] A thermal gradient test based on a laser heat source, schematically depicted in **Figure 8**a, has been recently developed.[59] Proper specimen design allows monitoring of not only the temperature at the surface and the backside of the substrate, but also near the TGO/TBC interface. Thermal histories can be accurately recorded and carefully manipulated using the laser power-up and -down rates (e.g., Figure 8b). In addition, the system is set up with blue LED illumination and suitable filters,[60] allowing visual monitoring of the coating surface during heating and cooling. The thermal history can then be cast in terms of ΔT_{sub} and $\Delta T_{sur/sub}$ (as discussed in the section on Understanding the driving force for thermomechanical failure), and used to calculate the strain energy buildup during cooling, Figure 8c. Specimens are then examined after testing to identify the type and extent of damage, Figure 8d–e, which can in turn be correlated to the thermal history. It is anticipated that this instrument will be invaluable in testing materials systems and in helping refine the models needed to build life prediction capabilities for TBCs with CMAS.

Outlook

The CMAS problem in thermal-barrier coatings (TBCs) is intrinsically thermomechanical, but thermochemical issues are relevant to formulating an effective mitigation strategy. Because the driving force for delamination scales with the square of the temperature drop, the problem is expected to increase in severity as TBCs are pushed to higher surface temperatures, while the TBC/thermally grown oxide interface remains near present levels. The grand challenge of the field is the search for a viable oxide that offers both CMAS resistance and adequate toughness. For zirconia/hafnia based systems, the challenge arises from the dichotomy in design approaches *viz*, CMAS resistant compositions require large concentrations of reactive dopants [Y, RE, Al], whereas tough compositions are based on tetragonal crystal structures with much lower dopant content.

Developing the science base to guide the materials development effort requires the effective integration of modeling and

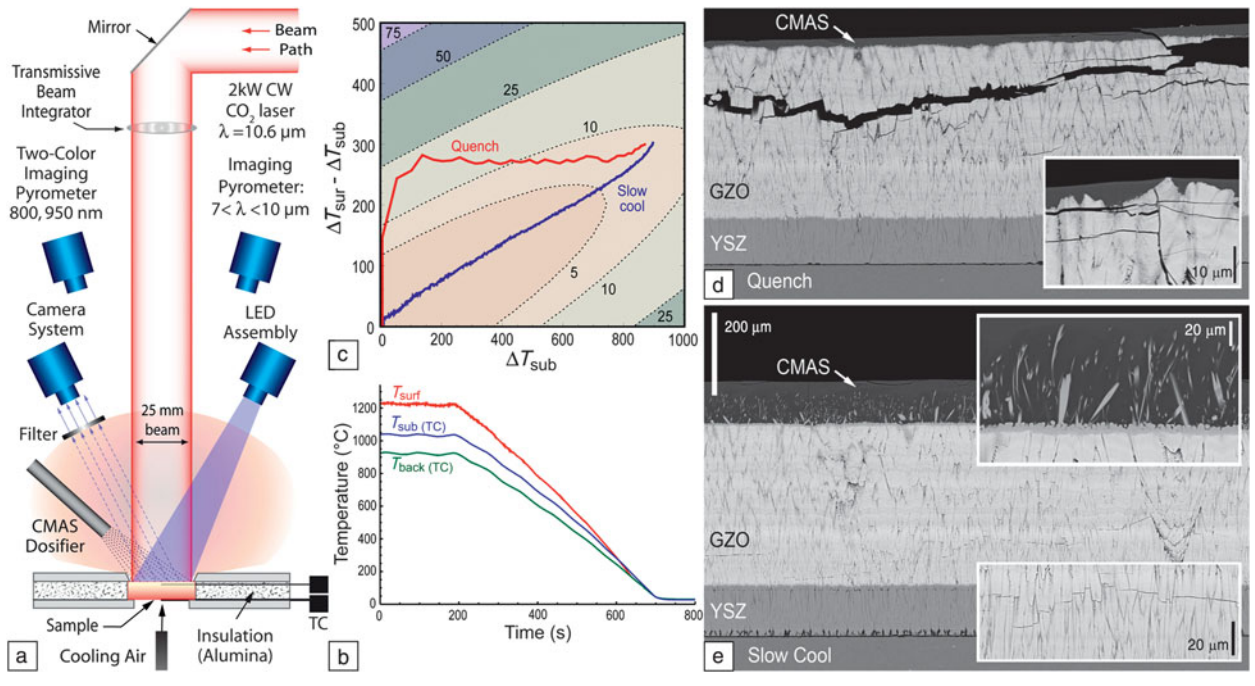

Figure 8. Illustration of a (a) thermal gradient test based on a continuous CO_2 laser with backside cooling and extensive instrumentation used to probe the response of coatings infiltrated with calcium-magnesium alumino-silicates to various thermal excursions. The thermal histories (e.g., (b)) can be varied over a substantial range, and ensuing thermal stresses and associated strain energies can be estimated based on models such as those described in the text; (c) projection of the surface in Figure 3 where the contours represent different levels of elastic energy and the paths are two representative thermal excursions corresponding to the samples whose micrographs are illustrated in (d) and (e). The insets show details of the cracks and in (e) the layer of reaction products on the surface of the GZO. Images courtesy of R.W. Jackson.

experimental activities, ideally under an integrated computational materials engineering (ICME) framework.[61] There is a paucity of thermodynamic information on the relevant multicomponent systems to help identify promising compositions that may enable both improvements in toughness and effective reactivity with CMAS melts, as well as to evaluate the sensitivity of candidate materials to the expected variability in melt compositions. Improvements are also needed in the modeling outlined in this article for predicting delamination driving forces, including, for example, assessment of the extent of stress relaxation at the highest temperatures and during cool-down and the interplay of multilayer architectures. Studies on the relevant infiltration, dissolution, and crystallization kinetics for the appropriate combinations of silicate melts and thermal barrier oxides are also essential. Once desirable compositions are identified, it would be necessary to develop the processing science to enable their optimal synthesis into coatings.

On the experimental side, there is a long-standing need for adequate methods for measuring and characterizing the mechanical and thermal properties of coatings at high temperatures, including microstructures produced by thermochemical interactions. It is worth noting that it has been a significant challenge for the field to devise methods to measure delamination toughness, yet this is crucial in developing design approaches to TBCs. Only within the past few years have experimental methods emerged that are capable of measuring coating and interface toughness with reasonable accuracy, but only at temperatures close to ambient. The challenges are daunting, but so are the needs for improving materials that would enable more efficient gas turbines for energy and propulsion.

Acknowledgments

This article draws on lessons from research supported by the Office of Naval Research (CGL) and the French Defense Research Organization (MHVS). The authors are indebted to Dr. M.J. Maloney (PWA) for use of the illustration in Figure 2, as well as to Drs. O. Lavigne (ONERA), D. Konitzer, and D. Lipkin (GE) and Professors N.P. Padture (Brown) and M.R. Begley (UCSB) for helpful discussions. The contributions of Drs. R.W. Jackson and S. Krämer at UCSB are gratefully acknowledged.

References

1. D.W. McKee, P.A. Siemers, *Thin Solid Films* **73**, 439 (1980).
2. A.S. Nagelberg, *J. Electrochem. Soc.* **132** (10), 2502 (1985).
3. R.L. Jones, C.E. Williams, *Surf. Coat. Technol.* 349 (1987).
4. C. Leyens, I.G. Wright, B.A. Pint, *Oxid. Met.* **54** (5/6), 401 (2000).
5. T.E. Strangman, *Thin Solid Films* **127**, 93 (1985).
6. T.E. Strangman, J. Neumann, A. Liu, "Thermal Barrier Coating Life—Prediction Model Development; Final Report" (NASA–Lewis Research Center, 1987).
7. R.L. Jones, "Experiences in Seeking Stabilizers for Zirconia having Hot Corrosion-Resistance and High Temperature Tetragonal (t') Stability" (NRL/MR/6170–96–7841, Naval Research Laboratory, 1996).
8. S. Raghavan, M.J. Mayo, *Surf. Coat. Technol.* **160**, 187 (2002).
9. F.M. Pitek, C.G. Levi, *Surf. Coat. Technol.* **201**, 6044 (2007).
10. M.A. Alvin, F.S. Pettit, G.H. Meier, N.M. Yanar, M. Chyu, D. Mazzotta, W. Slaughter, V. Karaivanov, B. Kang, C. Feng, R. Chen, T.C. Fu, in *5th International Conference on Advances in Materials Technology for Fossil Power Plants*, R. Viswanathan, D. Gandy, K. Coleman, Eds. (Electric Power Research Institute, Inc., Marco Island, FL, 2008), pp. 413–423.
11. J.L. Smialek, F.A. Archer, R.G. Garlick, *JOM* **46** (12), 39 (1994).
12. F.H. Stott, D.J. de Wet, R. Taylor, *MRS Bull.* **19** (10), 46 (1994).
13. M.P. Borom, C.A. Johnson, L.A. Peluso, *Surf. Coat. Technol.* **86–87**, 116 (1996).
14. S. Krämer, J.Y. Yang, C.A. Johnson, C.G. Levi, *J. Am. Ceram. Soc.* **89** (10), 3167 (2006).
15. K.M. Grant, S. Krämer, J.P.A. Löfvader, C.G. Levi, *Surf. Coat. Technol.* **202**, 653 (2007).
16. K.M. Grant, S. Krämer, G.G.E. Seward, C.G. Levi, *J. Am. Ceram. Soc.* **93** (10), 3504 (2010).
17. J.L. Smialek, "The Chemistry of Saudi Arabian Sand: A Deposition Problem on Helicopter Turbine Airfoils" (NASA TM-105234, NASA Lewis Research Center, 1991).
18. W. Braue, *J. Mater. Sci.* **44**, 1664 (2009).
19. A.G. Evans, D.R. Clarke, C.G. Levi, *J. Eur. Ceram. Soc.* **28** (7), 1405 (2008).
20. C. Mercer, S. Faulhaber, A.G. Evans, R. Darolia, *Acta Mater.* **53** (4), 1029 (2005).
21. S. Krämer, S. Faulhaber, M. Chambers, D.R. Clarke, C.G. Levi, J.W. Hutchinson, A.G. Evans, *Mater. Sci. Eng., A* **490**, 26 (2008).
22. V.K. Tolpygo, private communication.
23. K.M. Wessels, R.W. Jackson, D.G. Konitzer, T.M. Pollock, C.G. Levi, presented at the International Conference on Metallurgical Coatings and Thin Films, San Diego, CA, 2012.
24. L. Li, D.R. Clarke, *Int. J. Appl. Ceram. Technol.* **5** (3), 278 (2008).
25. J. Wu, H.B. Guo, Y.Z. Gao, S.K. Gong, *J. Eur. Ceram. Soc.* **31**, 1881 (2011).
26. W. Braue, P. Mechnich, *J. Am. Ceram. Soc.* **94** (12), 4483 (2011).
27. M.J. Maloney, in *Turbine Forum* (Forum of Technology, Germany, Nice-Port St. Laurent, France, 2006).
28. A.G. Evans, J.W. Hutchinson, *Surf. Coat. Technol.* **201**, 7905 (2007).
29. S. Sundaram, D.M. Lipkin, C.A. Johnson, J.W. Hutchinson, *J. Appl. Mech.* (2012), in press.
30. A. Aygun, A.L. Vasiliev, N.P. Padture, X. Ma, *Acta Mater.* **55** (20), 6734 (2007).
31. A.D. Gledhill, K.M. Reddy, J.M. Drexler, K. Shinoda, S. Sampath, N.P. Padture, *Mater. Sci. Eng., A* **528**, 7214 (2011).
32. P. Mechnich, W. Braue, U. Schulz, *J. Am. Ceram. Soc.* **94** (3), 925 (2011).
33. M.-P. Bacos, J.-M. Dorvaux, O. Lavigne, R. Mévrel, M. Poulain, C. Rio, M.-H. Vidal-Setif, in *Aerospace Lab: The ONERA Journal* (ONERA, Chatillon, France, 2011), issue 3.
34. R.A. Miller, J.L. Smialek, R.G. Garlick, in *Science and Technology of Zirconia*, A.H. Heuer, L.W. Hobbs, Eds. (The American Ceramic Society, Columbus, OH, 1981), vol. 3, pp. 241–253.
35. J.A. Krogstad, S. Krämer, D.M. Lipkin, C.A. Johnson, D.R.G. Mitchell, J.M. Cairney, C.G. Levi, *J. Am. Ceram. Soc.* **94** (S1), S168 (2011).
36. D.M. Lipkin, J.A. Krogstad, Y. Gao, C.A. Johnson, W.A. Nelson, C.G. Levi, *J. Am. Ceram. Soc.* (2012), in press.
37. M.J. Maloney, US Patent 6,177,200, 2001.
38. R. Vassen, A. Stuke, D. Stöver, *J. Therm. Spray Technol.* **18** (2), 181 (2009).
39. T.E. Strangman, D. Raybould, A. Jameel, W. Baker, *Surf. Coat. Technol.* **202**, 658 (2007).
40. W.E. Ford, in *Dana's Textbook of Mineralogy with an Extended Treatise on Crystallography and Physical Mineralogy, 4th Edition* (Wiley, New York, 1954).
41. PTI, "Material Safety Data Sheet: Airport Runway Sand" (2007); www.powdertechnologyinc.com/secondary/msds.php.
42. H.E. Taylor, F.E. Lichte, *Geophys. Res. Lett.* **7** (11), 949 (1980).
43. W. Chesner, R. Collins, M. MacKay, J. Emery, "User Guidelines for Waste and Byproduct Materials in Pavement Construction" (Federal Highway Administration, Washington, DC, 1997).
44. N. Chellah, M.-H. Vidal-Sétif, C. Petitjean, P.-J. Panteix, C. Rapin, M. Vilasi, in *8th International Symposium on High Temperature Corrosion and Protection of Materials (HTCPM8)* (Les Embiez, France, 2012).
45. T. Steinke, D. Sebold, D.E. Mack, R. Vaßen, D. Stöver, *Surf. Coat. Technol.* **205**, 2287 (2010).
46. A.K. Rai, R.S. Bhattacharya, D.E. Wolfe, T.J. Eden, *Int. J. Appl. Ceram. Technol.* **7** (5), 662 (2010).
47. J.M. Drexler, K. Shinoda, A.L. Ortiz, D. Li, A.L. Vasiliev, A.D. Gledhill, S. Sampath, N.P. Padture, *Acta Mater.* **58** 6835 (2010).
48. J.M. Drexler, A.L. Ortiz, N.P. Padture, *Acta Mater.* **60** 5437 (2012).
49. M.-P. Bacos, J.-M. Dorvaux, S. Landais, O. Lavigne, R. Mévrel, M. Poulain, C. Rio, M.-H. Vidal-Sétif, in *Aerospace Lab: The ONERA Journal* (ONERA, Chatillon, France, 2011), issue 3.
50. W.C. Hasz, C.A. Johnson, M.P. Borom, US Patent 5,660,885 (1997).

51. M. Fu, R. Darolia, M.D. Gorman, B.A. Nagaraj, US Patent 8,062,759 (2007).
52. N.P. Padture, K.W. Schlichting, T. Bhatia, A. Ozturk, B. Cetegen, E.H. Jordan, M. Gell, S. Jiang, T.D. Xiao, P.R. Strutt, E. Garcia, P. Miranzo, M.I. Osendi, *Acta Mater.* **49**, 2251 (2001).
53. S. Krämer, J.Y. Yang, C.G. Levi, *J. Am. Ceram. Soc.* **91** (2), 576 (2008).
54. J.M. Drexler, C.H. Chen, A.D. Gledhill, K. Shinoda, S. Sampath, N.P. Padture, *Surf. Coat. Technol.* **206**, 3911 (2012).
55. R.G. Wellman, J.R. Nicholls, *Tribol. Int.* **41**, 657 (2008).
56. R.V. Hillery, B.H. Pilsner, R.L. McKnight, T.S. Cook, M.S. Hartle, "Thermal Barrier Coating Life Prediction Model Development" (NASA CR 180807, General Electric, 1988).
57. E. Zaleski, R.W. Jackson, C. Ensslen, C.G. Levi, *8th International Symposium on High Temperature Corrosion and Protection of Materials (HTCPM8)* (Les Embiez, France, 2012).
58. J.M. Drexler, A. Aygun, D. Li, R. Vaßen, T. Steinke, N.P. Padture, *Surf. Coat. Technol.* **204** (16–17), 2683 (2010).
59. R.W. Jackson, E.M. Zaleski, M.R. Begley, C.G. Levi, in *International Conference on Metallurgical Coatings and Thin Films* (San Diego, CA, 2012).
60. M.D. Novak, F.W. Zok, *Rev. Sci. Instrum.* **82** (115101) (2012).
61. NRC, "Integrated Computational Materials Engineering: A Transformational Discipline for Improved Competitiveness and National Security" (9780309119993, The National Academies Press, Washington, DC, 2008). □